# SPOOL

# Cyber-physical Architecture #4

## Advancements in Designing, Producing, and Operating Off-Earth Infrastructure

V8/#2

ISSN 2215-0897
E-ISSN 2215-0900

VOLUME 8 . ISSUE 2

# SPOOL

VOLUME 8 . ISSUE 2

# Cyber-physical Architecture #4

## Editorial



## Articles



## Dialog

**SPOOL** - Journal of Architecture and the Built Environment

SPOOL is a journal initiative in the field of 'architecture and the built environment'. It puts a strong emphasis on specific topics: Science of Architecture; Landscape Metropolis; Energy Innovation, Cyber-physical Architecture and Climate Adaptation. These topics refer to existing and upcoming research programmes/interests in Europe and beyond, and ensure a steady stream of potential copy. Treating these topics as threads within one journal allows SPOOL to focus on the interrelationship between the fields, something that is often lost in specialised journals. SPOOL welcomes within this framework original papers and associated open data on research that deal with interventions in architecture and the built environment by means of design, engineering and/or planning.

**ISBN**
978-94-6366-459-2

**Cover images**
Front: Rhizomatic Off-Earth Habitat. Copyright Robotic Building Lab, TU Delft and Vertico
Back: Concept of a training campus for scientists on the Moon, featuring a semi-protected area for outside lunar operations. Student project Moon Campus. (MoonVillage Design studio, HB2, TU Wien, by B. Dogan, J. Oblitcova)

**Publisher**
TU Delft Open



ISSN 2215-0897
E-ISSN 2215-0900

www.spool.ac

EDITORIAL

# Advancements in Designing, Producing, and Operating Off-Earth Infrastructure

**Henriette Bier** [1, 2, 3], **Angelo Cervone** [1], **and Advenit Makaya** [4]

[1] *Delft University of Technology*
*Delft, the Netherlands*

[2] *Politecnico di Milano*
*Milan, Italy*

[3] *Anhalt University of Applied Sciences*
*Dessau-Rosslau, Germany*

[4] *European Space Agency*
*Noordwijk, Netherlands*

Sending humans to the Moon and Mars in the near future requires appropriate infrastructure to support and subsequently sustain human activities. This includes infrastructure to shield from environmental conditions, generate energy, and facilitate mobility and communication. Construction of such infrastructure aims to use in-situ resources and reduce the use of supplies from Earth. The establishment and maintenance of the required infrastructure, equipment, and hardware involves the development of adequate manufacturing techniques, which can enable maximal use of the local resources. Those techniques can be based on processing of local materials into construction materials, extraction of useful elements from local materials or in combination with materials brought from Earth. The required manufacturing techniques address the range of needs for sustained human activities, from smaller scale manufactured items to large built structures. The design of such structures is associated with a number of space systems' engineering challenges, ranging from the accurate definition of all resource budgets (mass, volume, power, data) to the design of the interfaces between all subsystems making use of these resources. The interplanetary spacecraft used to transport the required materials (and eventually, crew) from Earth to the final site would probably need to be designed ad-hoc for this specific application, given its peculiar mass and volume constraints, especially in case a reusable concept is adopted. Other engineering aspects involved in the design of the infrastructure systems include the selection of an appropriate power generation approach and the definition of the radiation environment in order to provide sufficient shielding to the habitats. This Spool CpA #4 issue investigates challenges of designing, engineering, constructing, operating, and maintaining off-Earth infrastructure.

These challenges are addressed with contributions from various disciplines ranging from (1) architecture to (2) materials engineering, involving In-Situ Resource Utilisation (ISRU) for manufacturing processes and (3) power generation:

## ARCHITECTURE

From reviews of previous designs to new design proposals, authors from academia and industry engage in investigations covering inter alia comfort, sustainability, and autarkic aspects in space architecture.

**Häuplik-Meusburger and Griffin** review concepts and designs that have been developed in the last 50 years. They all have been dealing with typical lunar challenges, such as lunar dust, microgravity, etc. The authors present them according to the class terminology of habitat design: Pre-integrated modules from Earth (class 1), prefabricated components assembled on-site (class 2), in-situ-resources (class 3), combination of all of the above, with examples included from space industry, space architecture community, as well as academia._

Somewhat similarly, **Konstantatou et al.** reflect on the value, applicability, and posed challenges of what has been designed so far and what could, and should, be designed in the future while taking into consideration the bi-directional relationship between off-Earth and on-Earth architecture and building construction. The paper focuses on past and contemporary structural design approaches – in particular component-based against continuous approaches – and assesses them in terms of sustainability, contribution to the space industry, and applicability to the on- and off-Earth context.

The third contribution with focus on architecture by **Bier et al.** briefly reviews a couple of contemporary off-Earth design proposals to then focus on presenting a novel idea to excavate into the ground in order to create subsurface habitats on Mars. By excavating, not only natural protection from radiation can be achieved, but also thermal insulation because the temperature is more stable underground. The excavated material is used for 3D printing the habitat with the ultimate goal of developing an autarkic system using solar and kite power (Corte Vargas et al., 2021) for building and inhabiting off-earth subsurface autarkic habitats.

In addition to this proposed 3D printing approach using locally sourced regolith, two papers address additive manufacturing (AM) concepts using lunar regolith:

## MATERIAL SCIENCE

**Laot et al.** explore functionally graded materials (FGM) as high-performance composite materials, offering several advantages, including localized tailoring of material properties, improved material boundary compatibility, and enhanced thermomechanical behaviour. The presented research is investigating the feasibility of an in-situ manufactured metallic-regolith FGM. Three AM techniques are assessed with respect to their capability to effectively consolidate regolith on its own and onto metallic substrates.

Furthermore, **Grundstrom et al.** present the use of a lunar regolith simulant as feedstock for a direct ink writing (DIW) AM process involving a bio-organic binder. The feasibility of this approach is demonstrated by manufacturing objects with various three-dimensional geometries. Of particular interest is the proposition to use these compounds as additives produced in-situ through photosynthesis for a future lunar base, utilising carbon dioxide exhaled by astronauts together with the available sunlight.

For such manufacturing processes as well as for habitation, considerable power supply is needed, which is addressed as follows:

## POWER GENERATION

**Corte Vargas et al.** present an energy generation approach that combines complementary resources for an effective renewable energy solution. In this work, a 10 kW microgrid solution is proposed, based on a pumping kite power system and photo-voltaic solar modules to power the construction as well as the subsequent use of the Mars habitat, as presented in the paper from Bier et al.

In addition to these contributions, a dialogue on architecture between experts is reported in the **Interview** section acknowledging that, while all contributions to this issue rely on learning from precedents and advancing development of new technologies, the challenge remains to efficiently transfer technology from on-Earth to off-Earth applications and vice versa.


### DOI

https://doi.org/10.7480/spool.2021.2.6056

# Additive Manufacturing and Spark Plasma Sintering of Lunar Regolith for Functionally Graded Materials

**Mathilde Laot** [1], **Belinda Rich** [2], **Ina Cheibas** [2], **Jia Fu** [1], **Jia-Ning Zhu** [1], **Vera A. Popovich** [1]

[1] **Delft University of Technology**
**Department of Materials Science and Engineering**
**Delft, the Netherlands**

[2] **ESA/ESTEC European Space Agency**
**Noordwijk, the Netherlands**

## Abstract

This study investigates the feasibility of in-situ manufacturing of a functionally graded metallic-regolith. To fabricate the gradient, digital light processing, an additive manufacturing technique, and spark plasma sintering were selected due to their compatibility with metallic-ceramic processing in a space environment. The chosen methods were first assessed for their ability to effectively consolidate regolith alone, before progressing to sintering regolith directly onto metallic substrates. Optimized processing conditions based on the sintering temperature, initial powder particle size, and different compositions of the lunar regolith powders were identified. Experiments have successfully proven the consolidation of lunar regolith simulants at 1050°C under 80 MPa with digital light processing and spark plasma sintering, while the metallic powders can be fully densified at relatively low temperatures and a pressure of 50 MPa with spark plasma sintering. Furthermore, the lunar regolith and $Ti_6Al_4V$ gradient was proven to be the most promising combination. While the current study showed that it is feasible to manufacture a functionally graded metallic-regolith, further developments of a fully optimized method have the potential to produce tailored, high-performance materials in an off-earth manufacturing setting for the production of aerospace, robotic, or architectural components.

## Keywords

In-Situ Resource Utilization (ISRU), Regolith, Functionally Graded Materials (FGM), Additive Manufacturing (AM), Digital Light Processing (DLP), Spark Plasma Sintering (SPS)

## DOI

https://doi.org/10.7480/spool.2021.2.5258

## Introduction

Lunar exploration is an essential step for long-term space expeditions. The Moon is exceptionally advantageous compared to other planetary bodies because of its proximity and fast communication times with Earth (Benaroya, 2018). It can serve as a strategic cornerstone of future technological developments in aerospace science and engineering, physics, and other disciplines (Eckart, 1999). Lunar infrastructure, such as space habitats and engineering tools, are critical for a successful mission. They must ensure high mechanical performance and safety against the harsh environmental conditions, such as radiation, meteoroids, thermal fluctuations, and ultra-high vacuum (Howe & Sherwood, 2009; Naser & Chehab, 2018). Furthermore, the ideal infrastructure would be autonomous, with build in-situ capabilities to substantially diminish the weight of payload brought from Earth (Frank et al., 2013). Thus, manufacturing proposals use local resources to design resilient and affordable human and robotic exploration tools. In-situ resource utilization (ISRU) is a key strategy for manufacturing space habitats and components (Kennedy, 2002; Sanders et al., 2005). Lunar soil or regolith is the primary material for ISRU and is most abundant on the Moon. Regolith is an abrasive and corrosive powder that contains several silicates (plagioclase, feldspar, pyroxene, olivine) and oxide minerals (ilmenite, spinel), see Table 1 (Edmunson & Rickman, 2012; Papike et al., 1982). These silicates and oxide minerals are abundant in metals such as silicon (Si), aluminium (Al), iron (Fe), titanium (Ti), and magnesium (Mg) (Mueller et al., 1988; Pieters, 1986; Prettyman et al., 2006; Taylor, 1987). The metals can be extracted by pyrometallurgy, electrometallurgy, and hydrometallurgy methods, with oxygen resulting as a by-product of this refining process (Agosto, 1981; Allen et al., 1996; Landis, 2007). However, metallic powders have not yet been investigated for lunar infrastructure fabrication. Current research focuses largely on the automated fabrication of structures from regolith simulants, which does not take full advantage of the ISRU potential.

The predominant construction approach for a permanent Moon base is additive manufacturing (AM). AM is divided into several families, namely material extrusion, material jetting, binder jetting, stereolithography or digital light processing, powder bed fusion, and direct energy deposition (F42 Committee, n.d.; Labeaga-Martínez et al., 2017). These AM methods are generally selected based on their technological feasibility for a lunar scenario and their expected performance (Dordlofva & Törlind, 2017). Material extrusion and binder jetting are promising techniques that use water with regolith in a concrete slurry (Cesaretti et al., 2014; Khoshnevis et al., 2005; Pilehvar et al., 2020). The disadvantages of these methods, however, include the large amount of water used, which is a highly scarce resource and valuable in space. Other fabrication methods are solar sintering and powder bed fusion, which involve the sintering of lunar regolith using solar light (Fateri, Meurisse, et al., 2019). Meurisse et. al. (2018) demonstrated the concept by manufacturing the first solar 3D-printed brick with lunar regolith simulant. This technique illustrates potential to use AM to build habitats or roads prior to astronaut' arrival (Fateri, Pitikaris, et al., 2019). Nevertheless, the vast majority of these studies employ components with inadequate mechanical properties (Goulas et al., 2018). The materials exhibit limited compressive or tensile strength and are not able to overcome the multitude of environmental requirements in space (Cesaretti et al., 2014; Goulas et al., 2017; Goulas & Friel, 2016; Meurisse et al., 2017; Neves et al., 2020). Such environmental factors include solar energetic particles (SEP), galactic cosmic rays (GCR), abrasion, wear, thermal fluctuations, refrigeration, ultra-high vacuum, resistance to fatigue, impact and pressurization, meteoroids and mechanical impacts, and biological and chemical inertness (Vaniman et al., 1991). Therefore, there is a need for resilient composites that can overcome all these environmental parameters and take full advantage of the potential of ISRU.

Functionally graded materials (FGM) are high-performance composites designed to achieve tailored features (Bever & Duwez, 1972). FGM can overcome the multitude of lunar requirements with functions or performance embodied in a graduated morphology. These materials are advantageous for maximizing ISRU capabilities due to their multi-material approach, which is high performance relative to monolithic

applications (Kim & Na, 1995; Srivastava et al., 2019; Suresh & Mortensen, 1997). FGM can improve mechanical behaviour via a specific distribution of materials in a graded layer. Several metal-ceramic gradients have been widely studied in recent years because of their highly attractive properties, such as high-temperature stability, high hardness, corrosion resistance, and versatility (Balla et al., 2007; Gong et al., 2018; Jin et al., 2018; Kamaruzaman et al., 2018; Katz-Demyanetz et al., 2019; Maseko et al., 2018; Popovich et al., 2018; Restivo et al., 2019; X. Zhang et al., 2018). A regolith to metal gradient can potentially be manufactured to combine ceramic-like properties with metal-like mechanical behaviour (Jin et al., 2018; Kamaruzaman et al., 2018). Such materials are expected to demonstrate improved resistance to thermal fatigue over conventional interfaces due to their graduated nature (Restivo et al., 2019), a crucial requirement for the dramatic thermal cycles experienced on the lunar surface, as well as high overall fracture toughness due to the presence of intermediate metallic-ceramic phases (Rattanachan et al., 2003). Compressive strength is expected to be in line with other regolith consolidation methods, in the range of 2 to 10 MPa (Altun et al., 2021).

The manufacturing technique plays an essential role in achieving such a gradient. Previous research investigated the powder characterization of regolith simulants to determine the feasibility of using AM to produce FGMs (Cheibas et al., 2020). Chemical composition, thermal characteristics, particle shape, and size distribution of the powders were analysed to determine regolith processability. This study found that digital light processing (DLP) and spark plasma sintering (SPS) are compatible consolidation techniques for both ceramic and metal powders, and thus FGMs (C. Zhang et al., 2019; Liu et al., 2019; Balla et al., 2012). Furthermore, preparation of the lunar simulant, particularly sieving and crushing, is necessary before consolidation due to the large particle size and shape.

## Materials and methods

### Powder characterisation

Three regolith simulants were evaluated for manufacture of a functionally-graded metallic-regolith: EAC-1A, LHS-1 (Lunar Highlands Simulant) and LMS-1 (Lunar Mare Simulant). The EAC-1A simulant was sourced from the European Astronaut Centre, Cologne, Germany, while LHS-1 and LMS-1 simulants were sourced from the CLASS Exolith Lab, Orlando, USA (CLASS Exolith Lab, n.d.-a; Engelschiøn et al., 2020). The use of simulant powders is necessary due to the limited availability of lunar soil. Thus, some differences between the terrestrial simulants and the actual lunar material are to be expected. Table 2 shows the similarity in oxide and mineralogical compositions between the chosen simulants and lunar Apollo samples. The element compositions of suite soils from the Apollo landing sites differ depending on the area of extraction: maria or highlands. The Apollo maria samples are similar to the LMS-1 simulant, with a higher concentration of titanium (Ti), ferrous oxides (FeO), and lower concentration of aluminium (Al). The highlands samples have a lower titanium (Ti) and iron (Fe) concentration, and higher aluminium in (Al) and calcium (Ca), similar to the LHS-1 simulant. The dominant mineralogical lunar content both for mare and highlands rock type is basaltic. The lunar highlands however, are more chemically simplified than the mare basalts. The highlands have different textural relationships dependent upon the degree of melting and recombination with other mineralogical components. Furthermore, essential differences exist between the Moon and Earth basalts. The key mineralogical difference in the lunar samples is the presence of FeO and $Fe^{2+}$, compared to terrestrial materials that typically consist of $Fe^{2+}$ and $Fe^{3+}$.

| | EAC-1A | LHS-1 | LMS-1 | MODAL PROPORTIONS |
|---|---|---|---|---|
| Plagioclase | 17.0 | 32.8 | 74.4 | 12.9 – 69.1 |
| Glass Mare | - | - | 24.2 | 0.9 – 17.2 |
| Glass Highlands | - | 24.5 | - | 3.8 – 25.0 |
| Basalt | - | 19.8 | 0.5 | - |
| Ilmenite | - | 11.1 | 0.4 | 0.0 – 12.8 |
| Pyroxene | 22.0 | 7.5 | 0.3 | 8.5 – 61.1 |
| Olivine | 14.0 | 4.3 | 0.2 | 0.2 – 17.5 |
| Iron Oxide | 13.0 | - | - | - |
| Other | 8.0 | - | - | - |
| **Total** | **74.0** | **100** | **100** | |

TABLE 1 Summary of mineralogical content (in wt.%) of three lunar regolith simulants (EAC-1A, LHS-1 and LMS-1) compared to the average volume percentages collected at the Apollo and Luna sites (Brown et al., 1975; Eckart, 1999).

| | EAC-1A | LHS-1 | LMS-1 | APOLLO MARIA | APOLLO HIGHLAND |
|---|---|---|---|---|---|
| $SiO_2$ | 43.70 | 44.18 | 42.18 | 45.4 | 45.50 |
| $TiO_2$ | 2.40 | 0.79 | 4.62 | 3.90 | 0.60 |
| $Al_2O_3$ | 12.60 | 26.24 | 14.13 | 14.90 | 24.00 |
| $Cr_2O_3$ | - | 0.02 | 0.21 | - | - |
| $Fe_2O_3$ | 12.00 | - | - | - | - |
| FeO | - | 3.04 | 7.87 | 14.10 | 5.90 |
| MgO | 11.90 | 11.22 | 18.89 | 9.20 | 7.50 |
| MnO | 0.20 | 0.05 | 0.15 | - | - |
| CaO | 10.80 | 11.62 | 5.94 | 11.80 | 15.90 |
| $Na_2O$ | 2.90 | 2.30 | 4.92 | 0.60 | 0.60 |
| $K_2O$ | 1.30 | 0.46 | 0.57 | - | - |
| $SO_3$ | - | 0.10 | 0.11 | - | - |
| **Total** | **98.40** | **100** | **99.56** | **99.9** | **100** |

TABLE 2 Oxide composition (given in wt.%) of three lunar regolith simulants (EAC-1A, LHS-1 and LMS-1 (Cannon, n.d.-a; Cannon, n.d.-b. Schleppi et al., 2018)) and the average of the lunar surface samples from Apollo maria and highlands regions (Mueller et al., 1988; Sibille et al., 2006).

Figure 1 (a) shows the particle size distribution of each simulant. All simulants exhibit a wide particle size range, namely 0.02 µm - 2000 µm for EAC-1A and <1 µm - 1000 µm for LHS-1 and LMS-1. The mean particle size is 10.5 µm for EAC-1A, 94 µm for LHS-1, and 63 µm for LMS-1 (CLASS Exolith Lab, n.d.-b; CLASS Exolith Lab, n.d.-c; Manick et al., 2018). The significant large grain fraction was predicted to cause difficulty in additive manufacturing, particularly in densification during sintering. Due to this, all three simulants underwent sieving through 50 or 100 µm mesh sieves to allow better sintering. A 30g batch of EAC-1A was milled in a Retsch planetary ball mill in an argon atmosphere using tungsten carbide balls (5 and 10 mm). The powder was milled for 30 hours at a speed of 300 rpm with a ball to powder mass ratio of 10:1. The contamination was kept very low, and the maximum particle size was reduced to 22 µm with mean particle size of 5 µm. Figure 1 (b) shows X-ray diffraction (XRD) patterns for all three lunar regolith simulants and confirms the presence of plagioclase, pyroxene. and iron oxide. Cheibas et al. conducted combined differential scanning calorimetry (DSC) and thermogravimetric analysis (TGA) to characterise the thermal behaviour of the given simulants (Cheibas et al., 2020). It was found that all three simulants exhibited a thermal transformation in the 1100°C - 1500°C temperature range, indicating partial melting taking place at these temperatures. Mass losses ranging from 0.97% to 2.75% were also observed in the simulants at temperatures above 1350°C, which is attributed to the loss of volatiles from the powder.

Regarding metal, several elements such as titanium, iron, and aluminium are abundant in lunar soil. Pure metallic powders have the potential to be extracted on the Moon and used to fabricate FGM. However, this research is a first step to determine the feasibility of a functionally graded regolith-metallic substrate. Due to the novelty of this study, an investigation is necessary to determine if the interface between the regolith and a terrestrial AM metallic powder is possible. Stainless steel 316L and $Ti_6Al_4V$ are high-grade metallic powders, frequently used in the aerospace industry for AM techniques (Mertens et al., 2014). These powders are selected because of their proven FGM potential and enhanced mechanical properties (Karami et al., 2020; Ruys et al., 2001). Therefore, in this study, the metallic powders used are stainless steel 316L and $Ti_6Al_4V$. The stainless steel powder was provided by Admatec (Alkmaar, The Netherlands) with a particle size range of <1 to 30 µm. The powder contains mainly austenite with a small portion of ferrite. $Ti_6Al_4V$ powder was provided by AP&C advanced powder & coatings, with a particle size range of 15 to 45 µm. The powder is composed solely of the alpha phase, an HCP lattice of $Ti_6Al_4V$.

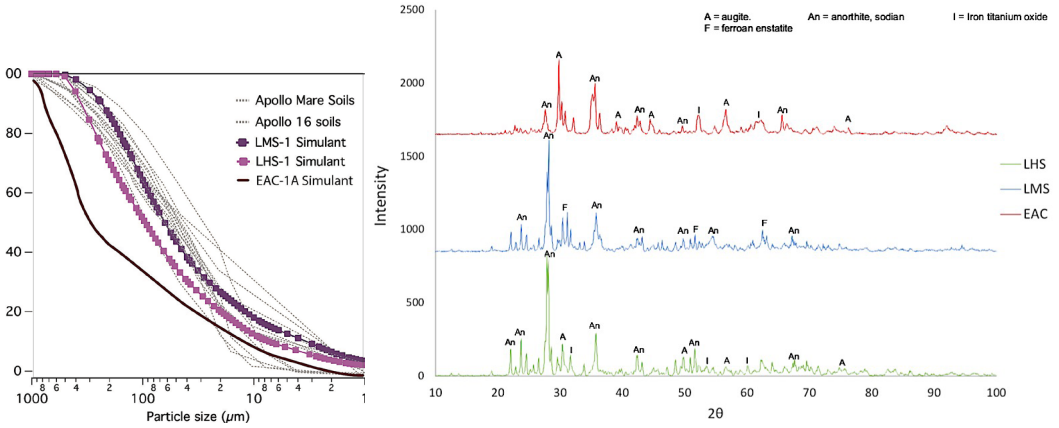


FIGURE 1 a) Average particle size distribution for EAC-1A, LHS-1 and LMS-1. Apollo data is shown for comparison and has been adjusted to remove the >1mm fraction. b) XRD patterns of the 3 lunar regolith simulants powders.

## Additive manufacturing consolidation techniques

Stereolithography, powder bed fusion, and direct energy deposition are AM methods able to process metal powders. However, the fabrication of functionally graded metallic-regolith has to be compatible with both the metal powders and lunar regolith. In the case of powder bed fusion and direct energy deposition, the current hardware to control a robust graded multi-material deposition is limited. Stereolithography, namely digital light processing (DLP), however, has the potential to achieve a metallic-regolith gradient and has been proven to work with lunar simulants (Altun et al., 2021). Therefore, DLP has a higher probability of success in consolidating the regolith and FGM as a proof of concept.

The DLP method is a liquid-based AM technique able to fabricate complex three-dimensional structures from ceramic or metallic powders. This vat polymerization method uses ultraviolet (UV) light to harden or cure a photopolymer resin. Meanwhile, a platform moves upward or downward after each new layer of the 3D printed object is cured (Chua et al., 2017; Zheng et al., 2012). The DLP method is divided into three steps: 1) printing the 3D model into the required shape; 2) debinding, to remove the polymeric binder; and 3) sintering as a final step aimed at full consolidation.

There are certain features of DLP which makes it incompatible with a lunar environment, such as scarcity and outgassing of the resin. A plausible scenario is to replace the conventional resin with a bio-inspired alternative to adapt this AM method to lunar infrastructure (Shiwei et al., 2020). Furthermore, the debinding step must be optimised for vacuum to prevent defect formation, which may occur when volatile products are unable to effectively escape the green body. This is more likely to occur in vacuum debinding than air debinding due to higher activation energy for binder degradation processes (Wright et al., 1989). Nonetheless, resin and debinding development is outside of the scope of this research.

In this study, DLP was performed using the EAC-1A powder. The original powder was sieved through a 30 µm sieve and the content of lunar regolith powder of the slurry was set to 41%. Rectangular bars were 3D-printed with a layer thickness of 50 µm and a depth of cure of 100 µm. Water debinding was performed for 1 day followed by debinding in a furnace. Debinding in the furnace involved slow heating in air with stops at 150, 300, 400, and 600°C to obtain the optimal removal of the resin and to reduce the remaining carbon as much as possible. The bars were then sintered in a standard furnace in an air atmosphere. The first sintering temperature was set to 1050°C and kept for 1 hour, with a slow heating rate of 100°C/h. An additional sintering run at 1075°C was carried out to improve sintering of the bars.

Printing and debinding were successfully performed in the DLP process. However, the standard sintering step required further optimisation to obtain good densification. Spark plasma sintering was then introduced to optimise the sintering parameters.

Spark plasma sintering (SPS) is a manufacturing technique that utilizes uniaxial pressure and pulsed or unpulsed DC or AC current to consolidate powders into the required shape (Munir et al., 2006). SPS has been previously studied as a technique to consolidate lunar regolith simulants, metal powders, or functionally graded materials (Long et al., 2013; Obadele et al., 2020; Radhamani et al., 2020; Tokita, 2003; X. Zhang et al., 2021). This study used a spark plasma sintering machine (SPS, FCT Group, Germany) operated under vacuum and a 20 mm graphite die with graphite punches. With this new sintering technique, the tool and the component are directly heated by DC current pulses to reduce cycle times to a few minutes. During SPS a direct pulsed current of 1000 A, voltage of 6V and pulse on/off 15:5 ms was applied. A pyrometer for process temperature regulation was focused on the inside of the top punch of the die. A 0.2 mm thick graphite foil was used to avoid adhesion and reaction between the powders and the graphite mould. Besides this foil, boron nitride spray was applied to reduce carbon diffusion into the sample. For this work, 4 mm high samples were pre-pressed to 10 kN before being set into the SPS machine. The sintering parameters used for the different regolith experiments are given in Table 3, while Table 4 shows the process parameters used to consolidate the metallic powders.

| NO. | LUNAR REGOLITH SIMULANT | SINTERING TEMPERATURE (°C) | PRESSURE ($MP_A$) | HOLDING TIME (min) | MAXIMUM PARTICLE SIZE (µm) |
|---|---|---|---|---|---|
| 1 | LHS-1 | 900 | 80 | 10 | 200 |
| 2 | LHS-1 | 975 | 80 | 20 | 100 |
| 3 | LHS-1 | 975 | 80 | 20 | 50 |
| 4 | LHS-1 | 1025 | 80 | 20 | 50 |
| 5 | LHS-1 | 1050 | 80 | 20 | 50 |
| 6 | LHS-1 | 1075 | 80 | 20 | 50 |
| 7 | LMS-1 | 1050 | 80 | 20 | 50 |
| 8 | EAC-1A | 1050 | 80 | 20 | 22 |
| 9 | EAC-1A | 1050 | 80 | 20 | 50 |
| 10 | EAC-1A | 1050 | 80 | 20 | 100 |

TABLE 3 Process parameters used for spark plasma sintering of lunar regolith.

| MATERIAL | SINTERING TEMPERATURE (°C) | PRESSURE (MPA) | HOLDING TIME (min) | MAXIMUM PARTICLE SIZE (µm) |
|---|---|---|---|---|
| Stainless Steel 316L | 1050 | 50 | 10 | 30 |
| | 1050 | 50 | 20 | 30 |
| | 1100 | 50 | 20 | 30 |
| $Ti_6Al_4V$ | 1000 | 50 | 10 | 45 |
| | 1050 | 50 | 10 | 45 |

TABLE 4 Process parameters used for spark plasma sintering of metallic powders.

Different experiments were performed to obtain FGM made of EAC-1A and one of the metallic powders: two-step experiments in which metal and lunar regolith were sintered separately under optimal parameters; and a one-step experiment in which both materials were sintered under the same parameters. First, EAC-1A was sintered under the optimal parameters (1050°C, 80 MPa, milled powder), then $Ti_6Al_4V$ was sintered at 1050°C, under 50 MPa with a holding time of 10 min. The optimal process parameters for stainless steel 316L were found to be 1100°C, 50 MPa, and a holding time of 20 min. The steel parameters were similar to those used for full sintering of crushed EAC-1A. The resulting parameters were then applied to another two-step experiment. The first step involved sintering of stainless steel in a layer under optimal parameters, followed by sintering of lunar regolith under its optimal conditions. Second, both layers were sintered under either optimal parameters for lunar regolith or 316L.

## Microstructural and morphological characterisation

XRD analysis was performed to determine the phases in the original powders and in the consolidated samples. The analysis was performed with a Bruker D8 Advance diffractometer using Cu K-alpha radiation. The step size used was 0.033° 2θ with 45 kV and 40 mA current in a 2θ range of 10°-100°. The samples were ground with SiC 180 to remove the remaining graphite foil and to enable XRD analysis.

The density of the samples was measured based on Archimedes' principle. The samples were cleaned with isopropanol, dried, and then weighed dry and immersed in distilled water. Three density measurements were taken per sample type and the mean and standard deviation were calculated to give an accuracy range. Spark plasma sintered samples were discs of 20 mm diameter and 4 mm thickness. The specimens were cut into 2 half-discs, then embedded into a conductive resin, ground (SiC 80, 180, 320, 800, 1200 and 2000) and polished (MD Mol 3 µm and MD Nap 1 µm). Optical microscopy (Olympus BX60M) and scanning electron microscopy (SEM) in both secondary and backscattered modes were used for microstructural characterization. Average porosity level and average relative sintered thickness were determined based on optical images. Porosity measurements were taken three times at 5 different locations; accuracy ranges were also taken based on the standard deviation. Energy dispersive spectroscopy (EDS) was performed to determine local composition and elemental distribution in the bulk and interface layers. Thermocalc® calculations were performed to determine the phases formed at the interface of FGM based on EDS results. Microhardness measurements were carried out using an automated Vickers hardness machine, Dura Scan (Struers). A load of 0.3 kgf (HV0.3) was used to measure the hardness of the lunar regolith sintered samples. It was observed that a higher load level results in severe cracking. For the metallic sintered samples, a load of 0.5 kgf (HV0.5) was used to measure their hardness. The hardness was measured at multiple locations on each sample and the average and standard deviation was calculated.

## Results and Discussion

### Consolidation of lunar regolith

### Digital Light Processing (DLP)

Figure 2 shows lunar regolith (EAC-1A) printed samples with a layer thickness of 50 µm. Four bars were successfully printed with a height and width of 5 mm and a length of 100 mm.

The debinding step was successful and the bars remained in their shape after being heat-treated. The colour of the samples after debinding was the same as the initial powder; hence no significant change of the composition of the powder should have occurred. It can thus be concluded that printing and debinding DLP steps can be performed without significant change in chemistry.

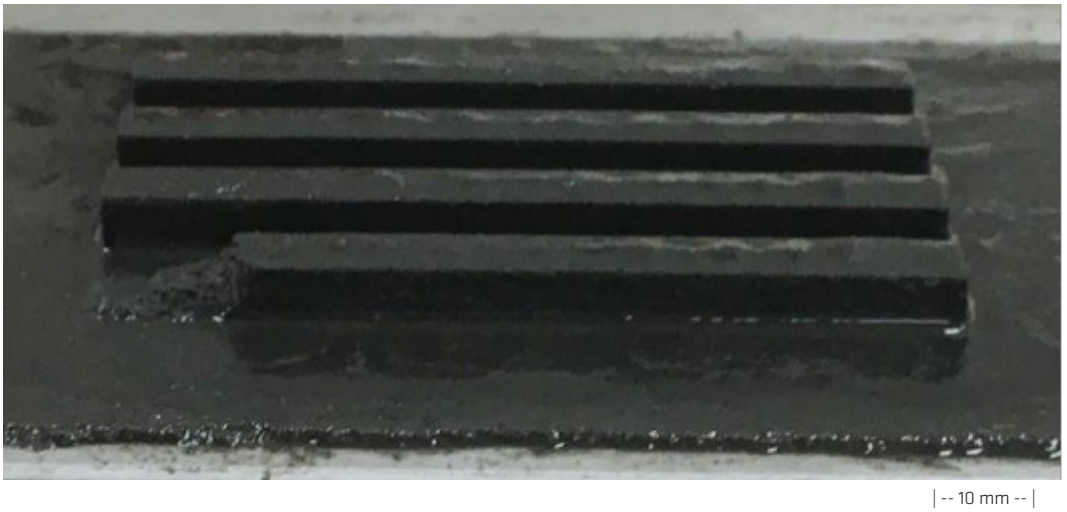

| -- 10 mm -- |

FIGURE 2 DLP printed bars made out of lunar regolith EAC-1A.

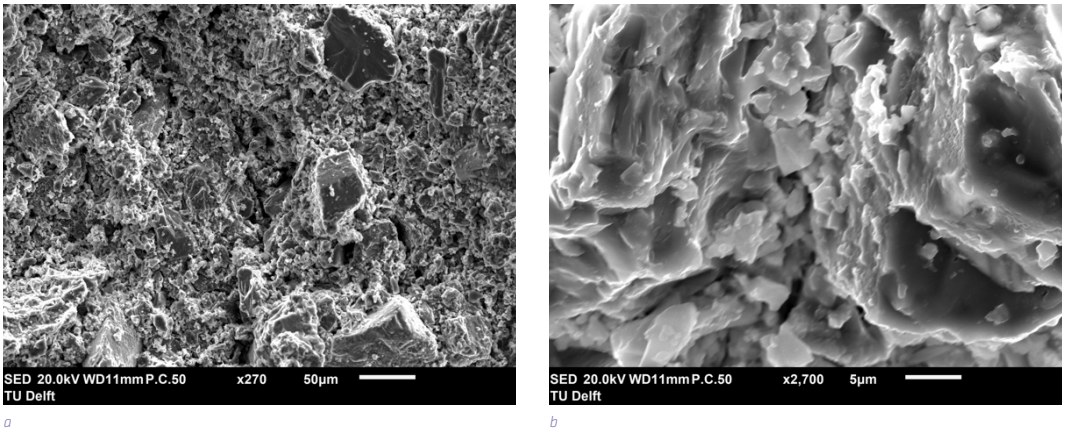


*a* *b*

FIGURE 3 SEM images of DLP samples sintered under standard in-air conditions: a) low and b) high magnifications.

After standard (in-air) sintering, the samples showed rather poor sintering characteristics: the bars did not keep their shape and cracked into small pieces. The sintered samples also changed in colour, to a light red. A similar colour change was also noticed by Liu et al. (2019), who found it to be associated with the transformation of $Fe^{2+}$ to $Fe^{3+}$ via oxidation reactions. Hence, standard in-air sintering is not suitable for this material and further optimization of the sintering step is required.

The microstructure of the samples showed poor sintering between particles (see Figure 3). However, the structure also shows larger particles surrounded by smaller particles, which would be beneficial for sintering as smaller particles can close the voids between coarser ones, resulting in better packing and densification. Furthermore, as shown in Figure 3b, some particles coalesced and exhibited necking. This partial necking indicates that EAC-1A can be sintered with digital light processing (DLP). However, the sintering process requires further optimization, which is the scope of the follow up sections.

## Spark Plasma Sintering (SPS)

SPS is proposed as a follow-up to DLP to increase densification of the lunar regolith. A number of experiments were performed using SPS techniques to optimize the technique. The results were analysed with respect to the sintering temperature, initial powder particle size, and different compositions in the lunar regolith powders.

## Effect of SPS temperature

Table 5 shows the effect of SPS temperature on density and hardness. As can be seen, SPS significantly increases the density and hardness while reducing the porosity of lunar regolith simulant samples. The density was found to increase with the sintering temperature, with the maximum density of 2.704 ± 0.025 $g.cm^{-3}$ achieved for the sample sintered at 1075°C. It should be noted that sintering at 1075°C led to partial melting and resulted in a non-stable process. It is therefore advisable to keep the sintering temperature below 1075°C.

| SPS TEMPERATURE (°C) | DENSITY (g/cm³) | POROSITY (%) | HARDNESS $HV_{0.3}$ |
|---|---|---|---|
| 1025 | 2.532 ± 0.046 | 23.7 ± 5.4 | 443 ± 56 |
| 1050 | 2.616 ± 0.060 | 21.0 ± 5.5 | 725 ± 77 |
| 1075 | 2.704 ± 0.025 | 11.7 ± 3.3 | 743 ± 142 |

TABLE 5 Density and Vickers hardness of SPS sintered lunar regolith (LHS) samples.

The microstructure of the samples was studied with SEM/EDS and their phases were determined with XRD (Figure 4 and 5). Three main phases were present in the samples at all sintering temperatures: an augite light grey phase $Ca(Mg,Fe,Al)(Si,Al)_2O_6$, a sodian anorthite dark grey phase $(Ca,Na)(Si,Al)_4O_8$ and a white phase corresponding to an iron titanium oxide (Figure 4). The sodian anorthite could have transformed to augite during the SPS experiment. The augite is often found in the form of "smashed" particles within the anorthite phase, as shown in Figure 5. This microstructure could be due to the pressure applied during the SPS process. The partially dissolved anorthite can be pushed between the smashed augite particles by applying external pressure. Anorthite has a lower melting point and a lower modulus than augite: anorthite is thus more prone to plastic deformation under the applied pressure and can fill the gaps between the smashed augite particles (X. Zhang et al., 2019). This specific microstructure was observed for all sintering temperatures.

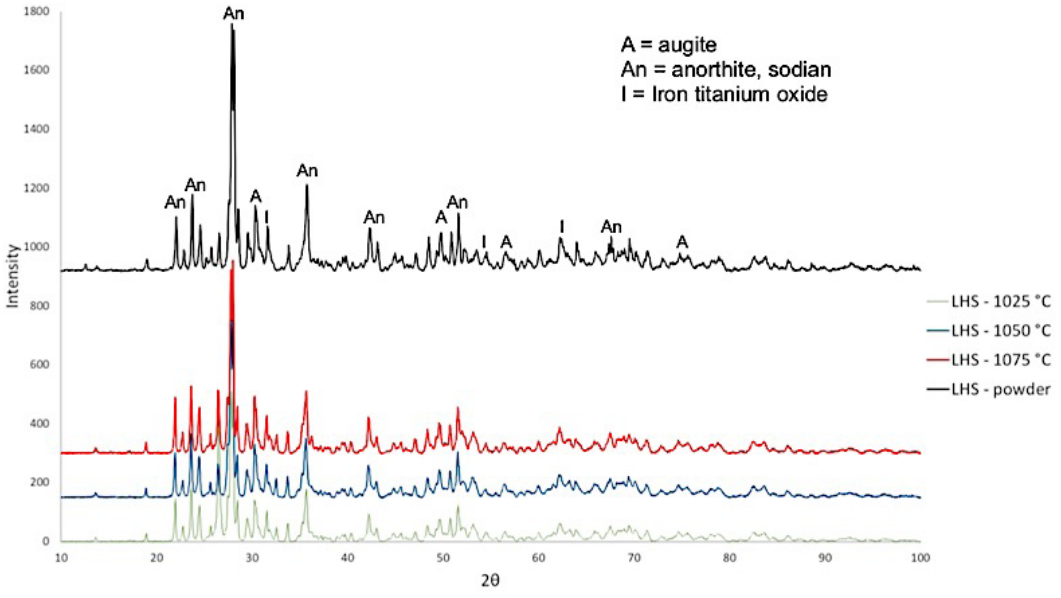


FIGURE 4 XRD patterns of LHS sintered samples as compared to the LHS as-received powder.

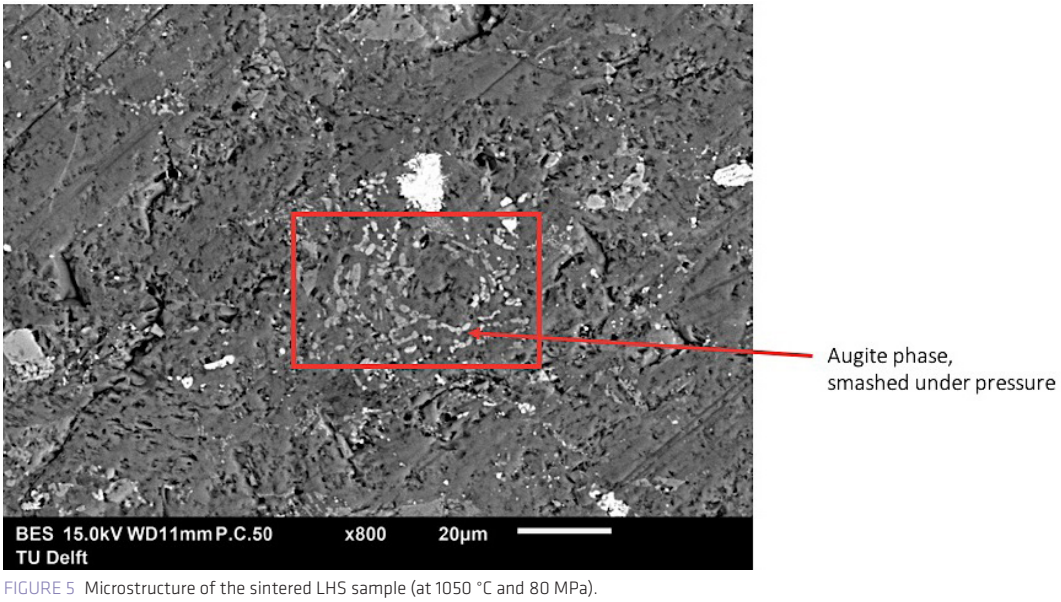


FIGURE 5 Microstructure of the sintered LHS sample (at 1050 °C and 80 MPa).

The XRD patterns for the three different sintering temperatures were very similar: all samples exhibited the same diffraction peaks and were thus composed of the same minerals. This is in accordance with the SEM images, with the same three phases are distinguished: augite, sodian anorthite, and an iron titanium oxide. The compositions of the sintered samples are very similar to the composition of the powder as it was received.

Carbon was detected using EDS only on the outer part of the samples. This carbon originates from the graphite foil used to prevent the powder from sticking to the mould during SPS. Boron nitride was sprayed on the graphite foil to avoid this diffusion, but a small portion of carbon can still diffuse into the samples. Carbon diffusion is a thermally activated process. It increases when using higher sintering temperatures

and higher pressure. Carbon only penetrates over a small layer of the sample and this layer can be removed by mechanical polishing. Viewed using EDS, the carbon was homogeneously present and had not formed any carbides.

Furthermore, the Vickers hardness also increased with the temperature. A significant increase was observed between the sintering temperatures of 1025°C and 1050°C. The hardness measurement is in accordance with the microstructure of the sintered samples. The high standard deviation is related to the different phases present in the specimens and the respective position of the measurement.

## Effect of particle size

In order to evaluate the effect of particle size, EAC regolith samples with sieved powders of maximum particle size 22, 50, and 100 µm were sintered at an optimal temperature of 1050°C and 80 MPa.

As can be seen in Table 6, samples with smaller particle size show higher densification. Moreover, the standard deviation is higher for samples with coarser particles, which indicates that the microstructure is more heterogeneous. It should also be noted that more macro-pores were observed in the coarser 100 µm sample. The presence of very coarse particles thus prevents good packing in the powder sample. The sample with the smallest initial particle size is the only sample that showed high vertical densification.

| PARTICLE SIZE (µm) | DENSITY (G/CM³) | POROSITY (%) | HARDNESS $HV_{0.3}$ |
|---|---|---|---|
| < 22 | 3.040 ± 0.046 | 4.3 ± 2.1 | 722 ± 35 |
| < 50 | 2.831 ± 0.077 | 15.5 ± 6.2 | 752 ± 74 |
| < 100 | 2.795 ± 0.078 | 21.4 ± 4.6 | 657 ± 46 |

TABLE 6 Density and Vickers hardness of SPS sintered lunar regolith (EAC) samples with different particle size.

The higher densification of samples with finer powders can be related to several densification mechanisms: rearrangement of the particles, formation and growth of the sintering necks between the particles, and plastic deformation and densification (Cheng et al., 2017). The smaller the particle size, the higher the surface energy driving force, given in Equation 1. The powder sintering is enhanced by the higher driving force. This causes migration of particles and increases the contact area between particles.

$$\Delta E = E_p - E_d \approx \gamma_{sv} W_m S_p \quad (1)$$

$$S_p \propto \frac{1}{R} \quad (2)$$

Equations 1 and 2

Equations 1 and 2 show the relationship between the powder properties and the driving force for sintering. ΔE is the intrinsic driving force, $E_p$ is the surface energy of the powder before sintering, $E_d$ the surface energy of powder after sintering, $\gamma_{sv}$ (J/m²) the solid-gas surface energy, $W_m$ (g/mol) the molar mass of material, $S_p$ (cm²/g) the specific surface area of powder, and R the radius of the particle.

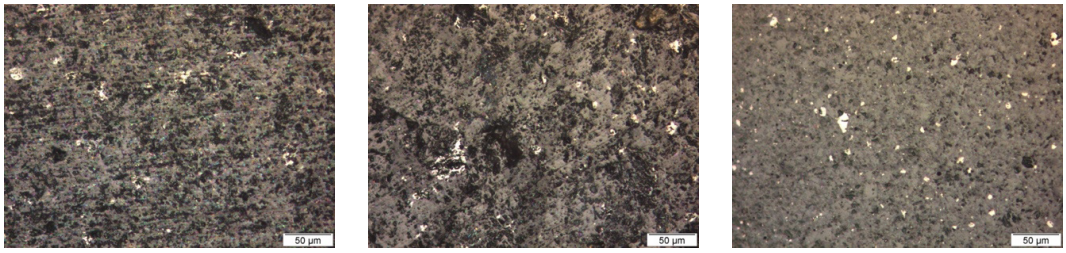


*a* *b* *c*

FIGURE 6 Optical microscopy images of EAC-1A sintered samples: a) 100 µm, b) 50 µm and c) 22 µm.

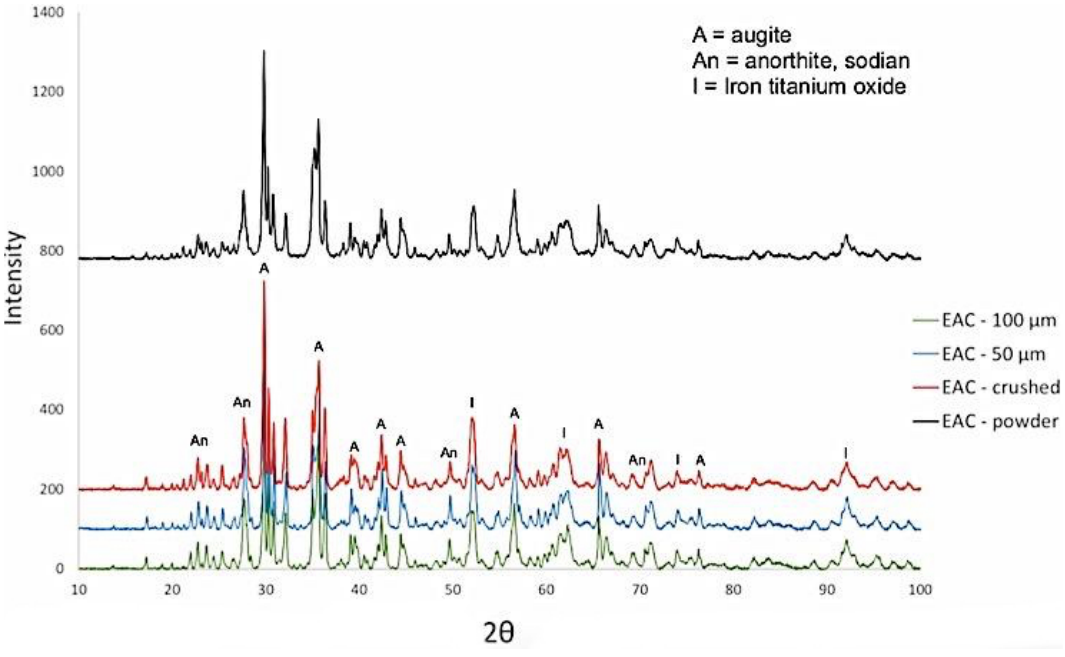


FIGURE 7 XRD patterns for SPS samples with different particle size as compared with as-received powder.

The tensile stress of the sintering necks increases with decreasing particle size, and the strength of the sintering necks is higher between smaller particles. Only the use of crushed EAC-1A powder (with resulting 22 µm particles) led to a fully dense sample (Figure 6c). In the case of SPS, the particle surface is heated to higher temperatures compared to the particle core due to spark discharge in the voids. The surface to volume ratio of smaller particles is bigger than for coarse particles. The amount of the powder subjected to high temperatures is higher in the case of smaller particles, which leads to more effective densification. XRD patterns (Figure 7) showed no significant differences between the samples consolidated with different particle sizes. The primary identified phases were plagioclase, pyroxenes (augite and diopside), and iron titanium oxide. The composition of the sintered samples is close to the composition of the initial powder.

The hardness of the sample with coarse particles is lower than for the other samples. The higher hardness for the sample with maximum particle size 50 µm is associated with a higher standard deviation due to the different hardness of the particles. Thus, the hardness of the 22 µm sample and the 50 µm sample are comparable. The hardness does not increase with powder milling as the phase composition remains similar, yet more homogeneously distributed.

## Effect of powder composition

In order to evaluate the effect of regolith simulants and their composition, the LHS-1, EAC-1A, and LMS-1 powders were spark plasma sintered at the previously determined optimal conditions of 1050°C, 80 MPa pressure, and maximum particle size of 50 µm with a holding time of 20 min.

Table 7 shows that all three simulants result in a similar densification level and none of the powders melted under these sintering conditions (1050°C, 80 MPa). The EAC-1A and LMS-1 samples displayed higher densification than the LHS-1 samples. It should however be noted that a thicker layer of fully dense material was measured for the LHS-1 sample. This indicates that the average porosity is lower for LMS-1 and EAC-1A, but LHS-1 has a more heterogeneous porosity with a highly densified part. All three simulants were found to be composed of the same oxides and minerals with comparable phase transition temperatures, and a similar expected behaviour for SPS.

The Vickers hardness of the samples was also not affected by the differences in simulant composition (Table 7). As LMS has more iron titanium oxide phases, the standard deviation could be influenced by these phases' presence at some material locations.

| LUNAR REGOLITH SIMULANT TYPE | DENSITY (g/cm$^3$) | POROSITY (%) | HARDNESS $HV_{0.3}$ |
|---|---|---|---|
| LHS-1 | 2.616 ± 0.060 | 21.0 ± 5.5 | 725 ± 77 |
| EAC-1A | 2.831 ± 0.077 | 15.5 ± 6.2 | 752 ± 74 |
| LMS-1 | 2.817 ± 0.083 | 21.6 ± 7.7 | 732 ± 167 |

TABLE 7 Density and Vickers hardness of SPS samples of different regolith simulants (max. particle size 50 µm).

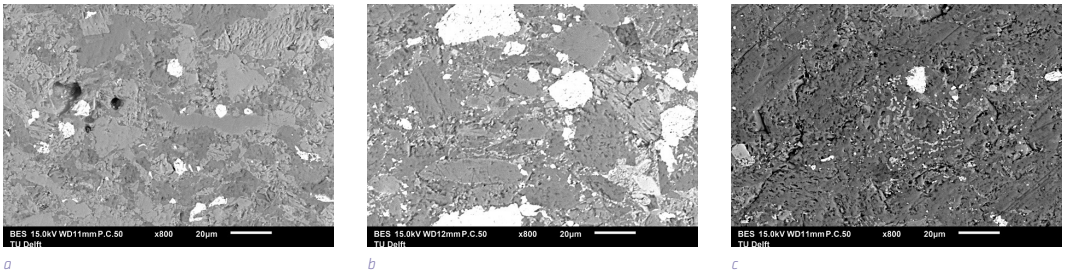


*a* *b* *c*

FIGURE 8 SEM images of SPS samples of three different lunar regolith simulants: a) EAC-1A, b) LMS-1 and c) LHS-1.

The microstructures of the sintered samples were also comparable and dense, with three main phases: augite, sodian anorthite, and iron titanium oxide. The LMS-1 samples showed a higher content of iron titanium oxide and coarser particles than the LHS-1 and EAC-1A samples (see white phases in Figure 8b).

## Consolidation of metallic powders

Consolidation of lunar regolith and metallic alloys has to be understood and optimised in order to develop a functionally graded material. The previous sections reviewed the consolidation of lunar regolith and the parameters influencing it. In this section, SPS consolidation of stainless steel and $Ti_6Al_4V$ will be addressed.

Table 8 shows the optimization of SPS parameters based on density and hardness. As can be seen, increasing the sintering temperature increases the density and hardness of stainless steel. The density decrease is relatively low with increased holding time, although other authors observed the opposite trend (Marnier et al., 2014). In our study, the lower density could be due to poor rearrangement of the particles during sintering, preventing the pores from closing. The different balance between open pores and closed pores may also play a role, as the Archimedes measurements only take into account the open pores. However, when porosity is measured using optical techniques, the porosity reduces with increasing temperature.

All $Ti_6Al_4V$ samples showed good densification and almost zero porosity. The applied uniaxial pressure of 50 MPa helps to rearrange the particles, breaking the agglomerates and inducing plastic deformation at high temperatures. The Joule heating effect derived from the pulsed current is another important densification mechanism. The current can flow through the highly conductive powdered sample, heating up the particles, especially on the particle surfaces. The temperature is thus higher at the contact point between particles. Diffusion thus increases and leads to higher and easier densification (Crosby et al., 2014).

Table 8 shows that the hardness for both alloys increased with rising sintering temperature. The hardness of samples sintered at 1050°C is in the order of the hardness of the cast annealed 316 alloys. The samples sintered at 1100°C show a much higher hardness. The hardness was homogeneous across the whole sample and the standard deviation is relatively small for all samples, indicating that the microstructure and composition are also likely homogeneous. SEM analysis revealed a homogeneous microstructure for all samples and did not show any precipitates. Some nano-precipitates could be present, such as carbides due to carbon diffusion. However, they are not visible at the magnification used. Some authors reported the presence of carbides on grain boundaries (Marnier et al., 2014). Nevertheless, these carbides were found only on the thin edges of the samples.

| MATERIAL | TEMPERATURE / HOLDING TIME | DENSITY (g/cm³) | POROSITY (%) | HARDNESS $HV_{0.5}$ |
|---|---|---|---|---|
| Stainless Steel 316 | 1050 °C/10 min | 7.642 ± 0.046 | 3 ± 1.2 | 158 ± 5 |
| | 1050 °C/20 min | 7.556 ± 0.015 | 1.4 ± 0.4 | 164 ± 6 |
| | 1100 °C/20 min | 7.834 ± 0.010 | 0.9 ± 0.3 | 191 ± 5 |
| $Ti_6Al_4V$ | 1000 °C/10 min | 4.391 ± 0.018 | 1.2 ± 0.5 | 322 ± 11 |
| | 1050 °C/10 min | 4.389 ± 0.006 | 0.7 ± 0.2 | 341 ± 23 |

TABLE 8 Density and Vickers hardness of sintered stainless steel and $Ti_6Al_4V$ (under 50 MPa pressure).

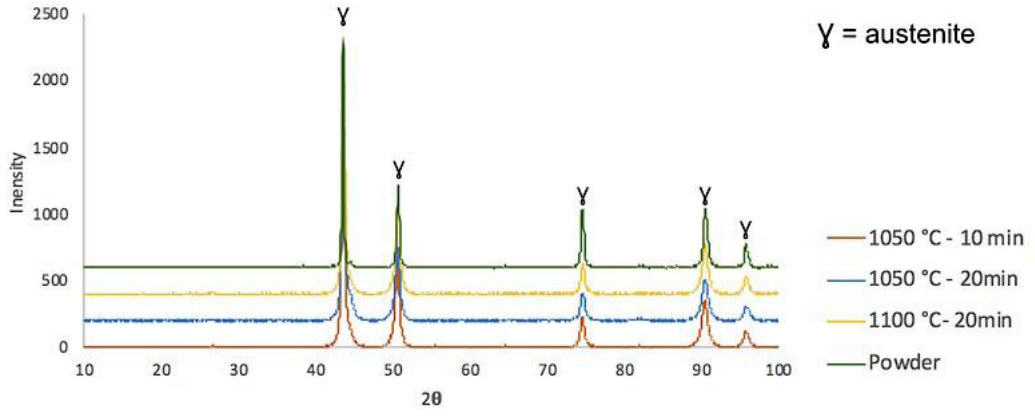


FIGURE 9 XRD of SPSed stainless steel 316 samples and of as-received powder.

The Vickers hardness for $Ti_6Al_4V$ was found to be 341 $HV_{0.5}$ for the samples sintered at 1050°C, compared to 322 $HV_{0.5}$ for the sample sintered at 1000 °C. These values are in the order of the Vickers hardness for $Ti_6Al_4V$ cast alloys (Poondla et al., 2009).

The XRD results in Figure 9 reveal only austenite phases present in all 316L samples. This fully austenitic microstructure was also observed by Keller et al. (2016).

For $Ti_6Al_4V$ alloys, the elements Ti, Al, and V were found to be evenly distributed, and no precipitates formed during the sintering process. The XRD results in Figure 10 show that the same phases form at the two different sintering temperatures. The α-Ti phase is present as in the as-received powder, but a second phase is detected for both samples: $Ti_{0.8}V_{0.2}$, which is a β-Ti structure.

Microstructural analysis revealed the presence of clusters of grains elongated in the same direction. Recrystallization is not hindered by the presence of intermetallics at the grain boundaries or by interstitial solute atoms, as shown by Long et al. (2013).

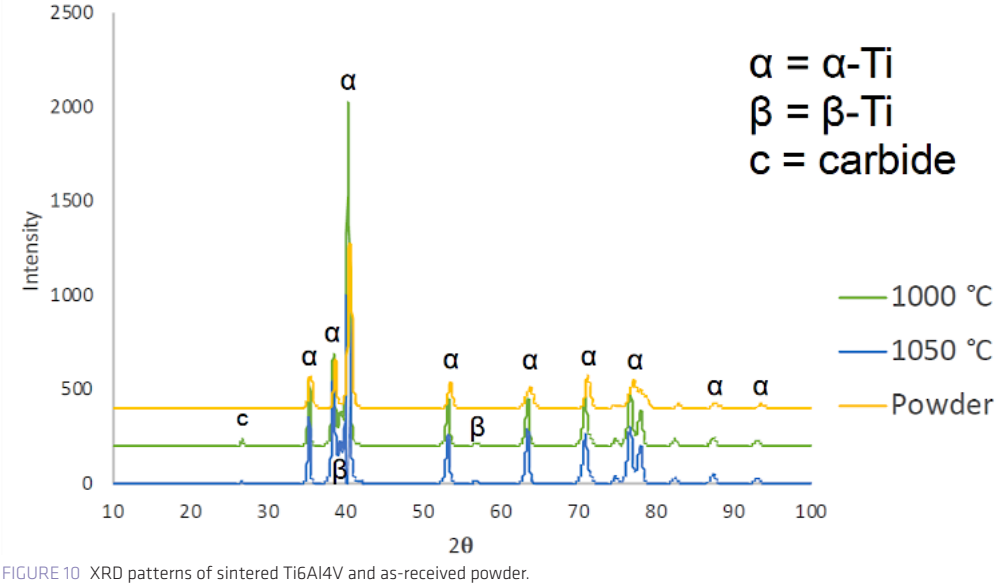


FIGURE 10 XRD patterns of sintered Ti6Al4V and as-received powder.

## Consolidation of functionally graded material (FGM)

The optimized parameters for FGM samples are based on the sintering results from regolith simulant and the individual metallic powders. The optimal SPS parameters for each material are displayed in Table 9.

| MATERIAL | SINTERING TEMPERATURE (°C) | PRESSURE (MPA) | HOLDING TIME (MIN) | MAXIMUM PARTICLE SIZE (MM) |
|---|---|---|---|---|
| Lunar regolith simulant EAC-1A | 1050 | 80 | 20 | 22 |
| Stainless steel 316L | 1100 | 50 | 20 | 30 |
| Ti6Al4V | 1050 | 50 | 10 | 45 |

TABLE 9 Optimal parameters for SPS of FGM based on lunar regolith simulant, stainless steel and titanium alloy.

### 3.3.1. FGM based on lunar regolith and stainless steel

The sintering was initially performed in one step by combining both lunar regolith (EAC-1A) and 316L green bodies. The experiment resulted in an inconsistent FGM and interfacial cracking. The one-step sintering at 1100°C under 50 MPa completely melted the lunar regolith simulant, which was squeezed out of the SPS mould. The surface of the metallic part did not show any remnants of the lunar regolith. This experiment highlights that sintering at 1100°C under 50 MPa is not suitable for the FGM lunar regolith simulant.
When sintering both powders at 1050°C under 50 MPa, the FGM did not keep its shape and the EAC-1A and stainless-steel layers did not bond. Both layers exhibited cracks and porosity at the FGM interface, see Figure 11. Thus, pressure of 50 MPa proved too low to allow for good sintering of the two powders.
A minimal pressure of 80 MPa seemed to be required to sinter the lunar regolith, and a higher pressure may be required to allow for interfacial sintering.
Therefore, a two-step sintering was introduced and proved to be more successful. The thin layer of EAC-1A remained in contact with the metal. However, the FGM fractured within the lunar regolith layer upon removal from the SPS mould. This might be caused by the thermal expansion coefficient of stainless steel 316, which is twice as high as the lunar regolith (Ray et al., 2010). This mismatch in thermal properties induces thermal stresses during SPS cooling. These stresses can explain why the FGMs cracked post-sintering.
However, the interface between the two dissimilar materials remained intact. SEM images revealed the presence of a grey phase at the interface, featuring higher chromium concentration than in the inner layers (Figure 13a). Chromium tends to diffuse from the stainless steel to the interface and form a high-content Cr phase; according to Thermocalc® calculations and composition from EDS, this is likely to be a BCC-A2 phase (Figure 12). Figure 13 shows the 316L/EAC functionally graded material hardness profile. The interface has a hardness much closer to the metallic alloy and does not exhibit a gradual transition, which is preferred for FGMs. Each hardness value was averaged based on 10 measurements for each location. Since the change in hardness between the interface and the lunar regolith is relatively large, it could explain the poor sintering properties of this type of FGM.

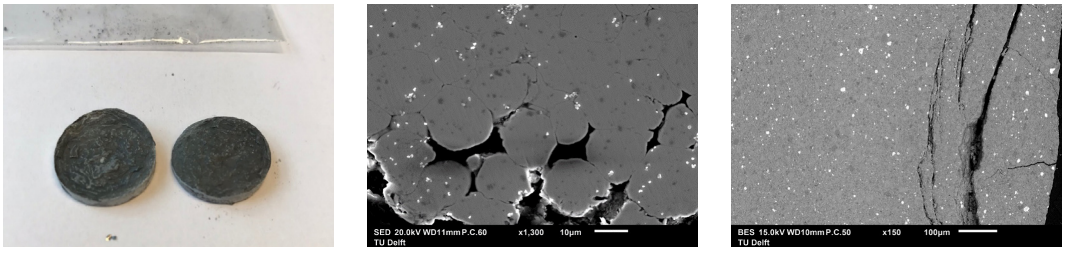


a b c

FIGURE 11 a) FGM 316/EAC after sintering at 1050°C. SEM images of the interface between the two materials: b) SS 316L and c) EAC-1A.

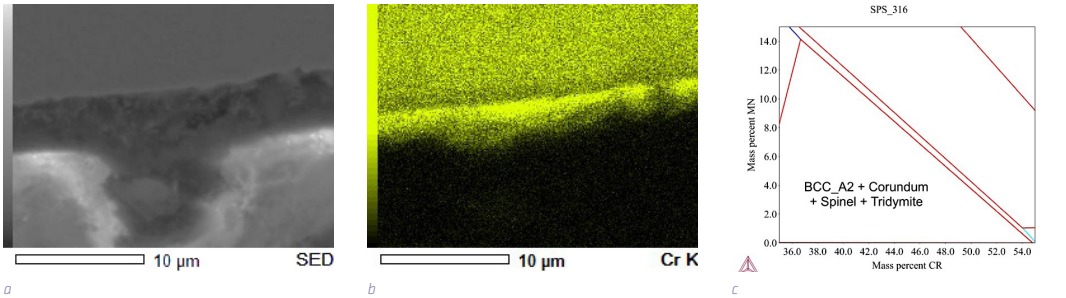


a b c

FIGURE 12 a) SEM image of interface of FGM 316/EAC, b) EDS map of Cr at the interface of FGM 316/EAC and c) Thermocalc graph for Cr diffusion.

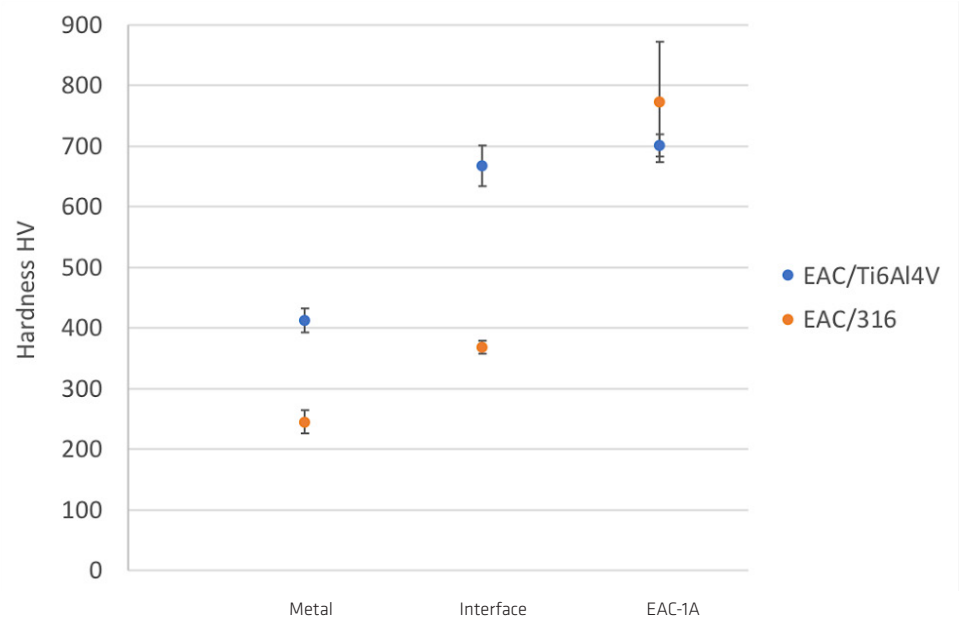


FIGURE 13 Vickers hardness profile of the functionally graded materials.

### 3.3.2. FGM based on lunar regolith and $Ti_6Al_4V$ alloy

$Ti_6Al_4V$ is the second alloy, selected for its good compatibility with lunar regolith. The FGM samples (Figure 14) produced did not show any fractures, cracking, or interfacial porosity, which were characteristic of the previous 316L/EAC FGM. As shown in Figure 13b, white particles, identified as titanium oxide, are present at the interface between the lunar regolith and $Ti_6Al_4V$. Moreover, EDS measurements reveal a potential segregation of silicon at the interface (Figure 15b), which forms the phase HCP_A3 ($Ti_xSi_y$) according to Thermocalc® calculations (Figure 15c).

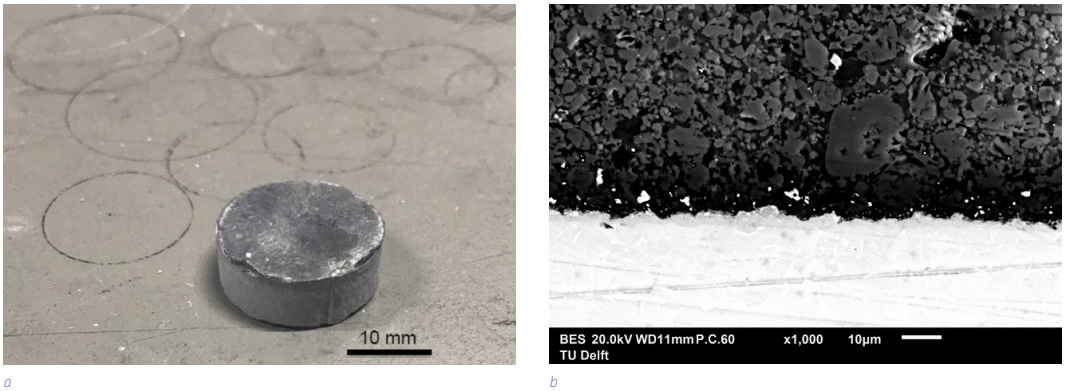


*a* *b*

FIGURE 14 a) FGM $Ti_6Al_4V$/EAC-1A after sintering in 2 steps and b) SEM image of the interface between $Ti_6Al_4V$ (light, below) and EAC-1A (dark, above).

The Vickers hardness profile of this FGM shows a gradual transition from one material to another at interface (Figure 13). The hardness of the interface is close to the hardness of the lunar regolith. The coefficient of thermal expansion of $Ti_6Al_4V$ and lunar regolith simulant are very close, about $8x10^{-6}$ $K^{-1}$ for both materials (Karami et al., 2020; Ray et al., 2010; Yakout et al., 2020). The similar coefficients help to prevent high thermal stresses during sintering, and especially during the cooling stage.

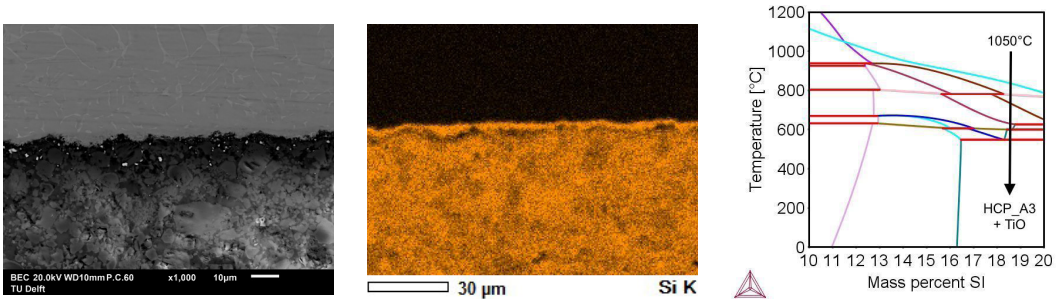


a b c

FIGURE 15 a) SEM image of interface of FGM Ti6Al4V/EAC, b) EDS of Si at the interface of FGM and Ti6Al4V c) Thermocalc graph for Ti6Al4V/EAC interface.

## Conclusions

In-situ resource utilization and advanced materials are essential for future space habitation on the Moon. In this study, additive manufacturing and spark plasma sintering were used to investigate the feasibility of a functional graded metallic-regolith. First, lunar regolith simulants were printed and debinded using digital light processing. Second, spark plasma sintering was applied and optimized using different sintering conditions, namely temperature, particle size, and composition. Then, the same SPS approach was applied to the metallic powders. Finally, the optimal processing conditions were developed for consolidation of functionally graded metallic-regolith with respect to densification, microstructural, compositional, and microhardness characteristics. The following conclusions are drawn from this study:

Lunar regolith simulants can be successfully additively manufactured via a combination of digital light processing and spark plasma sintering at 1050°C under 80 MPa. For best densification, it is necessary to sieve or mill the powders to 20-50 µm range. A higher pressure could be used to avoid the milling step. The composition of the sintered samples is similar to the powder composition: mainly augite, sodian anorthite, and iron titanium oxide.

Increasing the temperature and reducing the particle size in this process was found to increase densification and Vickers micro-hardness.

Metallic powders can be fully densified with SPS at relatively low temperature and a pressure of 50 MPa. Both stainless steel and $Ti_6Al_4V$ showed a homogeneous structure without precipitates or carbides.

FGMs were made using the optimal SPS parameters. The combination of lunar regolith and $Ti_6Al_4V$ has proven to be the most promising gradient. The hardness profile showed a gradual transition between these two layers, while the interface was found to be strong enough to avoid cracking.

This FGM feasibility study showed promising results for using additive manufacturing and in-space resources. The authors recommend the following aspects for follow-up research:

Investigations of the mechanical properties of regolith-metallic FGMs are needed, in particular of compressive strength, fracture toughness, and thermal fatigue behaviour for lunar construction applications, and wear resistance for coating applications. Thermal and wear properties are thought likely to be improved over metallic substrate alone, whereby fracture resistance will be greater than regolith alone. Understanding these properties is a major next step toward validating this method for lunar applications.

The combination of regolith with other metals in pure composition, such as pure aluminium, iron, and titanium powders, is needed to determine optimal FGM manufacturing in conditions closer to a lunar scenario.

In order to adapt the DLP method for lunar infrastructure, the next step is to investigate compatible resins. Furthermore, the debinding step should be optimised for the lunar environment to prevent charcoal formation and defects by tailoring powder morphology, resin, heating rate, and geometry.

Moreover, the SPS technique would have to be modified to be employed on the Moon for large-scale production. This study showed local melting of the powder at 1075 °C. Thus, laser-based additive manufacturing techniques could be investigated as a method for applying lunar regolith as a coating onto metallic surfaces to achieve better wear, corrosion, and thermal resistance.

The DLP process holds a uniquely high potential for printing complex geometries. Further studies could investigate methods for high-pressure sintering of complex green bodies in order to make full use of the DLP potential for FGM manufacture.

## Acknowledgments

The authors would like to acknowledge the support of the European Space Agency (ESA) via the Ariadna 19-D-A-02 research funding. Furthermore, we would like to express gratitude to the ESA technicians at the European Space Research and Technology Centre (ESTEC), in particular to Advenit Makaya, Sarah Rodríguez Castillo, and Martina Meisnar, as well as Jaap Hooijmans at Admatec for his assistance in performing DLP.

## References


AGOSTO, W. (1981, May). BENEFICIATION AND POWDER METALLURGICAL PROCESSING OF LUNAR SOIL METAL. *4th Space Manufacturing; Proceedings of the Fifth Conference*. https://doi.org/10.2514/6.1981-3263

Allen, C. C., Morris, R. V., & McKay, D. S. (1996). Oxygen extraction from lunar soils and pyroclastic glass. *Journal of Geophysical Research: Planets*, *101*(E11), 26085–26095. https://doi.org/10.1029/96je02726

Altun, A. A., Ertl, F., Marechal, M., Makaya, A., Sgambati, A., & Schwentenwein, M. (2021). Additive manufacturing of lunar regolith structures. *Open Ceramics*, *5*, 100058. https://doi.org/10.1016/j.oceram.2021.100058

Balla, V. K., Bandyopadhyay, P. P., Bose, S., & Bandyopadhyay, A. (2007). Compositionally graded yttria-stabilized zirconia coating on stainless steel using laser engineered net shaping (LENSTM). *Scripta Materialia*, *57*(9), 861–864. https://doi.org/10.1016/j.scriptamat.2007.06.055

Balla, V. K., Roberson, L. B., O'Connor, G. W., Trigwell, S., Bose, S., & Bandyopadhyay, A. (2012). First demonstration on direct laser fabrication of lunar regolith parts. *Rapid Prototyping Journal*, *18*(6), 451–457. https://doi.org/10.1108/13552541211271992

Benaroya, H. (2018). *Building Habitats on the Moon: Engineering Approaches to Lunar Settlements (Springer Praxis Books)* (1st ed.). Springer.

Bever, M., & Duwez, P. (1972). Gradients in composite materials. *Materials Science and Engineering*, *10*, 1–8. https://doi.org/10.1016/0025-5416(72)90059-6

Brown, G. M., Peckett, A., Emeleus, C. H., Phillips, R., & Pinsent, R. H. (1975). *Petrology and mineralogy of Apollo 17 mare basalts*. 1–13.

Cannon, K. (n.d.-a). *LHS-1 Lunar Highlands Simulant*. Planetary Simulant Database. Retrieved November 25, 2020, from https://simulantdb.com/simulants/lhs1.php

Cannon, K. (n.d.-b). *LMS-1 Lunar Mare Simulant*. Planetary Simulant Database. Retrieved November 25, 2020, from https://simulantdb.com/simulants/lms1.php

Cesaretti, G., Dini, E., De Kestelier, X., Colla, V., & Pambaguian, L. (2014). Building components for an outpost on the Lunar soil by means of a novel 3D printing technology. *Acta Astronautica*, *93*, 430–450. https://doi.org/10.1016/j.actaastro.2013.07.034

Cheibas, I., Laot, M., Popovich, V. A., Rich, B., & Castillo, S. R. (2020). *Additive Manufacturing of Functionally Graded Materials with In-Situ Resources*. Aerospace Europe Conference, Bordeaux, France.

Cheng, Y., Cui, Z., Cheng, L., Gong, D., & Wang, W. (2017). Effect of particle size on densification of pure magnesium during spark plasma sintering. *Advanced Powder Technology*, *28*(4), 1129–1135. https://doi.org/10.1016/j.apt.2017.01.017

Chua, C. K., Wong, C. H., & Yeong, W. Y. (2017). *Standards, Quality Control, and Measurement Sciences in 3D Printing and Additive Manufacturing*. Academic Press.

*CLASS Exolith Lab*. (n.d.-a). Center for Lunar & Asteroid Surface Science. Retrieved November 6, 2020, from https://sciences.ucf.edu/class/exolithlab/

CLASS Exolith Lab. (n.d.-b). *LHS-1 Lunar Highlands Simulant Fact Sheet*. Exolith Lab. Retrieved November 6, 2020, from https://exolithsimulants.com/collections/regolith-simulants/products/lhs-1-lunar-highlands-simulant

CLASS Exolith Lab. (n.d.-c). *LMS-1 Lunar Mare Simulant Fact Sheet*. Exolith Lab. Retrieved November 6, 2020, from https://exolithsimulants.com/collections/regolith-simulants/products/lms-1-lunar-mare-simulant

Crosby, K., Shaw, L. L., Estournes, C., Chevallier, G., Fliflet, A. W., & Imam, M. A. (2014). Enhancement in Ti–6Al–4V sintering via nanostructured powder and spark plasma sintering. *Powder Metallurgy*, *57*(2), 147–154. https://doi.org/10.1179/1743290113y.0000000082

Dordlofva, C., & Törlind, P. (Eds.). (2017). *Qualification Challenges with Additive Manufacturing in Space Applications*. .

Eckart, P. (1999). *The Lunar Base Handbook (Space Technology Series)* (1st ed.). McGraw-Hill Primis Custom Publishing.

Edmunson, J., & Rickman, D. L. (2012). A Survey of Geologic Resources. In V. Badescu (Ed.), *Moon* (pp. 1–21). Springer. https://doi.org/10.1007/978-3-642-27969-0_1

Engelschiøn, V. S., Eriksson, S. R., Cowley, A., Fateri, M., Meurisse, A., Kueppers, U., & Sperl, M. (2020). EAC-1A: A novel large-volume lunar regolith simulant. *Scientific Reports*, *10*(1). https://doi.org/10.1038/s41598-020-62312-4

F42 Committee. (n.d.). *Terminology for Additive Manufacturing Technologies*. ASTM International. https://doi.org/10.1520/F2792-12A

Fateri, M., Meurisse, A., Sperl, M., Urbina, D., Madakashira, H. K., Govindaraj, S., Gancet, J., Imhof, B., Hoheneder, W., Waclavicek, R., Preisinger, C., Podreka, E., Mohamed, M. P., & Weiss, P. (2019). Solar Sintering for Lunar Additive Manufacturing. *Journal of Aerospace Engineering*, *32*(6), 04019101. https://doi.org/10.1061/(asce)as.1943-5525.0001093

Fateri, M., Pitikaris, S., & Sperl, M. (2019). Investigation on Wetting and Melting Behavior of Lunar Regolith Simulant for Additive Manufacturing Application. *Microgravity Science and Technology*, *31*(2), 161–167. https://doi.org/10.1007/s12217-019-9674-5

Frank, J., Spirkovska, L., McCann, R., Lui Wang, Pohlkamp, K., & Morin, L. (2013). Autonomous mission operations. *2013 IEEE Aerospace Conference*, 1–20. https://doi.org/10.1109/aero.2013.6496927

Gong, F., Zhao, J., Li, Z., Sun, J., Ni, X., & Hou, G. (2018). Design, fabrication and mechanical properties of multidimensional graded ceramic tool materials. *Ceramics International*, *44*(3), 2941–2951. https://doi.org/10.1016/j.ceramint.2017.11.046

Goulas, A., Binner, J. G., Engstrøm, D. S., Harris, R. A., & Friel, R. J. (2018). Mechanical behaviour of additively manufactured lunar regolith simulant components. *Proceedings of the Institution of Mechanical Engineers, Part L: Journal of Materials: Design and Applications*, *233*(8), 1629–1644. https://doi.org/10.1177/1464420718777932

Goulas, A., Binner, J. G., Harris, R. A., & Friel, R. J. (2017). Assessing extraterrestrial regolith material simulants for in-situ resource utilisation based 3D printing. *Applied Materials Today*, *6*, 54–61. https://doi.org/10.1016/j.apmt.2016.11.004

Goulas, A., & Friel, R. J. (2016). 3D printing with moondust. *Rapid Prototyping Journal*, *22*(6), 864–870. https://doi.org/10.1108/rpj-02-2015-0022

Howe, A. S., & Sherwood, B. (2009). *Out of this world: The new field of space architecture*. American Institute of Aeronautics & Astronautics.

Jin, Q., Ren, X. P., Hou, H. L., Zhang, Y. L., & Qu, H. T. (2018). In Situ Synthesis and Structural Design of Ti/TiC Functionally Graded Materials. *Materials Science Forum*, *913*, 515–521. https://doi.org/10.4028/www.scientific.net/msf.913.515

Kamaruzaman, F. F., Nuruzzaman, D. M., Ismail, N. M., Hamedon, Z., Iqbal, A. K. M. A., & Azhari, A. (2018). Microstructure and properties of aluminium-aluminium oxide graded composite materials. *IOP Conference Series: Materials Science and Engineering*, *319*, 012046. https://doi.org/10.1088/1757-899x/319/1/012046

Karami, K., Blok, A., Weber, L., Ahmadi, S. M., Petrov, R., Nikolic, K., Borisov, E. V., Leeflang, S., Ayas, C., Zadpoor, A. A., Mehdipour, M., Reinton, E., & Popovich, V. A. (2020). Continuous and pulsed selective laser melting of $Ti_6Al_4V$ lattice structures: Effect of post-processing on microstructural anisotropy and fatigue behaviour. *Additive Manufacturing*, *36*, 101433. https://doi.org/10.1016/j.addma.2020.101433

Katz-Demyanetz, A., Popov, V. V., Kovalevsky, A., Safranchik, D., & Koptyug, A. (2019). Powder-bed additive manufacturing for aerospace application: Techniques, metallic and metal/ceramic composite materials and trends. *Manufacturing Review*, *6*, 5. https://doi.org/10.1051/mfreview/2019003

Keller, C., Tabalaiev, K., Marnier, G., Noudem, J., Sauvage, X., & Hug, E. (2016). Influence of spark plasma sintering conditions on the sintering and functional properties of an ultra-fine grained 316L stainless steel obtained from ball-milled powder. *Materials Science and Engineering: A*, *665*, 125–134. https://doi.org/10.1016/j.msea.2016.04.039

Kennedy, K. (2002). The Vernacular of Space Architecture. *AIAA Space Architecture Symposium*. https://doi.org/10.2514/6.2002-6102

Khoshnevis, B., Bodiford, M., Burks, K., Ethridge, E., Tucker, D., Kim, W., Toutanji, H., & Fiske, M. (2005). Lunar Contour Crafting - A Novel Technique for ISRU-Based Habitat Development. *43rd AIAA Aerospace Sciences Meeting and Exhibit*. https://doi.org/10.2514/6.2005-538

Kim, B.-H., & Na, Y.-H. (1995). Fabrication of fiber-reinforced porous ceramics of Al2O3-mullite and SiC-mullite systems. *Ceramics International*, *21*(6), 381–384. https://doi.org/10.1016/0272-8842(95)94461-i

Labeaga-Martínez, N., Sanjurjo-Rivo, M., Díaz-Álvarez, J., & Martínez-Frías, J. (2017). Additive manufacturing for a Moon village. *Procedia Manufacturing*, *13*, 794–801. https://doi.org/10.1016/j.promfg.2017.09.186

Landis, G. A. (2007). Materials refining on the Moon. *Acta Astronautica*, *60*(10–11), 906–915. https://doi.org/10.1016/j.actaastro.2006.11.004

Liu, M., Tang, W., Duan, W., Li, S., Dou, R., Wang, G., Liu, B., & Wang, L. (2019). Digital light processing of lunar regolith structures with high mechanical properties. *Ceramics International*, *45*(5), 5829–5836. https://doi.org/10.1016/j.ceramint.2018.12.049

Long, Y., Zhang, H., Wang, T., Huang, X., Li, Y., Wu, J., & Chen, H. (2013). High-strength Ti–6Al–4V with ultrafine-grained structure fabricated by high energy ball milling and spark plasma sintering. *Materials Science and Engineering: A*, *585*, 408–414. https://doi.org/10.1016/j.msea.2013.07.078

Manick, K., Gill, S.-J., Rumsey, M. S., Smith, C. L., Duvet, L., Miller, C. G., & Jones, C. (2018, March). *The European Space Agency Exploration Sample Analogue Collection (Esa2c) And Curation Facility – Present And Future* [Paper presentation]. 49th Lunar and Planetary Science Conference, The Woodlands, Texas.

Marnier, G., Keller, C., Noudem, J., & Hug, E. (2014). Functional properties of a spark plasma sintered ultrafine-grained 316L steel. *Materials & Design*, *63*, 633–640. https://doi.org/10.1016/j.matdes.2014.06.053

Maseko, S. W., Popoola, A. P. I., & Fayomi, O. S. I. (2018). Characterization of ceramic reinforced titanium matrix composites fabricated by spark plasma sintering for anti-ballistic applications. *Defence Technology*, *14*(5), 408–411. https://doi.org/10.1016/j.dt.2018.04.013

Mertens, A. I., Reginster, S., Paydas, H., Contrepois, Q., Dormal, T., Lemaire, O., & Lecomte-Beckers, J. (2014). Mechanical properties of alloy Ti–6Al–4V and of stainless steel 316L processed by selective laser melting: influence of out-of-equilibrium microstructures. *Powder Metallurgy*, *57*(3), 184–189. https://doi.org/10.1179/1743290114y.0000000092

Meurisse, A., Beltzung, J. C., Kolbe, M., Cowley, A., & Sperl, M. (2017). Influence of Mineral Composition on Sintering Lunar Regolith. *Journal of Aerospace Engineering*, *30*(4), 04017014. https://doi.org/10.1061/(asce)as.1943-5525.0000721

Meurisse, A., Makaya, A., Willsch, C., & Sperl, M. (2018). Solar 3D printing of lunar regolith. *Acta Astronautica*, *152*, 800–810. https://doi.org/10.1016/j.actaastro.2018.06.063

Mueller, S., Taylor, G. J., & Phillips, R. J. (1988). Lunar composition: A geophysical and petrological synthesis. *Journal of Geophysical Research*, *93*(B6). https://doi.org/10.1029/jb093ib06p06338

Munir, Z. A., Anselmi-Tamburini, U., & Ohyanagi, M. (2006). The effect of electric field and pressure on the synthesis and consolidation of materials: A review of the spark plasma sintering method. *Journal of Materials Science*, *41*(3), 763–777. https://doi.org/10.1007/s10853-006-6555-2

Naser, M. Z., & Chehab, A. I. (2018). Materials and design concepts for space-resilient structures. *Progress in Aerospace Sciences*, *98*, 74–90. https://doi.org/10.1016/j.paerosci.2018.03.004

Neves, J. M., Ramanathan, S., Suraneni, P., Grugel, R., & Radlińska, A. (2020). Characterization, mechanical properties, and microstructural development of lunar regolith simulant-portland cement blended mixtures. *Construction and Building Materials*, *258*, 120315. https://doi.org/10.1016/j.conbuildmat.2020.120315

Obadele, B. A., Adesina, O. S., Oladijo, O. P., & Ogunmuyiwa, E. N. (2020). Fabrication of functionally graded 316L austenitic and 2205 duplex stainless steels by spark plasma sintering. *Journal of Alloys and Compounds*, *849*, 156697. https://doi.org/10.1016/j.jallcom.2020.156697

Papike, J. J., Simon, S. B., & Laul, J. C. (1982). The lunar regolith: Chemistry, mineralogy, and petrology. *Reviews of Geophysics*, *20*(4), 761. https://doi.org/10.1029/rg020i004p00761

Pieters, C. M. (1986). Composition of the lunar highland crust from near-infrared spectroscopy. *Reviews of Geophysics*, *24*(3). https://doi.org/10.1029/rg024i003p00557

Pilehvar, S., Arnhof, M., Pamies, R., Valentini, L., & Kjøniksen, A. L. (2020). Utilization of urea as an accessible superplasticizer on the moon for lunar geopolymer mixtures. *Journal of Cleaner Production*, *247*, 119177. https://doi.org/10.1016/j.jclepro.2019.119177

Poondla, N., Srivatsan, T. S., Patnaik, A., & Petraroli, M. (2009). A study of the microstructure and hardness of two titanium alloys: Commercially pure and Ti–6Al–4V. *Journal of Alloys and Compounds*, *486*(1–2), 162–167. https://doi.org/10.1016/j.jallcom.2009.06.172

Popovich, V. A., Borisov, E. V., Heurtebise, V., Riemslag, T., Popovich, A. A., & Sufiiarov, V. S. (2018). Creep and Thermomechanical Fatigue of Functionally Graded Inconel 718 Produced by Additive Manufacturing. *TMS 2018 147th Annual Meeting & Exhibition Supplemental Proceedings*, 85–97. https://doi.org/10.1007/978-3-319-72526-0_9

Prettyman, T. H., Hagerty, J. J., Elphic, R. C., Feldman, W. C., Lawrence, D. J., McKinney, G. W., & Vaniman, D. T. (2006). Elemental composition of the lunar surface: Analysis of gamma ray spectroscopy data from Lunar Prospector. *Journal of Geophysical Research: Planets*, *111*(E12). https://doi.org/10.1029/2005je002656

Radhamani, A. V., Lau, H. C., Kamaraj, M., & Ramakrishna, S. (2020). Structural, mechanical and tribological investigations of CNT-316 stainless steel nanocomposites processed via spark plasma sintering. *Tribology International*, *152*, 106524. https://doi.org/10.1016/j.triboint.2020.106524

Rajan, T. P. D., & Pai, B. C. (2014). Developments in Processing of Functionally Gradient Metals and Metal–Ceramic Composites: A Review. *Acta Metallurgica Sinica (English Letters)*, *27*(5), 825–838. https://doi.org/10.1007/s40195-014-0142-3

Rattanachan, S., Miyashita, Y., & Mutoh, Y. (2003). Microstructure and fracture toughness of a spark plasma sintered Al2O3-based composite with BaTiO3 particulates. *Journal of the European Ceramic Society*, *23*(8), 1269–1276. https://doi.org/10.1016/s0955-2219(02)00294-7

Ray, C. S., Reis, S. T., Sen, S., & O'Dell, J. S. (2010). JSC-1A lunar soil simulant: Characterization, glass formation, and selected glass properties. *Journal of Non-Crystalline Solids*, *356*(44–49), 2369–2374. https://doi.org/10.1016/j.jnoncrysol.2010.04.049

Restivo, T. A. G., Beccari, R. F., Padilha, W. R., Durazzo, M., Telles, V. B., Coleti, J., Yamagata, C., Silva, A. C. D., Suzuki, E., Soares Tenório, J. A. S., & Mello-Castanho, S. R. H. (2019). Micrograded ceramic-metal composites. *Journal of the European Ceramic Society*, *39*(12), 3484–3490. https://doi.org/10.1016/j.jeurceramsoc.2019.03.018

Ruys, A. J., Popov, E. B., Sun, D., Russell, J. J., & Murray, C. C. J. (2001). Functionally graded electrical/thermal ceramic systems. *Journal of the European Ceramic Society*, *21*(10–11), 2025–2029. https://doi.org/10.1016/s0955-2219(01)00165-0

Sanders, G. B., Romig, K. A., Larson, W. E., Johnson, R., Rapp, D., Johnson, K. R., Sacksteder, K., Linne, D., Curreri, P., Duke, M., Blair, B., Gertsch, L., Boucher, D., Rice, E., Clark, L., McCullough, E., & Zubrin, R. (2005). *Results from the NASA Capability Roadmap Team for In-Situ Resource Utilization (ISRU)*. International Lunar Conference.

Schleppi, J., Gibbons, J., Groetsch, A., Buckman, J., Cowley, A., & Bennett, N. (2018). Manufacture of glass and mirrors from lunar regolith simulant. *Journal of Materials Science*, *54*(5), 3726–3747. https://doi.org/10.1007/s10853-018-3101-y

Shiwei, N., Dritsas, S., & Fernandez, J. G. (2020). Martian biolith: A bioinspired regolith composite for closed-loop extraterrestrial manufacturing. *PLOS ONE*, *15*(9), e0238606. https://doi.org/10.1371/journal.pone.0238606

Sibille, L., Carpenter, P., Systems, B., Schlagheck, R., & French, R. A. (2006, September). *Lunar Regolith Simulant Materials: Recommendations for Standardization, Production, and Usage* (NASA/TP—2006-214605). George C. Marshall Space Flight Center.

Srivastava, M., Rathee, S., Maheshwari, S., & Kundra, T. K. (2019). Design and processing of functionally graded material: review and current status of research. In L. Kumar, P. Pandey, & D. Wimpenny (Eds.), *3D Printing and additive manufacturing technologies* (pp. 243–255). Springer, Singapore

Suresh, S., & Mortensen, A. (1997). Functionally graded metals and metal-ceramic composites: Part 2 Thermomechanical behaviour. *International Materials Reviews*, *42*(3), 85–116. https://doi.org/10.1179/imr.1997.42.3.85

Taylor, S. R. (1987). The unique lunar composition and its bearing on the origin of the Moon. *Geochimica et Cosmochimica Acta*, *51*(5). https://doi.org/10.1016/0016-7037(87)90220-1

Tokita, M. (2003). Large-Size-WC/Co Functionally Graded Materials Fabricated by Spark Plasma Sintering (SPS) Method. *Materials Science Forum*, *423–425*, 39–44. https://doi.org/10.4028/www.scientific.net/msf.423-425.39

Vaniman, D., Reedy, R., Heiken, G., Olhoeft, G., & Mendell, W. (1991). The Lunar Environment. In G.H. Heiken, D.T. Vaniman, & B.M. French (Eds.), *Lunar Sourcebook: A User's Guide to the Moon*, Cambridge University Press, Cambridge, (pp. 27–60).

Wright, J. K., Evans, J. R. G., & Edirisinghe, M. J. (1989). Degradation of Polyolefin Blends Used for Ceramic Injection Molding. *Journal of the American Ceramic Society*, *72*(10), 1822–1828. https://doi.org/10.1111/j.1151-2916.1989.tb05985.x

Yakout, M., Elbestawi, M. A., & Veldhuis, S. C. (2020). A study of the relationship between thermal expansion and residual stresses in selective laser melting of Ti-6Al-4V. *Journal of Manufacturing Processes*, *52*, 181–192. https://doi.org/10.1016/j.jmapro.2020.01.039

Zhang, C., Chen, F., Huang, Z., Jia, M., Chen, G., Ye, Y., Lin, Y., Liu, W., Chen, B., Shen, Q., Zhang, L., & Lavernia, E. J. (2019). Additive manufacturing of functionally graded materials: A review. *Materials Science and Engineering: A*, *764*, 138209. https://doi.org/10.1016/j.msea.2019.138209

Zhang, X., Chen, Y., & Hu, J. (2018). Recent advances in the development of aerospace materials. *Progress in Aerospace Sciences*, *97*, 22–34. https://doi.org/10.1016/j.paerosci.2018.01.001

Zhang, X., Gholami, S., Khedmati, M., Cui, B., Kim, Y.-R., Kim, Y.-J., Shin, H.-S., & Lee, J. (2021). Spark plasma sintering of a lunar regolith simulant: effects of parameters on microstructure evolution, phase transformation, and mechanical properties. *Ceramics International*, *47*(4), 5209–5220. https://doi.org/10.1016/j.ceramint.2020.10.100

Zhang, X., Khedmati, M., Kim, Y.-R., Shin, H.-S., Lee, J., Kim, Y.-J., & Cui, B. (2019). Microstructure evolution during spark plasma sintering of FJS-1 lunar soil simulant. *Journal of the American Ceramic Society*, *103*(2), 899–911. https://doi.org/10.1111/jace.16808

Zheng, X., Deotte, J., Alonso, M. P., Farquar, G. R., Weisgraber, T. H., Gemberling, S., Lee, H., Fang, N., & Spadaccini, C. M. (2012). Design and optimization of a light-emitting diode projection micro-stereolithography three-dimensional manufacturing system. Review of Scientific Instruments, 83(12), 125001. https://doi.org/10.1063/1.4769050

# Design-to-Robotic-Production of Underground Habitats on Mars

**Henriette Bier** [1,2,3], **Edwin Vermeer** [1], **Arwin Hidding** [1], **Krishna Jani** [1]

[1] *Delft University of Technology*
*Delft, the Netherlands*

[2] *Politecnico di Milano*
*Milan, Italy*

[3] *Anhalt University of Applied Sciences*
*Dessau-Rosslau, Germany*

## Abstract

In order for off-Earth top surface structures built from regolith to protect astronauts from radiation, they need to be several meters thick. Technical University Delft (TUD) proposes to excavate into the ground to create subsurface habitats. By excavating, not only can natural protection from radiation be achieved but also thermal insulation, as the temperature is more stable underground. At the same time, valuable resources can be excavated via in-situ resource utilization (ISRU). In this process, a swarm of autonomous mobile robots excavate the ground in a downwards sloping spiral movement. The excavated regolith will be mixed with cement, which can be produced on Mars through ISRU, in order to create concrete. The concrete is then 3D printed/sprayed onto the excavated tunnel to reinforce it. As soon as the tunnels are reinforced, the material between the tunnels can be removed in order to create a larger cavity that can be used for habitation. The proposed approach relies on design-to-robotic-production (D2RP) technology developed at TUD for on-Earth applications. The rhizomatic 3D-printed structure is a structurally optimized, porous shell structure with increased insulation properties. In order to regulate the indoor pressurised environment, an inflatable structure is placed inside the 3D-printed cavity. This inflatable structure is made of materials that can at some point also be produced on Mars via ISRU. Depending on location, the habitat and the production system are powered by a system combining solar and kite-power. The ultimate goal is to develop an autarkic D2RP system for building subsurface autarkic habitats on Mars from locally-obtained materials.

## Keywords

Data-driven design, robotic production and operation, habitat, renewable energy, autarkic system

## DOI

https://doi.org/10.7480/spool.2021.2.6075

## Introduction

Building habitats on Mars requires the acknowledgement of three interconnected aspects. First, the design-to-robotic-production (D2RP) method developed at Technical University Delft (TUD) for on-Earth applications has to be adapted to Mars conditions. Second, the geology and available materials, the climate and possible hazards and their impact on the D2RP process have to be considered. Third, the limits in terms of mass and volume for interplanetary space travel have to be acknowledged.
Currently, Mars is within reach for interplanetary habitation based on the current and expected level of technology readiness level likely to be reached in the near future. According to previous research, regolith, crushed rock and dust found on Mars can potentially be used as a construction material (inter al. Spiero and Dunand, 1997; Happel, 1993) and regolith constructions can potentially protect astronauts from large amounts of radiation. However, galactic cosmic rays would require a regolith layer several meters thick in order to sufficiently protect the astronauts. Furthermore, thermal stresses that occur f rom large temperature changes during the day night cycle on Mars are a challenge, as is the absence of an atmosphere, which could further increase stresses on the building envelope when creating a pressurized environment.

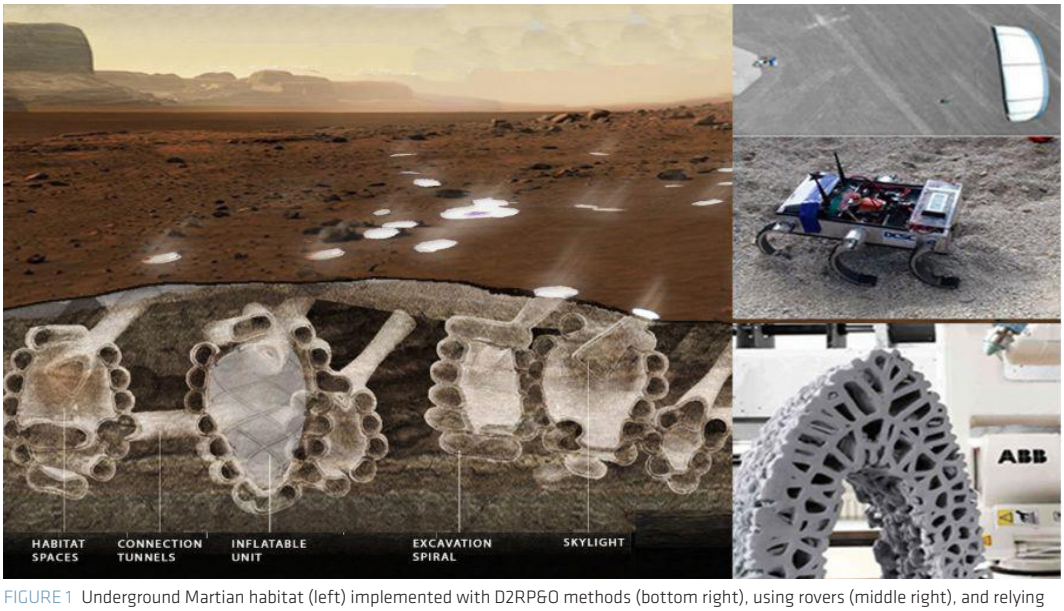


FIGURE 1 Underground Martian habitat (left) implemented with D2RP&O methods (bottom right), using rovers (middle right), and relying on renewable energy generation (top right).

Precedent case studies counteract these challenges in various ways. For instance, (i) the Mars Ice House developed by the National Aeronautics and Space Administration (NASA) uses ice as a main construction material, as it is more effective against radiation than regolith-based construction. Measures are taken to keep the ice from sublimating into the air by relying on inflatable plastics.[1] The Foster and Partners (ii) autonomous habitation sintering approach uses regolith as main construction material. Instead of printing it, they fuse the layers together using an autonomous swarm of robots.[2] And, (iii) Apis Cor's X-House is a 3D-printed habitat that uses Martian concrete reinforced with basalt fibers and expandable polyethylene

1 https://www.nasa.gov/feature/langley/a-new-home-on-mars-nasa-langley-s-icy-concept-for-living-on-the-red-planet

2 https://www.fosterandpartners.com/projects/lunar-habitation/

foam.[3] Furthermore, (iv) AI Space Factory's MARSHA is a 3D-printed habitat using a biopolymer basalt composite material for 3D printing, which is effective against stress and, to some degree, against radiation as the material has a high hydrogen concentration[4].
All these examples are NASA 3D-printed habitat proposals and all of them are meant for the surface. The TUD team sees an opportunity to investigate possibilities for autonomous robots to drill into and/or excavate off-Earth and to 3D print/spray a subsurface habitat, while also considering the restraints of interplanetary travel. The main idea is to develop a D2RP method that facilitates excavation and 3D printing in order to produce subsurface habitats. Subsurface habitation has the advantage of natural protection from radiation while also being less affected by thermal stresses because the temperature is more stable underground. At the same time, excavation involves mining valuable resources for in-situ resource utilization (ISRU). Design methodologies are, however, restricted by the method of production and the materials available. The use of locally-obtained materials via excavation and the naturally-obtained shelter represent the advantages over other design proposals.

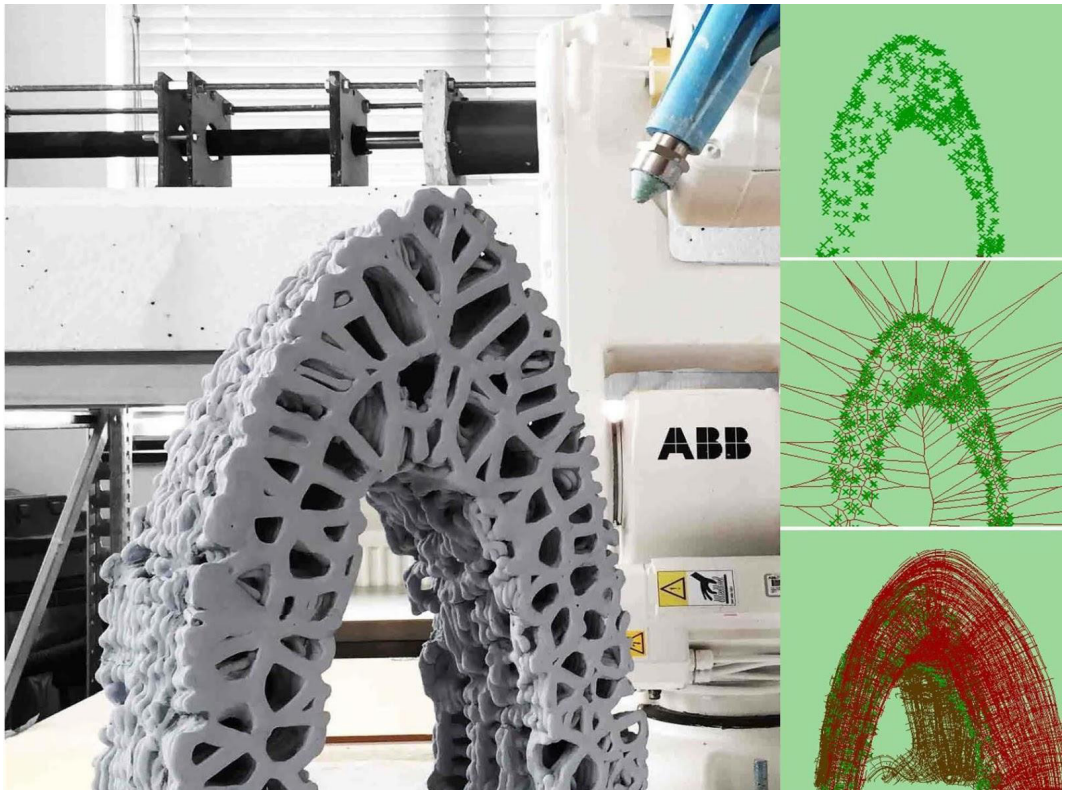


FIGURE 2 Additive D2RP using ceramic clay and relying on structural analysis, and robotic path optimisation.

The idea developed by the TUD team for the Open Space Innovation Campaign's 'Off-Earth Manufacturing and Construction' competition, which was put forward by the European Space Agency (ESA), involves autonomous mobile robots that will excavate the ground in a downwards sloping spiral movement. Initially, the idea was that the excavated regolith would be mixed with liquid sulphur to create concrete, which

3 http://www.spacexarch.com

4 https://www.aispacefactory.com/marsha

would then be used by the 3D printing/spraying rovers to stabilize the excavated tunnels. Now, the team rather proposes using cement-based concrete because of the extensive experience in using this material for on-Earth habitats as well as the available expertise and technology of the industry partner, Vertico. While cement can be produced on Mars, infrastructure for producing it needs to be in place. This implies that the structure would be built at a later stage of colonisation with the excavated tunnels first being stabilized using shotcrete. This would allow, in a second step, for removal of the material in between the tunnels and the creation of a larger cavity that could be used for habitation.

## Description

This idea proposes adapting several technologies developed for on-Earth application to off-Earth conditions. This paper focuses on the architecture-related aspects and in particular on the data-driven design-to-robotic production and operation (D2RP&O) processes.

**1. Data-driven D2RP** integrates advanced computational design with robotic techniques in order to produce architectural formations by directly linking design to building production (Bier et al. 2018). The overall design of the habitat relies on data-driven simulations of the underground rhizomatic structure (figure 1). In collaboration with experts from Civil Engineering and Geosciences (CEG), TUD, , suitable locations for excavation will be identified by analysing the composition of the terrain. The first case study is for a 60-80 $m^2$ habitat that can be extended over time.

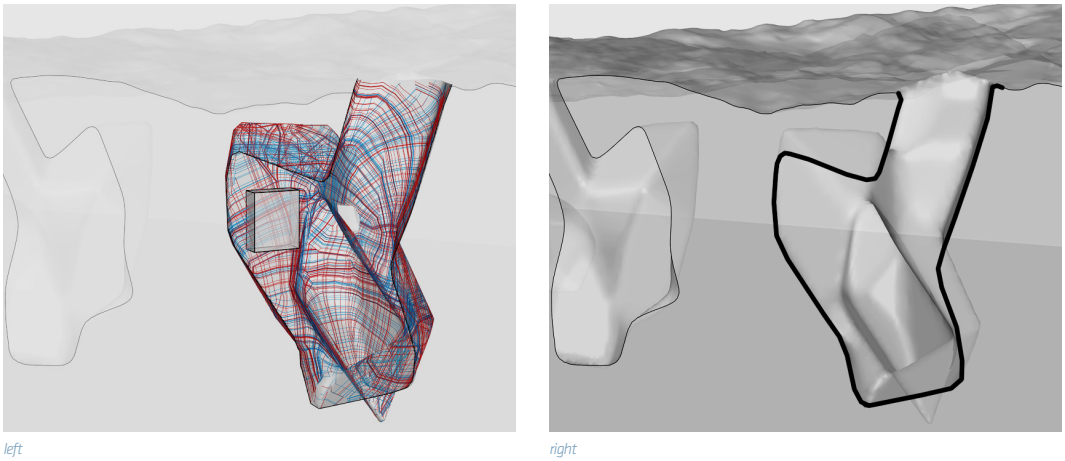

*left* *right*

FIGURE 3 Section through underground structure (right) and structural analysis with a fragment chosen for further development (left).

Subtractive and additive D2RP will be employed in the following sequence:

**1.1 Subtractive D2RP** involving excavation following a regular mining approach developed at CEG is proposed. Excavation is to be implemented with rovers similar to the ones developed at TUD[5] in a controlled downwards spiral movement (figure 1). D2RP involving milling, drilling, cutting as explored at the Robotic

5 https://tudelftroboticsinstitute.nl/robots/zebro or https://www.delftsepost.nl/nieuws/algemeen/772027/tu-delft-studenten-bouw-en-aan-eerste-nederlandse-maanrover

Building (RB), TUD[6] will be employed at the later stages of construction when the interior architecture of the habitats is created.

**1.2 Additive D2RP** as explored in the RB lab with ceramic clay[7] (figure 2) and thermoplastic elastomers (TPE)[8] represents the basis for the AM approach with regolith that is proposed in this project. Furthermore, the industrial partner, Vertico, has expertise in robotic 3D printing with concrete. The idea is to connect the printing/spraying system to a swarm of rovers. The assumption is that this will generate a structurally optimized porous structure with increased insulation properties (figure 2) and requiring less material and printing time.
Both additive and subtractive D2RP will be powered by the airborne energy[9] system combined with solar cells[10] (Vargas et al., 2021). In order for the built structures to be habitable, environmental control, life support, and energy requirements need to be considered.

**2. Data-driven D2RO** links the design to building operation (*inter al.* Bier et al. 2018). It takes sensor-actuator systems into account that are required for environmental control and life-support. The system supplies air, water and food and relies on filtration systems for human waste disposal and air production requiring an average power for a habitat on Mars of 1600 W for a crew of 6 people (Santovincenzo, 2004). Water needs to be stored, used, and reclaimed (from wastewater), although Mars missions may also utilise water from the atmosphere or ice deposits. Oxygen comes from electrolysis, which uses electricity from solar panels or kite-power to split water into hydrogen gas and oxygen gas. Temperature regulation is achieved using both passive and active systems, which protect from overheating, either by thermal insulation and by heat removal from internal sources (such as the heat emitted by electronic equipment) and protect from cold, by thermal insulation and by heat release from internal sources. Furthermore, shielding against harmful external influences such as radiation and micro-meteorites is necessary. This is achieved by placing the habitat below ground level. In addition, an inflatable structure is proposed to counteract Mars' low atmospheric pressure, which is a threat to human health. The inflatable structure that regulates the indoor pressurised environment is placed within the 3D-printed structure. This inflatable structure requires materials such as neoprene, vectran, kevlar, etc. These materials can also be produced on Mars through ISRU of silicon, which is proven to be available in abundance on Mars.

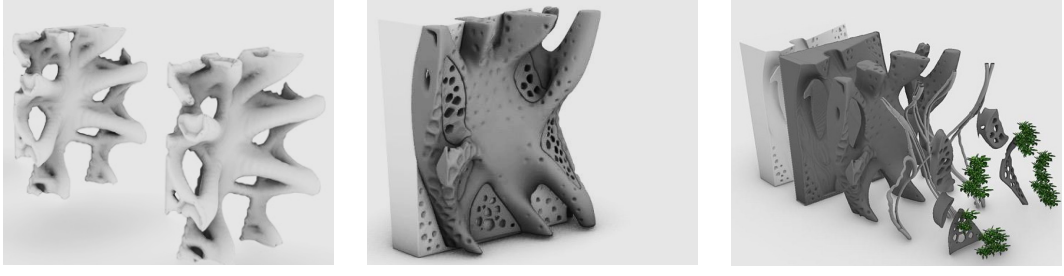

*left* *middle* *right*

FIGURE 4 Structure based on stress lines analysis (left), structural mesh with acoustic optimization pattern (middle), and exploded axonometric view showing excavated layer, 3D-printed/sprayed layer, sensor-actuators, and plant pods layers (right),

6 http://100ybp.roboticbuilding.eu/index.php/WorkshopHvA

7 http://www.roboticbuilding.eu/project/scalable-porosity/

8 http://www.roboticbuilding.eu/project/variable-stiffness/

9 http://www.roboticbuilding.eu/project/kite-powered-d2rp/

10 https://www.tudelft.nl/en/eemcs/the-faculty/departments/electrical-sustainable-energy/photovoltaic-materials-and-devices/

Life support systems could include a plant cultivation system, which could also replenish water and oxygen. Such a system could reuse nutrients via waste composting, which is then used to fertilize crops.

Research results of the Micro-Ecological Life Support System Alternative (MELiSSA)[11], which is a ESA-led initiative, aiming to understand the behaviour of artificial ecosystems in order to develop technology for a future regenerative life support system, could be integrated into the proposed project. The life-support system is, however, not discussed in this paper in more detail.

**Energy generation** by means of solar panels and airborne wind energy is considered as described by Vargas, et al. (2021) and is not discussed in this paper. Instead, the plant cultivation system is shortly addressed.

## Case study

The proposed idea has been tested in a case study by means of D2RP&O, which involved the development of a 1:1 scale prototype as a proof of concept for habitat envelope components that facilitate cultivation of plants. The structure is analysed for structural stresses and the output result is derived in the form of tension and compression lines (figure 3). A 1-meter by 1-meter fragment of the envelope is selected for further development. The fragment is developed considering structural loads and the result is topologically optimized (figure 4). This structural mesh is designed based on the results of the analysis and sensor-actuators that enable and regulate plant growth are integrated within it.

The underground is excavated and is reinforced with concrete. The milled and reinforced surface serves a dual purpose; it supports the cave-like structure and also has acoustical properties generated by surface tectonics (figures 4 and 5). The structural mesh is sprayed and/or 3D printed. The sensors and wires are integrated, while detachable 'plant pods' are overlaid on the structural mesh (figure 5). The detachability is for ease of maintenance. A selection of plants such as lettuce, basil, mint, dill, rosemary, thyme, and soybeans was identified in dialogue with the University of Wageningen (Wamelink et al., 2014).

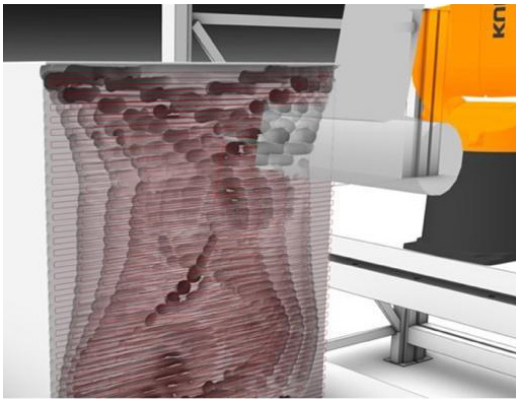

*left*

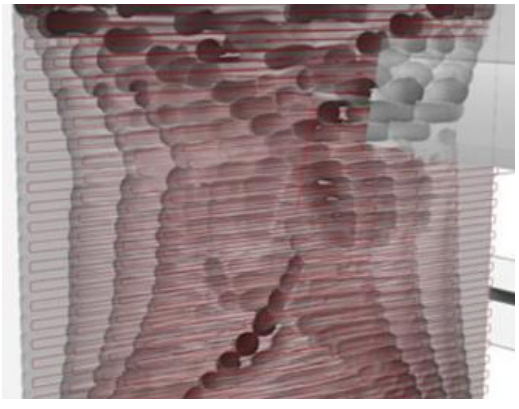

*right*

FIGURE 5 Simulated toolpaths for subtractive D2RP.

11 https://www.esa.int/Enabling_Support/Space_Engineering_Technology/MELiSSA_life_support_project_an_innovation_network_in_support_to_space_exploration

The robotic production was digitally simulated to optimize the robotic path and the first tests were implemented by milling expanded polystyrene (EPS) and 3D printing with fibre-reinforced TPE. The aim was to emulate the process that is to be implemented on Mars. The tests identified that it is necessary to adjust the surface tectonics because the material deposition during printing introduced a considerable flattening of the acoustic patterns. In the next step, prototyping will be implemented with improved patterns and with commercially available regolith simulants and cement. The 3D-printed porous structure will then be compared with a non-porous structure in order to identify differences in structural and insulation properties.

## Conclusion

The presented project investigates possibilities to develop Martian subsurface habitats while also considering the constraints of interplanetary travel. The paper presents the overall framework within which such an approach could be implemented and discusses a case study that describes the subtractive and additive D2RP approach. While digital prototyping has been successfully implemented, the physical robotic prototyping is still a work in progress.

### Acknowledgements:

This paper has profited from the contribution of teams from the faculties of Aerospace Engineering, Maritime, Material, and Mechanical Engineering, Civil Engineering, and Architecture. Furthermore, it has profited from the contribution of Wieger Wamelink from the University of Wageningen and Advenit Makaya from ESA.

## References


Bier, H., Liu Cheng, A., Mostafavi, S., Anton, A., & Bodea, S. (2018). Robotic Building as Integration of Design-to-Robotic-Production and -Operation. In H. Bier (Ed.), Robotic Building (pp. 97–120). Springer International Publishing. https://doi.org/10.1007/978-3-319-70866-9_5

Happel, J. A. (1993). Indigenous Materials for Lunar Construction. Applied Mechanics Reviews, 46(6), 313–325. https://doi.org/10.1115/1.3120360

Khoshnevis, B., Yuan, X., Zahiri, B., Zhang, J., & Xia, B. (2016). Construction by Contour Crafting using sulfur concrete with planetary applications. Rapid Prototyping Journal, 22(5), 848–856. https://doi.org/10.1108/RPJ-11-2015-0165

Kootstra, G., Bender, A., Perez, T., & van Henten, E. J. (2020). Robotics in Agriculture. In M. H. Ang, O. Khatib, & B. Siciliano (Eds.), Encyclopedia of Robotics (pp. 1–19). Springer Berlin Heidelberg. https://doi.org/10.1007/978-3-642-41610-1_43-1

Santovincenzo, A. (2004). CDF Study Report Human Missions to Mars Overall Architecture Assessment [ESA Technical Report CDF-20(A),]. http://emits.sso.esa.int/emits-doc/1-5200-RD20-HMM_Technical_Report_Final_Version.pdf

Spiero, F., & Dunand, D. (1997). Simulation of Martian Materials and Resources Exploitation on a Variable Gravity Research Facility. In T. Meyer (Ed.), The Case for Mars IV: The International Exploration of Mars—Consideration for Sending Humans, Proceedings of the fourth Case for Mars Conference, Univelt for the American Astronautical Society (p. 356).

Wamelink, G. W. W., Frissel, J. Y., Krijnen, W. H. J., Verwoert, M. R., & Goedhart, P. W. (2014). Can Plants Grow on Mars and the Moon: A Growth Experiment on Mars and Moon Soil Simulants. PLoS ONE, 9(8), e103138. https://doi.org/10.1371/journal.pone.0103138

Wan, L., Wendner, R., & Cusatis, G. (2016). A novel material for in situ construction on Mars: Experiments and numerical simulations. Construction and Building Materials, 120, 222–231. https://doi.org/10.1016/j.conbuildmat.2016.05.046

# Learning lessons from Earth and Space towards Sustainable Multi-planetary Design

**Marina Konstantatou** [1], **Miriam Dall'Igna** [1], **Samuel Wilkinson** [1], **Irene Gallou** [1], **Daniel Piker** [1]

[1] *Foster + Partners*
*London, United Kingdom*

## Abstract

Off-Earth structural design has been a subject of fascination and research for decades. Given that the vision of permanent lunar and Martian human presence is materialising, it is an opportune moment to reflect on the future applicability and challenges of off-Earth design. This article investigates contemporary thinking about off-Earth structural design – specifically focused on large-scale infrastructure such as habitats – and assesses it in terms of its sustainability. We suggest that the extra-terrestrial setting, which is characterised by resource, construction, and labour constraints, is to be analysed as an extreme case of the built environment on Earth. Subsequently, we propose that structural design methodologies originating on Earth can benefit both the off-Earth context, through their inherent material efficiency and use of local materials, and the on-Earth context, where unsustainable growth and material inefficiency dominate our built environment. As our planet rapidly heads towards a scarcity of construction materials and disruptive environmental change, what sustainability lessons can we learn from our past, and how can we apply these to extra-terrestrial construction? Finally, how can we use these lessons to futureproof our built environment?

## Keywords

Off-Earth Design, Space Architecture, In-Situ Resource Utilisation (ISRU), Material Efficiency, Reusability, Sustainability, Form-Finding, Structural Design

## DOI

https://doi.org/10.7480/spool.2021.2.5431

## Context

As public and private international initiatives to construct a permanent presence on the lunar surface come closer to reality, so too do the challenges faced by construction here on Earth. Specifically, material scarcity, climate change, and loss of biodiversity are beginning to impact our well-being and society.

In this paper we give an overview of contemporary engineering and design approaches for extra-terrestrial habitations, comparing them with pre-industrial vernacular and contemporary terrestrial structural design approaches. By identifying the similarities, lessons learnt from one can be applied to the other; for instance, in terms of material efficiency, use of local materials, and construction approaches.

Current thinking would position off-world construction as a largely separate field to conventional construction practice, rather than as an extreme example of it. In drawing the two domains closer together, we aim to create more of a bi-directional relationship, where off-Earth construction acts as a catalyst for change here, and on-Earth structures as a precedent for lunar and Martian construction.

### Off-Earth structures

In this paper, we will use a broad definition of off-Earth construction, including any enabling infrastructure, such as berms, landing pads, roads, and habitation. Assuming a phased approach with increasing complexity of habitations over time, we can distinguish five classes of off-Earth construction: Class I are single prefabricated pressurised modules, such as the Apollo lunar lander; Class II are multiple such modules connected together on the surface; and Class III combines multiple modules plus structures built from in-situ materials (Howe et al., 2013). Extending this, Class IV would be constructed solely from local materials, and in Class V the construction machines would themselves be fabricated in-situ (Wilkinson et al., 2016a). Our focus here is on Class III, using in-situ resources for construction of heavy-weight infrastructure, such as a regolith shield.

For protection from radiation over extended periods, the construction of a regolith shield is a logical alternative to transporting heavy shielding from Earth. Other in-situ resource utilisation (ISRU) radiation protection options exist, such as water or extracted metals, which may provide a thinner structure, yet regolith is abundant and easily collected, and therefore assumed to be a principal construction material at the outset. A shield built from surface regolith has many advantages: protection from cosmic radiation, solar flares, dust storms, micro-meteorites, and temperature variations, as well as increasing the durability of the habitat modules within (Mueller et al., 2016).

### On-Earth structures

In contrast to its off-Earth counterpart, on-Earth construction has evolved over the course of human history, from caves to primitive forms of shelter – in ancient vernacular periods – to the contemporary technological advances in computational methods for form-finding, topological optimisation, and automation in fabrication and construction.

Over the years, humanity has collectively built a vocabulary of infrastructures using diverse techniques and materials to withstand the test of time in different climatic environments (Oliver, 1997). From monolithic to component-based structures, natural and synthetic materials, we have a long history of on-site physical experimentation to learn from. In addition, with the advent of and advances in computation, we can now simulate structures in-silico with sophisticated methods. These enable us to input the physical properties of materials, forces, and environmental conditions to produce reliable and ever more precise predictions of structural behaviour and form. Furthermore, these can be combined with fabrication and construction automation techniques which have become feasible through the development of industrial, or bespoke, robotic and machinery systems. As a result, we have never been in a better position to simulate the behaviour and engineer the construction of off-Earth structures by adapting the vernacular and contemporary methods widely used on Earth.

## Societal and environmental

Automotive, aerospace, and defence industries tend to push technological development by operating in the context of extreme cases and environments. Technologies developed for these industries can find applications in the most diverse sectors such as health, energy, environment, education, mobility, information technology, and commerce. However, in some cases these applications are identified as by-products. If we take the reciprocal nature of off- and on-Earth construction research into account from the start, we might be able to increase the range and societal impact of extra-terrestrial construction.

In the contemporary era, it is widely accepted that on-Earth construction faces many challenges. One urgent demand relates to our environment. As our resources head swiftly towards scarcity, the architectural, engineering, and construction industries are more actively considering circularity and material lifecycles (De Wolf et al., 2020) as a paramount constraint to preserve life as we know it on our planet.

Off-earth, supply redundancy rather than circularity has so far driven human exploration missions (Owens et al., 2017; Owens and DeWeck, 2016). At the same time, due to scarcity of resources and economical constraints intrinsic to human exploration of space, longer presences in hostile environments could benefit from the circularity paradigm. Specifically, the circularity of resources is an emerging topic of future sustainable human exploration, as it relates to the survival and preservation of the human and machine presence in space. For example, ESA astronaut Alexander Gerst recently installed the ESA's advanced closed loop system (2019) on the ISS. It produces water from carbon dioxide, which in turn is used to produce oxygen. Other related emerging fields are the lifecycles and reusability of structural infrastructure. These are also particularly relevant for Earth, where material waste and inefficiencies in the construction industry are linked to a lack of integrated end-of-life strategies (Brütting et al., 2019). Construction materials have traditionally been seen as essentially infinite and of low value when compared with other industries, leading to little emphasis on significant efficiency savings. Another challenge is the high embodied energy of materials such as cement, aluminium, steel, fixtures, and fittings – all multiplied by the massive quantities used and wasted annually. Advances in space research with regards to ISRU, manufacturing, recycling and even regenerative life support systems (Häder et al., 2018) can inform, if not be integrated, with advances in terrestrial construction processes in the future.

## Research questions & statement

Given the extreme extra-terrestrial construction conditions – i.e., scarcity of processed structural materials, imports from Earth, machinery, and labour – the architectural and structural design of off-Earth infrastructure will have to be dictated by what is feasible in terms of available material properties and construction methods. This contrasts with the contemporarily prevalent form-centric architectural vision in terrestrial architecture developed often in isolation from structural performance and material considerations.

The off-Earth context is akin to the one that dominated our architectural and construction history for millennia, in which the resulting form of dwellings, landmarks, and infrastructure was largely dictated by the availability and properties of local construction materials accessible to the various civilisations and cultures. For example, the shape of gothic cathedrals is directly related to, and an outcome of, the material properties of masonry and the geometries that can be in structural equilibrium within it (Heyman, 1995). It should be noted that at the time, these shapes were a result of trial and error over long spans of time without their creators necessarily being conscious of their unique geometrical and mechanical properties. In the contemporary context, these have been deciphered, researched, and developed into methodologies that can result in materially efficient structures by taking into consideration the structural performance in the early design phase. This field of research is broadly known today as form-finding.

This innovative subject is thus closely related to traditional vernacular construction and, due to its intrinsic characteristics, can benefit both on-Earth and off-Earth design and construction. In this context we pose the following two research statements.

Firstly, extra-terrestrial structures and architectural visions proposed in the literature primarily focus on continuous monolithic structures, yet their discrete counterparts – as observed on Earth – could have comparative advantages, which may make them more appropriate or robust for early lunar infrastructure.

Such possible advantages include:

- Reusability – if the constituting modules can be recycled for the construction of multiple infrastructure projects, the structural material and subsequent energy spent on constructing them corresponds to multiple uses rather than a single one.

- End-of-life behaviour – if the structures can be fully disassembled and the site left in its initial state after the infrastructure is decommissioned, the phenomenon of empty and abandoned structures, similar to the accumulated space junk currently orbiting the Earth, can be avoided.

- Constructability and repair – if the modules can be fabricated, and repaired, individually using regolith processing methods, component-based structures could minimise their embodied energy and maximise their lifespan through component repair or replacement within the structure.

- Lastly, given possible seismic activity, such as moonquakes, a comparison of the seismic performance of continuous and discrete-element structures would be an additional element of a holistic design for the off-Earth environment. For example, such a study should assess deformation demands imposed by the moonquakes on the structures, to prevent the formation of cracks that could hinder structural durability, safety, and serviceability.

Secondly, whilst we can apply terrestrial structural techniques to other worlds, we can also use advances from extra-terrestrial structures to inform contemporary terrestrial ones. Even though there is a rich history

of vernacular component-based architecture and construction on Earth, and of contemporary form-finding, which is increasingly applied to architectural and engineering design, our built environment is predominantly characterised by material inefficiency and a lack of recyclability, as described above.

This can be attributed to the fact that today's capabilities have changed dramatically. In other words, we build inefficient structures because we can afford to – the progress of structural materials and the construction processes at our disposal allow us to detach design from performance, at least at the early stages, and imagine the form in isolation knowing that it is probably possible to construct it somehow. The materially-efficient structures observed throughout our vernacular and masonry construction heritage were directly related to an abundance of constraints which are largely obsolete today. In this context, we can observe how the extra-terrestrial built environment is an extreme, and heavily constrained, case of our present situation, and, remarkably, a very similar case to our past.

Characteristics such as material efficiency and reusability are a necessity when it comes to research and development on the design and construction of permanent extra-terrestrial outposts. This developing body of knowledge can be enriched by our past and, in turn, inform our future, with a focus on energy and waste minimisation in conjunction with maximising material efficiency.

## Literature review

### On-Earth, component-based, design and construction systems

Over the last few millennia, numerous vernacular design and construction methods have been developed by using predominantly local resources (ISRU) and following structurally efficient geometries as a result of trial-and-error processes.

Many of these methods are based on component-based systems comprising bricks, structural tiles, masonry elements (voussoirs), or topologically interlocking components. These can be observed throughout several historical periods and geographical areas spanning from the vernacular construction of vaults in sub-Saharan Africa and Persia to the stereotomy methods of Gothic cathedrals (Oliver, 1997; Fitchen, 1981). When it comes to brick-based methods, which require mortar but no, or minimal, scaffolding (Fig. 1b), these can be observed in structures such as: vernacular Nubian and Persian vaults (Wendland, 2004); Brunelleschi's domes in Italy (Paris et al., 2020); and more recently, Guastavino structural tile vaulting techniques (Ochsendorf, 2010). Additionally, stereotomy methods, which involve the cutting of 3-dimensional solids such as masonry into specific shapes that can be fit together to form spatial structures, can be potentially mortar-less and in some cases even scaffold-less. These have been applied to the development of structures such as Gothic cathedrals (Fitchen, 1981) (Fig. 1c), Byzantine vaults (Choisy, 1883), topologically interlocking structures for floor slabs (Fig. 1e) (Frézier, 1738), lighthouses such as the Eddystone lighthouse designed by John Smeaton (Fig. 1d), dry-stone constructions, e.g., the walls of the Maya civilisation, and the characteristic dome-shaped limestone trulli dwellings of the Puglia region in Italy (Fig. 1a) (Todisco et al., 2017).

These methods, being potentially mortar-less and scaffold-less, hold promise for the development of extra-terrestrial structural systems where structural material, scaffolding, and binders are sparse and prohibitively expensive to transport from Earth. What is more, mortar-less, component-based infrastructure has the potential for reuse through a sustainable construct and deconstruct cycle in which one type of infrastructure can be converted to another depending on the ever-changing needs of a growing settlement.

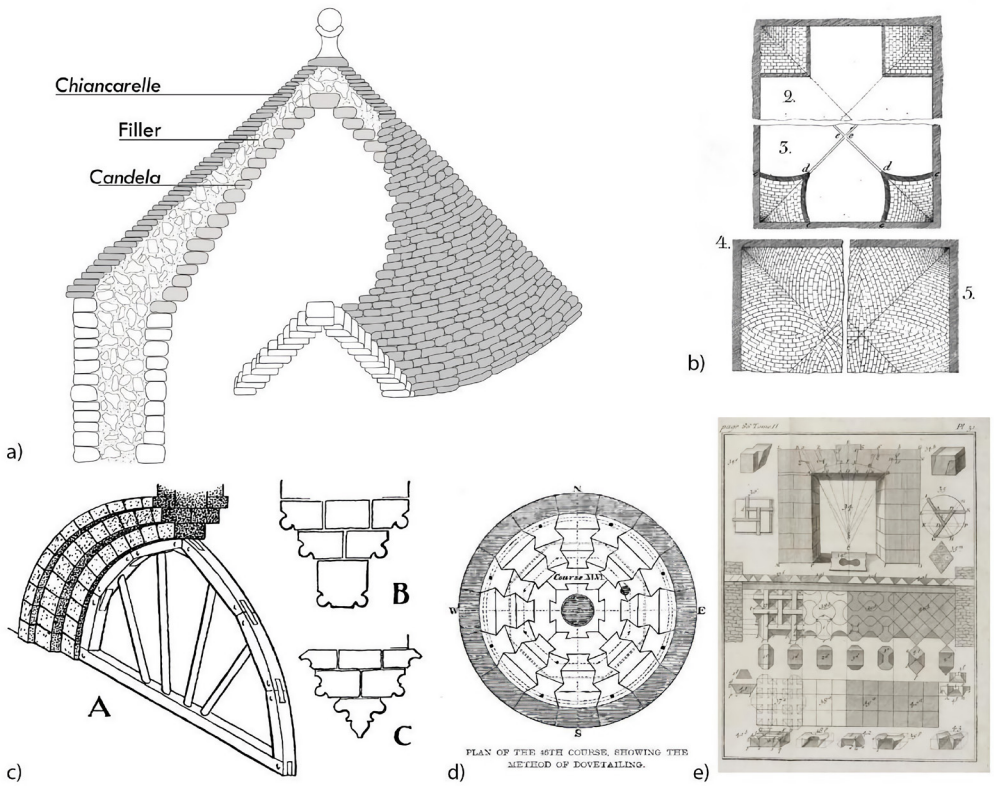


FIGURE 1 a) Dry stone domes as seen in the traditional trulli constructions of Puglia, Italy from Todisco et al. (2017); b) Brick cross vault with self-supporting courses (Wendland, 2004); c) Masonry arch of a Gothic cathedral comprising voussoirs (Fitchen, 1981); d) Masonry lighthouse comprising dovetail interlocking components; e) Flat vaults and floor slabs constructed from interlocking components (Frézier, 1738).

## Form-finding frameworks

Form-finding comprises several different approaches and methods but can be broadly defined as "the forward process in which parameters are explicitly/directly controlled to find an 'optimal' geometry of a structure which is in static equilibrium" (Adrianssens et al., 2014). The earliest – and perhaps most well-known – examples of form-finding are physical models such as chains suspended from two points which result in tension-only structures, and equivalently compression-only arches when inverted (Fig. 2a), similarly 3-dimensional hanging chain models used by Gaudi for the Sagrada Familia form studies (Fig. 2b), 3-dimensional hanging fabric models developed by Heinz Isler for his concrete shell explorations, and soap film structures used by Frei Otto for modelling lightweight tensile structures (Fig. 2c).

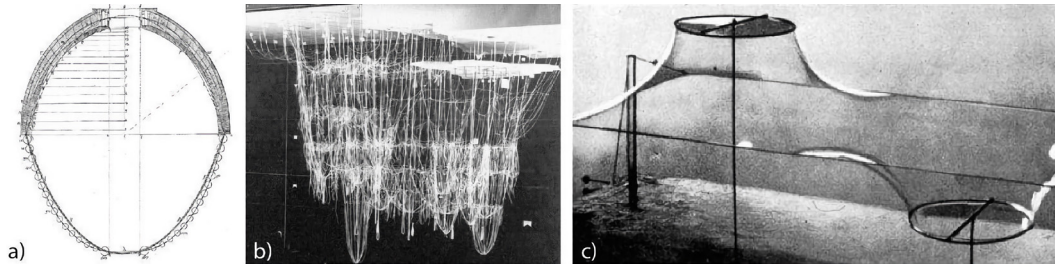


FIGURE 2 a) The geometry of a hanging chain in tension can be used for the safety assessment of masonry structures as depicted here by Poleni (1748) for St. Peter's basilica; b) Spatial hanging chain model used for the form-finding of Sagrada Familia by Gaudi (image credits: Institute for Lightweight Structures, Stuttgart); c) Soap film studies for the form-finding explorations of tensile structures by Frei Otto.

In the realm of contemporary form-finding for structurally efficient geometries, techniques such as dynamic relaxation (Day, 1965) and force density (Schek, 1974) have been proposed. Specifically, by defining parameters such as the boundary conditions and the state of stresses of the structure, it is possible to find the corresponding geometry which is in static equilibrium. As a result, the structural analysis and boundary conditions are the input, and the form is the corresponding output rather than the design preceding the analysis phase. Related examples of application of these methods include the grid-shell of the Great Court Roof of the British Museum (Fig. 3b) which was designed by Foster + Partners and form-found by Chris Williams (Williams, 2001) using dynamic relaxation, and the works of Frei Otto such as the Mannheim grid-shell and the German Pavillion at the 1967 expo in Montreal (Liddell, 2015).

FIGURE 3 The Great Court Roof grid-shell of the British Museum form-found by Chris Williams (image credits: Foster + Partners, Nigel Young).

Component-based structural systems are experiencing a resurgence due to their versatility and lightweight, material efficient nature in conjunction with progress in computer aided design (CAD). When it comes to masonry, the fundamental theory of thrust lines and thrust surfaces has been extensively studied in recent decades, most notably by Heyman (1995). It is experiencing numerous modern-day computational applications through digital stereotomy and robotic manufacturing, which enable the precise design and cutting of the voussoir geometries (Rippmann et al., 2012). Also, research into topologically interlocking components is an active field, specifically their generalisation in doubly-curved spatial structures (Loing et al., 2020). Moreover, academic interest in the subject is reflected in the work of research groups pursuing it and developing prototype structures such as the Armadillo Vault (Block et al., 2017) (Fig. 4a). It was exhibited at the Architectural Venice Biennale in 2016 and comprises robotically-cut, custom made voussoirs which form a shell without the need for mortar. Further example are the long-span shell of the Mapungubwe National Park Interpretive Centre made of structural tiles (Ramage et al., 2009) (Fig. 4b), and the hybrid timber shell structure comprising interlocking components (Mesnil et al., 2018).

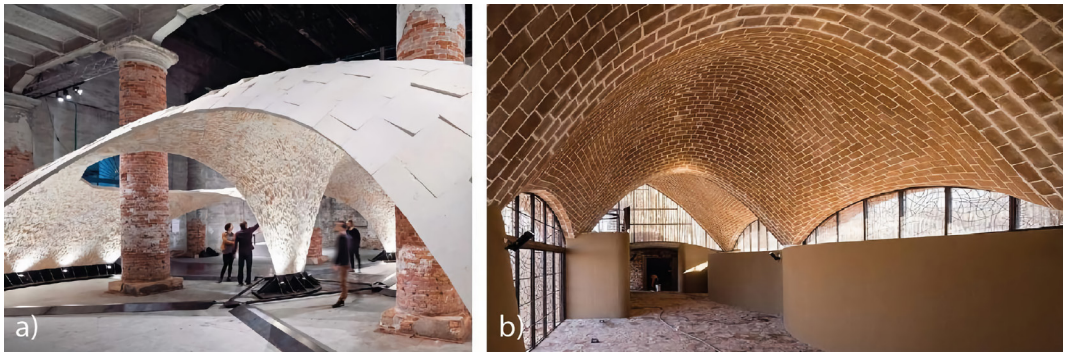


FIGURE 4 a) The mortar-less 'armadillo' vault as exhibited at the Venice Biennale in 2016 (Block et al., 2017); b) The long-span shell of the Mapungubwe National Park comprising structural tiles (image credits: Iwan Baan).

These component-based precedents are successful examples of materially efficient and lightweight structures that strive to merge contemporary CAD advancements, fundamental structural theory, structural insight from previous centuries, and in some cases vernacular construction methods. At the same time, they could not necessarily be used in the extra-terrestrial context since they require scaffolding or mortar, or they consist of too many different pieces that cannot be easily reused in other infrastructure types and geometries.

## Construction methods

Machines have been used since ancient times to assist people in construction. Iconic historic buildings such as the pyramids, the Colosseum, and St. Peter's Basilica materialised via a combination of sheer manpower and simple yet effective tools. Since the industrial revolution, building construction has evolved significantly in two ways. Firstly, building materials can be mass-produced in factories, which allows for a more efficient and standardised supply. At the same time, there was a slow yet continuous demise in craftsmanship and the use of natural materials. Secondly, advancements in construction machines and technologies led to a significant reduction in the labour required. Buildings became larger and stronger, and the building process faster and more standardised. But when it comes to automation, and specifically to the use of robotics, the construction industry lags significantly behind. This discrepancy presents an untapped opportunity for the construction industry due to the inherent advantages of robotics. Specifically, robotic systems are less dangerous, can work for 24 hours a day without losing focus or making errors, and are unfazed by extreme environments.

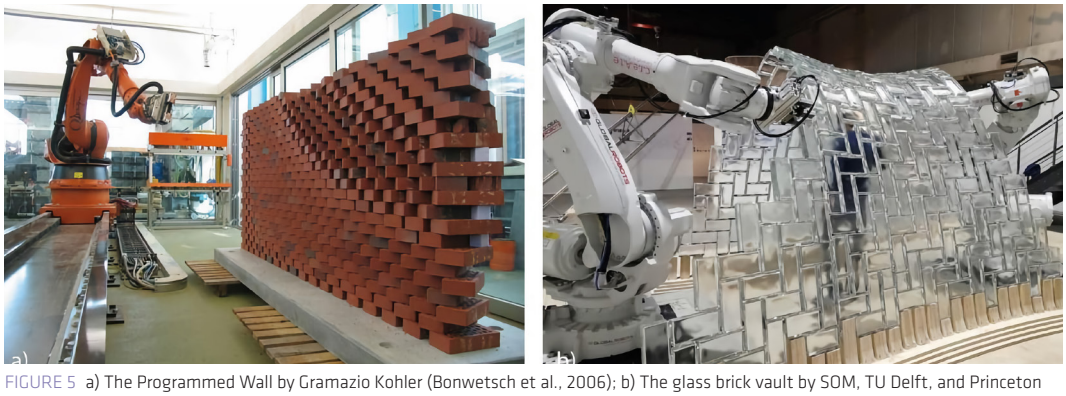

FIGURE 5 a) The Programmed Wall by Gramazio Kohler (Bonwetsch et al., 2006); b) The glass brick vault by SOM, TU Delft, and Princeton (image credits: SOM).

## Robotics

Applications and built prototypes of robotically assembled component-based systems include the Programmed Wall (Fig. 5a) by Gramazio Kohler research of ETH Zurich (Bonwetsch et al., 2006) and the glass brick vault (Fig. 5b) by SOM, TU Delft, and Princeton (Parascho et al., 2020). In the former, the bricks are placed in precise and predefined locations by a fully automated robotic system. This methodology can allow for the construction of brick walls with geometries that would have been prohibitively complicated by means of human labour. At the same time, glue used in the interface between adjacent bricks prohibits their reusability, whilst the possibility of varying the dimensions of the bricks in conjunction with the robotic capabilities has not been investigated. The latter is a collaboration between human and robotic labour in which humans perform complex tasks that require adaptability, such as placing mortar between bricks, and the robots perform precise and laborious tasks, such as placing the bricks in their predefined locations. Operating in complex environments such as on the Moon and Mars requires robotic systems characterised by autonomy and redundancy. One solution proposed to increase redundancy is multi-robot systems or robotic swarms, collectively interpreting their environment and displaying emergent behaviour through a simple set of rules. In the context of remote, extra-terrestrial construction, Foster + Partners has proposed the idea of an autonomous robot swarm that can use indigenous materials to build protective shells (Fig. 6a) (Wilkinson et al., 2016b). Other recent advances in robotics pave the way for a potentially robust technical framework that could allow for off-Earth construction. Specifically, these include the capabilities of the Spot robot – developed by Boston Dynamics – in uncalibrated terrains and (Fig. 6b) of swarm robotic systems in assembling brick-based systems (Werfel et al., 2014) (Fig. 6c).

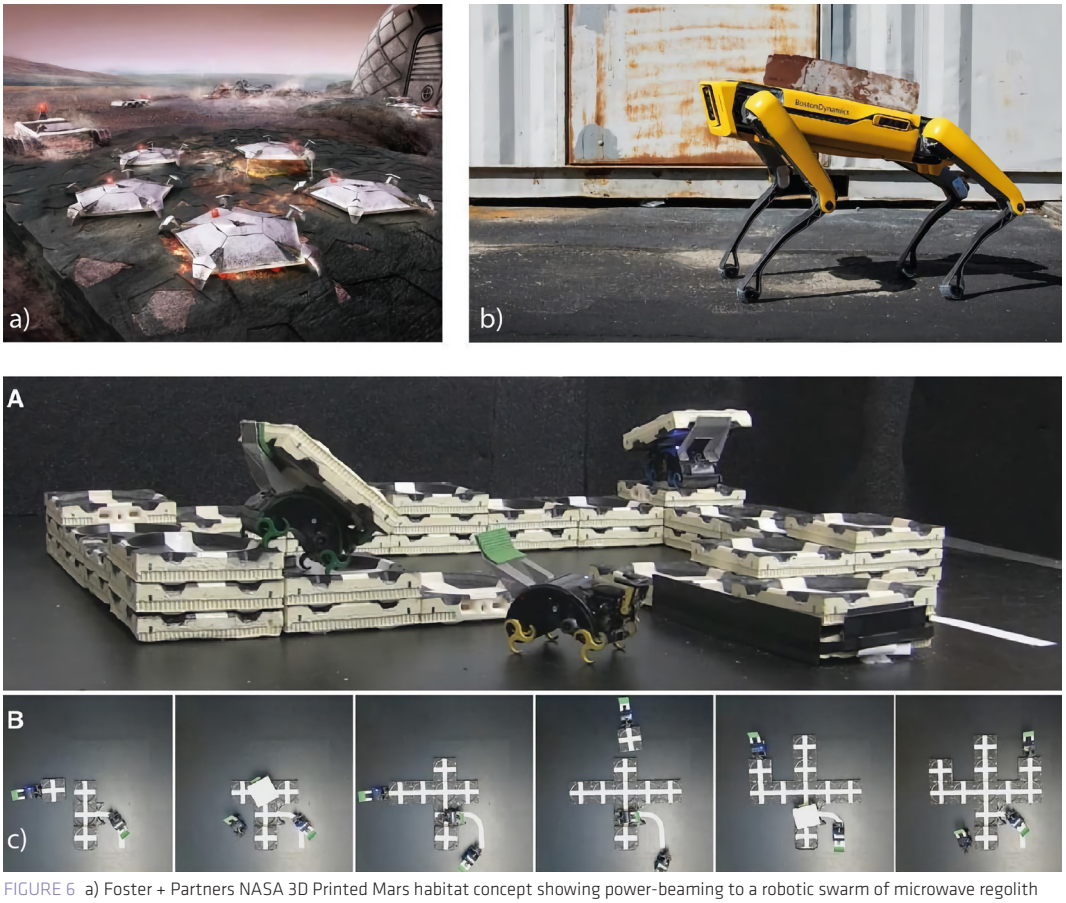


FIGURE 6 a) Foster + Partners NASA 3D Printed Mars habitat concept showing power-beaming to a robotic swarm of microwave regolith sintering (Wilkinson et al., 2016b); b) The Spot robot developed by Boston Dynamics could potentially be used for transferring and assembling bricks on uncalibrated terrains; c) Self-organising robots working like termites can build structures independently (Werfel et al., 2014).

## Off-Earth design

### Engineering proposals

The design of off-Earth structures has been studied by numerous researchers over the previous decades from a structural engineering point of view (Kalapodis et al., 2020). The proposed solutions span a wide range of different methods: from inflatable habitats, to rigid deployable structures, and 3D-printed domes. These studies provide valuable insights in terms both of possible extra-terrestrial structures and of their subsequent structural analysis and performance given the specific harsh environmental conditions that they will need to withstand. At the same time, if we assess them from a sustainability perspective – in terms of their reusability – they mainly investigated monolithic or continuous structures which cannot be easily disassembled and recycled for other infrastructure, while also not allowing for flexibility and geometric adaptability. As a result, locally sourced and produced structural materials, energy consumption during construction, and imported materials from Earth correspond to only one extra-terrestrial structure and cannot contribute to the construction of other infrastructure. Moreover, these approaches concern predominantly simple geometries such as circular barrel vaults, cylinders, and parabolic arches, thus limiting the architectural vocabulary and array of possible functions.

### Architectural proposals

The speculative architectural design of off-Earth structures has drawn renewed attention in recent years (Mueller et al., 2019). Particularly, structures such as habitat shells have largely monopolised this attention due to their expressive, organic nature. Specifically, and in the lunar context, recent contributions include: 3D-printed monolithic vaults designed by Foster + Partners (Fig. 7a) utilising an optimised structural material distribution based on bone formation (Cesaretti et al., 2014); 3D-printed infrastructure of toroidal structures designed and developed by NASA, BIG, SEArch+, and ICON (2020) (Fig. 7c); and an inflatable moon village (2019) jointly proposed by SOM, ESA, and MIT (Inocente et al., 2019) (Fig. 7b). In the Martian context, architectural proposals include: the 3D-printed Mars Ice House from SEArch+ (2016) (Fig. 7d); 3D-printed monolithic vaults designed by Foster + Partners, which employ a swarm robot system to print the structure in layers (Fig. 7e) (Wilkinson et al., 2016b); the 3D-printed Mars habitat domes from AI space factory, who developed the MARSHA Architecture on Mars (2018) project (Fig. 7f); and the habitat structures proposed by Hassell studio (Fig. 7g) in the context of the NASA 3D-printed habitat challenge (2018). All of these approaches comprise continuous monolithic structures that are not suitable for reconfiguration. As a result, there is scope for the development of methodologies that take recyclability into consideration for the design of extra-terrestrial infrastructure.

### Component-based systems

Component-based structural systems have already been proposed in the extra-terrestrial context. In particular, Dyskin et al. (2005) and Imhof et al. (2017) studied the potential of topological interlocking elements. Specifically, the RegoLight project focused on component-based infrastructure (Fig. 8) composed of interlocking tetrahedral-based elements (Imhof et al., 2017). These approaches resulted in a potentially mortar-less and scaffold-less construction process and apply to planar elements such as walls, and standard curved geometries, such as barrel and corbel vaults.

However, the range of applicable geometries is limited, as is the potential for reuse. This is because a departure from the applicable geometries would require scaffolding and numerous different brick geometries. This hinders the reusability potential of the infrastructure, because bricks designed for spatial, curved infrastructure geometries cannot be easily reused for planar ones. This is an inherent issue in stereotomy approaches in which the geometry of the brick is fully dictated and in return fully dictates the global geometry. Thus there is little versatility in terms of reusability.

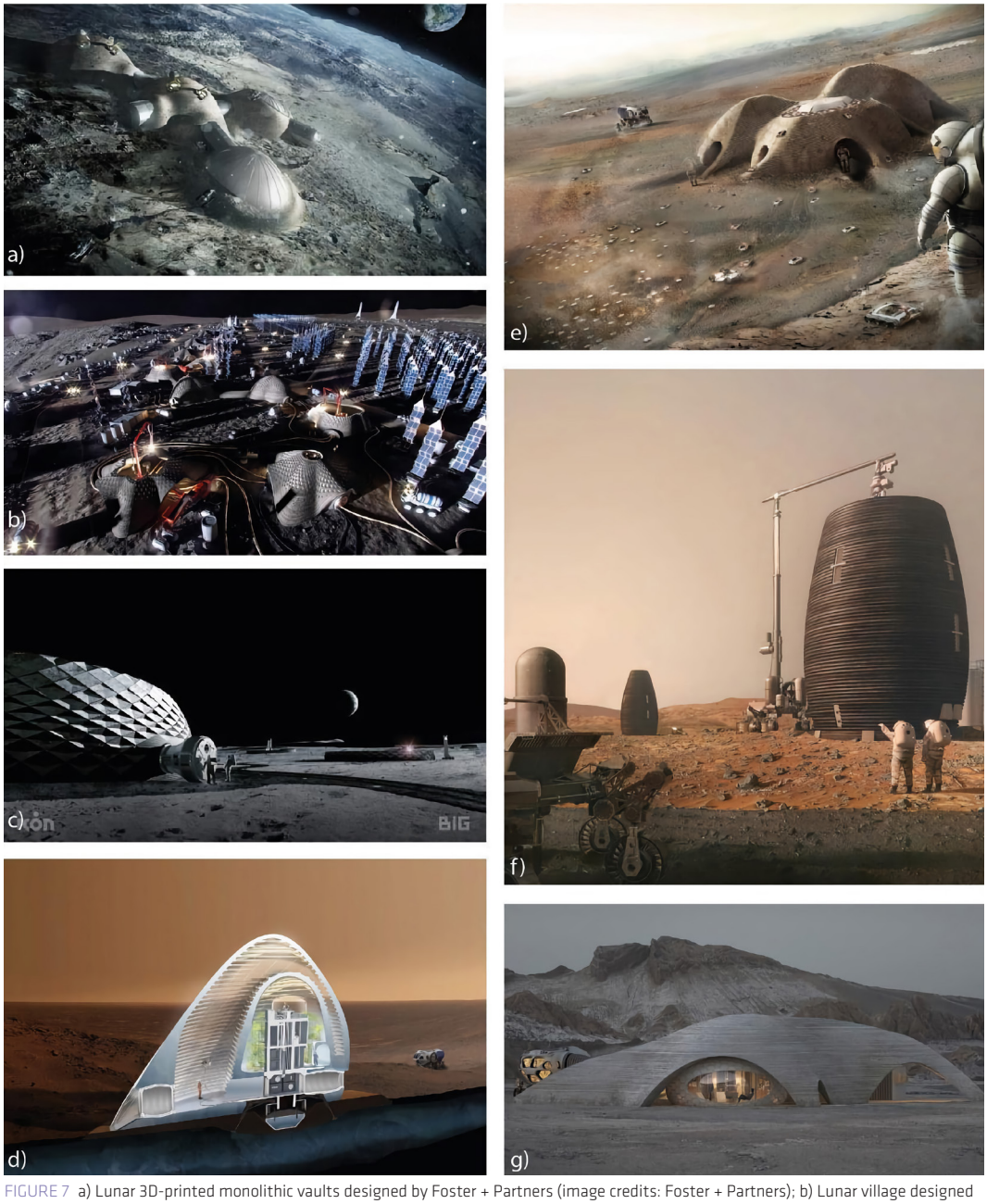


FIGURE 7 a) Lunar 3D-printed monolithic vaults designed by Foster + Partners (image credits: Foster + Partners); b) Lunar village designed by SOM (image credits: SOM); c) 3D-printed lunar infrastructure designed by BIG and ICON (image credits: BIG and ICON); d) Martian 3D-printed habitat (ice house) developed by SEArch+ (image credits: SEArch+); e) Martian 3D-printed monolithic vaults designed by Foster + Partners (image credits: Foster + Partners); f) Martian 3D-printed habitats designed by AI space factory (image credits: AI space factory); g) Martian 3D-printed habitats designed by Hassell studio (image credits: Hassell studio).

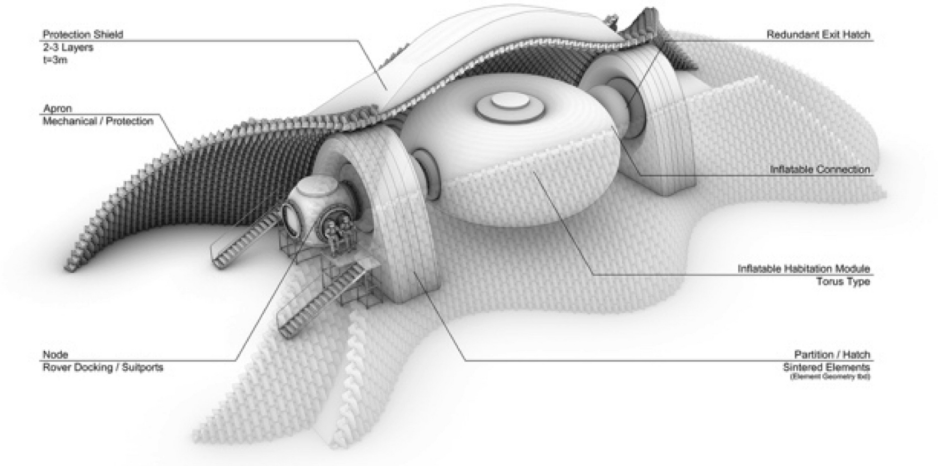


FIGURE 8 Habitat geometry comprising interlocking components as suggested by the RegoLight project (Imhof et al., 2017).

## Innovation of proposed design and construction system

Within the literature and canon of works envisioning off-Earth structures, there is a strong tendency towards continuous structures constructed using additive manufacture, including in our own previous proposals for lunar and Martian habitats. And yet, discrete structures have certain clear advantages that may make them more amenable to the immediate task. By discrete structures, we refer to those which do not behave monolithically due to being composed of many smaller elements, i.e., bricks, blocks, or tiles, and minimal use of binding. As discussed in previous sections, bricks, tiles, and stone blockwork have a long history on Earth, influenced by parameters such as available materials, processes for hardening, ability to form or cut, and handling. Their use has run parallel to continuous structural methods, like wattle and daub, rammed earth, and concrete.

We suggest that a component-based (Fig. 9b), rather than continuous (Fig. 9a), approach to designing and constructing extra-terrestrial structures could be beneficial in terms of maximising the sustainability of space exploration and permanent human presence beyond our planet. This design methodology is based on identical components that interlock via a system of grooves on their bottom side and a system of pins on their upper side. In this way, the component shape does not define, and is not defined by, the global geometry of the structure as in the case of stereotomy techniques. Moreover, the assembled configuration contains within its geometry a form-found compression-only surface, thus maximising material efficiency by minimising tension and bending. In particular, the proposed design and construction paradigm is underpinned by the following principles:

– Reusability: This will be achieved by developing mortarless design systems based on the interlocking properties of adjacent components. In this way, the system compensates for the lack of mortar and binders, which can hinder reconfigurability. As a result, the first unique advantage of discrete systems is their potential for reuse over time. Structures exist to serve a function, which may change or cease over the course of a settlement's lifetime. Discrete bricks can be deconstructed and reconfigured into new structures with some ease. Moreover, in the same fashion as some vernacular examples of dry-stone construction, the design of the components should be generic – one geometry that can be used for multiple configurations and uses – rather than specialised in terms of where the component is placed within the global infrastructure geometry.

– Efficiency: This will be achieved by using form-finding techniques which can derive global geometries in structural equilibrium with specific mechanical properties – e.g., compression-only doubly curved shells. In this way, the generated infrastructure forms comply with, and are a result of, the properties of the available ISRU structural material, which as suggested from the relevant contemporary literature will be adequate mostly in terms of compression strength – similar to vernacular brick-based vaults, dry-stone domes, rammed earth structures, and masonry cathedrals. Also, since the structures will not be monolithic, replacement and repair could take place in a component-based fashion without jeopardising the serviceability of the whole infrastructure.

– Economy: This will be achieved by using each component, and hence its corresponding material and fabrication energy, not only for multiple structures within its lifespan but also for other uses during construction - e.g., temporary scaffolding during erection. What is more, as showed by both vernacular analogues and contemporary research (Imhof et al., 2017), interlocking, component-based systems hold the promise of minimising the need for scaffolding, if not making it obsolete, showing the potential of free-standing structures during erection, and hence unsupported overhangs. This allows for overhanging features such as arches, domes, or slopes. Furthermore, the decommissioning of structures and evolution of the human outpost will not result in abandoned ruins, unusable structural material, nor, ultimately, in the permanent transformation of the lunar and Martian landscape.

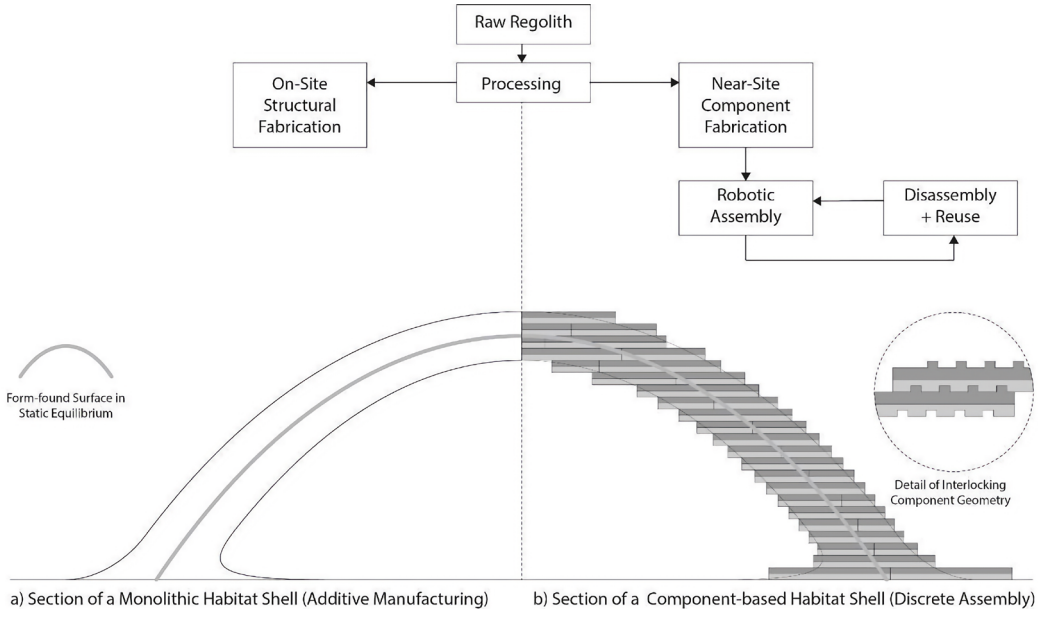


FIGURE 9 a) Section of a monolithic 3D-printed vault that cannot be recycled; b) Section of a component-based, mortar-less and scaffold-less vault, the components of which can be reused.

Lastly, bricks offer the strong benefit that they, due to their small size, can be fabricated in a controlled environment (e.g., thermally or atmospherically). This does not preclude additive manufacture use for bricks, which may be preferable for the robots and tools in a controlled or semi-controlled environment such as a pressurised workshop. Similarly to continuous structures, discrete systems can also achieve adaptable and complex forms. We need only look to the wide range of applications and creativity of brick structures found on Earth.

## Conclusions

In this research paper, we proposed that a component-based design methodology may hold comparative advantages over its continuous counterparts, which currently dominate the literature and architectural discourse of off-Earth design. Specifically, we suggested that this system could be based on a synthesis of ancient vernacular and cutting-edge form-finding knowledge on structural design and construction. We discussed how extra-terrestrial infrastructure design has striking similarities with the past and present tradition of the built environment in the Earth context and suggested that it should be seen as an extreme case of our design and construction practises on Earth rather than as an isolated field. Moreover, we put forward a bi-directional relationship, in which off-Earth construction acts as a catalyst for change here, and on-Earth structures as a precedent for lunar and Martian construction. In this context, we highlighted how industries on Earth have much to learn from the extreme constraints characterising space missions. These lessons could lead to structures that are not only lightweight yet strong but also environmentally efficient and recyclable.

## References


Adriaenssens, S., Block, P., Veenendaal, D., & Williams, C. (2014). *Shell structures for architecture: Form Finding and Optimization*. Routledge.

Block, P., Van Mele, T., Rippmann, M., & Paulson, N. (2017). *Beyond Bending*. DETAIL.

Bonwetsch, T., Kobel, D., F., G., & Kohler, M. (2006). The informed Wall: Applying additive digital fabrication techniques on architecture. *Synthetic Landscapes [Proceedings of the 25th Annual Conference of the Association for Computer-Aided Design in Architecture*, 489–495.

Brütting, J., De Wolf, C., & Fivet, C. (2019). The reuse of load-bearing components. *IOP Conference Series: Earth and Environmental Science*, *225*, 012025. https://doi.org/10.1088/1755-1315/225/1/012025

Cesaretti, G., Dini, E., De Kestelier, X., Colla, V., & Pambaguian, L. (2014). Building components for an outpost on the Lunar soil by means of a novel 3D printing technology. *Acta Astronautica*, *93*, 430–450.

Choisy, A. (1883). *L'art de bâtir chez les Byzantins. Librairie de la Société anonyme de publications périodiques*.

Day, A. S. (1965). An introduction to dynamic relaxation. *The Engineer*, *219*, 218–221.

De Wolf, C., Hoxha, E., & Fivet, C. (2020). Comparison of environmental assessment methods when reusing building components: A case study. *Sustainable Cities and Society*, *61*, 102322. https://doi.org/10.1016/j.scs.2020.102322

Dyskin, A. V., Estrin, Y., Pasternak, E., Khor, H. C., & Kanel-Belov, A. J. (2005). The principle of topological interlocking in extraterrestrial construction. *Acta Astronautica*, *57*(1), 10–21. https://doi.org/10.1016/j.actaastro.2004.12.005

European Space Agency. (2019). *Advanced Closed Loop System*. ESA. https://www.esa.int/Science_Exploration/Human_and_Robotic_Exploration/Research/Advanced_Closed_Loop_System

Fitchen, J. (1981). *The Construction of Gothic Cathedrals*. The University of Chicago Press.

Frézier, A. F. (1738). *La théorie et la pratique de la coupe des pierres et des bois, pour la construction des voûtes et autres parties des bâtiments civils et militaires, ou Traité de stéréotomie à l'usage de l'architecture*. Doulsseker.

Häder, D.-P., Braun, M., & Hemmersbach, R. (2018). Bioregenerative Life Support Systems in Space Research. In M. Braun, M. Böhmer, D.-P. Häder, R. Hemmersbach, & K. Palme, *Gravitational Biology I* (pp. 113–122). Springer International Publishing. https://doi.org/10.1007/978-3-319-93894-3_8

Hassell & Eckersley O'Callaghan. (2018). *NASA 3D Printed Habitat Challenge*. Hassell. https://www.hassellstudio.com/project/nasa-3d-printed-habitat-challenge

Heyman, J. (1995). *The Stone Skeleton*. Cambridge University Press.

Hilburg, J. (2020, October 2). *NASA, BIG, SEArch+, and ICON team up to develop a lunar city*. The Architect's Newspaper. https://www.archpaper.com/2020/10/nasa-big-search-icon-project-olympus/

Howe, S. A., Wilcox, B. H., McQuin, C., Townsend, J., Rieber, R. R., Barmatz, M., & Leichty, J. (2013). Faxing structures to the moon: Freeform additive construction system (FACS. *AIAA SPACE 2013 Conference and Exposition*, 5437.

Imhof, B., Urbina, D., Weiss, P., Sperl, M., Hoheneder, W., Waclavicek, R., Madakashira, H. K., Salini, J., Govindaraj, S., Gancet, J., Mohamed, M. P., Gobert, T., Fateri, M., Meurisse, A., Lopez, O., & Preisinger, C. (2017). Advancing Solar Sintering for Building A Base On The Moon. In *69th International Astronautical Congress (IAC)*.

Inocente, D., Koop, C., Petrov, G. I., Hoffman, J. A., Sumini, V., Makaya, A., Arnhof, M., Lakk, H., Lamaze, B., Cowley, A., Binns, D., Landgraf, M., Messina, P., & Haingeré, C. (2019). Master Planning and Space Architecture for a Moon Village. In *70th International Astronautical Congress (IAC)*.

Kalapodis, N., Kampas, G., & Ktenidou, O.-J. (2020). A review towards the design of extraterrestrial structures: From regolith to human outposts. *Acta Astronautica*, *175*, 540–569. https://doi.org/10.1016/j.actaastro.2020.05.038

Liddell, I. (2015). Frei Otto and the development of gridshells. *Case Studies in Structural Engineering*, *4*, 39–49. https://doi.org/10.1016/j.csse.2015.08.001

Loing, V., Baverel, O., Caron, J.-F., & Mesnil, R. (2020). Free-form structures from topologically interlocking masonries. *Automation in Construction*, *113*, 103117. https://doi.org/10.1016/j.autcon.2020.103117

*MARSHA by AI SpaceFactory*. (2018). AI SpaceFactory. https://www.aispacefactory.com/marsha

Mesnil, R., Douthe, C., Gobin, T., & Baverel, O. (2018). *Form Finding and Design of a Timber Shell-Nexorade Hybrid*. Advances in Architectural Geometry.

Mueller, R., Howe, S., Kochmann, D., Ali, H., Andersen, C., Burgoyne, H., Chambers, W., Clinton, R., De Kestellier, X., Ebelt, K., & Gerner, S. (2016). Automated additive construction (AAC) for Earth and space using in-situ resources. *Proceedings of Earth & Space 2016*.

Mueller, R., Prater, T. J., Roman, M., Edmunson, J. E., Fiske, M., & Carrato, P. (2019). NASA Centennial Challenge: Three Dimensional (3D) Printed Habitat. *70th International Astronautical Congress (IAC*, *3*.

Ochsendorf, J. (2010). *Guastavino Vaulting: The Art of Structural Tile*. Princeton Architectural Press.

Oliver, P. (1997). *Encyclopedia of vernacular architecture of the world*. Cambridge University Press.

Owens, A., & DeWeck, O. (2016). Systems Analysis of In-Space Manufacturing Applications for International Space Station in Support of the Evolvable Mars Campaign. *Proceedings of the American Institute of Aeronautics and Astronautics SPACE Forum*.

Owens, A., DeWeck, O., Stromgren, C., Goodliff, K. E., & Cirillo, W. (2017). Supportability Challenges, Metrics, and Key Decisions for Human Spaceflight. *Proceedings of the American Institute of Aeronautics and Astronautics (AIAA)*.

Parascho, S., Han, I. X., Walker, S., Beghini, A., Bruun, E. P. G., & Adriaenssens, S. (2020). Robotic vault: A cooperative robotic assembly method for brick vault construction. *Construction Robotics*, *4*(3–4), 117–126. https://doi.org/10.1007/s41693-020-00041-w

Paris, V., Pizzigoni, A., & Adriaenssens, S. (2020). Statics of self-balancing masonry domes constructed with a cross-herringbone spiraling pattern. *Engineering Structures*, *215*, 110440. https://doi.org/10.1016/j.engstruct.2020.110440

Poleni, G. (1748). *Memorie Istoriche della Gran Cupola del Tempio Vaticano*. Stamperia del Seminario di Padova.

Ramage, M., Ochsendorf, J., & Rich, P. (2009). Sustainable shells: New African vaults built with soil-cement tiles. *Proceedings of the International Association for Shell and Spatial Structures (IASS) Symposium*.

Rippmann, M., Lachauer, L., & Block, P. (2012). Interactive Vault Design. *International Journal of Space Structures*, *27*(4), 219–230. https://doi.org/10.1260/0266-3511.27.4.219

Schek, H.-J. (1974). The force density method for form finding and computation of general networks. *Computer Methods in Applied Mechanics and Engineering*, *3*(1), 115–134. https://doi.org/10.1016/0045-7825(74)90045-0

Todisco, Skidmore, Owings & Merrill. (2019, April 9). *SOM Releases Concept for Moon Village, the First Permanent Human Settlement on the Lunar Surface*. SOM. https://www.som.com/news/som_releases_concept_for_moon_village_the_first_permanent_human_settlement_on_the_lunar_surface

L., Sanitate, G., & Lacorte, G. (2017). Geometry and Proportions of the Traditional Trulli of Alberobello. *Nexus Network Journal*, *19*(3), 701–721. https://doi.org/10.1007/s00004-016-0326-4

Space Exploration Architecture & Clouds AO. (2016). *Mars Ice House*. SEArch+. http://www.spacexarch.com/mars-ice-house

Wendland, D. (2004). Free-handed vault construction in the European building tradition: Vaulting patterns in half-stone vaults. *13th International Brick and Block Masonry Conference*.

Werfel, J., Petersen, K., & Nagpal, R. (2014). Designing collective behavior in a termite-inspired robot construction team. *Science*, *343*(6172), 754–758.

Wilkinson, S., Musil, J., Dierckx, J., Gallou, I., & Kestelier, X. (2016). Concept Design of an Outpost for Mars using Autonomous Additive Swarm Construction. *ESA Acta Futura Special Issue*, *10*, 121–129.

Wilkinson, S., Musil, J., Dierckx, J., Maddock, R., Yanga, X., Dall'Igna, M., Gheorghiu, O., & De Kestelier, X. (2016). Preliminary findings from a multi-robot system for large-scale extra-planetary additive construction. In *67th International Astronautical Congress (IAC)*.

Williams, C. (2001). The analytic and numerical definition of the geometry of the British Museum Great Court Roof. *Mathematics & Design*, 434–440.

# Additive manufacturing of Lunar Regolith Simulant using Direct Ink Writing

**Billy Grundström** [1], **Timon Schild** [2], **Aidan Cowley** [1]

[1] *Northvolt*
*Västerås, Sweden*

[2] *ESA/EAC - European Astronaut Centre*
*Cologne, Germany*

[3] *European Space Agency - ESA*
*Cologne, Germany*

## Abstract

This work explores the use of a lunar regolith simulant as feedstock for the direct ink writing additive manufacturing process as an option to enable future lunar in-situ resource utilisation. The feasibility of this approach is demonstrated in a laboratory setting by manufacturing objects with different geometries, using methyl cellulose or sodium alginate as binding agents, water and lunar regolith simulant to create a viscous, printable 'ink'. A custom three-axis gantry system is used to produce green bodies for subsequent sintering. The sintered objects are characterised using compressive strength measurements and scanning electron microscopy (SEM). It is proposed that the bioorganic compounds used in this work as additives could be produced in situ for a future lunar base through photosynthesis, utilising carbon dioxide exhaled by astronauts together with the available sunlight. Thus, all the components used for the dispersion – additive, water, and regolith – are available in situ. The compressive strength for sintered samples produced with this method was measured to be 2.4 MPa with a standard deviation of 0.2 MPa (n = 4). It is believed, based on the high sample porosity observed during SEM analysis, that the comparatively low mechanical strength of the samples is due to a low sintering temperature, and that the mechanical strength could be increased by optimising the sintering process further.

## Keywords

ISRU, additive manufacturing, 3D printing, direct ink writing, lunar regolith, sintering

## DOI

https://doi.org/10.7480/spool.2021.2.5268

## Context

A limiting factor for human space exploration is the restricted amount of mass that can be transported into space due to the high cost of space travel (Anand et al., 2012). Even though this cost is expected to decrease with the further development of reusable launch systems, the cost per transported mass is likely to remain high due to intrinsic limitations in the storage capacity of spacecraft related to the required propulsion mass (Sherwood, 2019)"ISSN":"00945765","abstract":"NASA planning for the human space flight frontier is coming into alignment with the goals of other planetary-capable national space agencies and independent commercial actors. US Space Policy Directive 1 made this shift explicit: "the United States will lead the return of humans to the Moon for long-term exploration and utilization". The stage is now set for public and private American investment in a wide range of lunar activities. Assumptions about Moon base architectures and operations are likely to drive the invention of requirements that will in turn govern development of systems, commercial-services purchase agreements, and priorities for technology investment. Yet some fundamental architecture-shaping lessons already captured in the literature are not clearly being used as drivers, and remain absent from typical treatments of lunar base concepts. A prime example is general failure to recognize that most of the time (i.e., before and between intermittent human occupancy. The cost associated with sending one pound – approximately 0.45 kg – of mass into orbit has been estimated to be at least $10,000 (Montes et al., 2015).

In-situ resource utilisation (ISRU) is a methodology for reducing the amount of material needed to be sent from Earth by using resources available at the destination during coming missions to the Moon or to Mars. Such an example of ISRU is the planned demonstration of oxygen production from atmospheric CO2 by the Mars rover Perseverance, launched in 2020 by the National Aeronautics and Space Administration (NASA) (Hinterman, 2020). Another example would be the use of native construction materials for buildings and infrastructure on the Moon or on Mars. One such material that has attracted significant interest in the context of space exploration is regolith, which is an umbrella term for the compositionally and morphologically heterogeneous surface layer of rock and fine particles on celestial bodies. The use of regolith has been studied extensively for ISRU applications (Anand et al., 2012; Nieke et al., 2019; Schleppi et al., 2019; Sherwood, 2019; Song et al., 2019).

Additive manufacturing (AM) – or three-dimensional (3D) printing – is a manufacturing process that has raised much interest in the last couple of decades. This is due to its ability for rapid prototyping as well as the high level of design freedom enabled by the technology compared to traditional subtractive manufacturing (SM) technologies. These and other features makes AM an attractive technology for future ISRU applications in remote locations (Jakus et al., 2015; Schlordt et al., 2013; Taylor et al., 2017). During the AM process, an object is built in a layer-by-layer fashion. There exists a multitude of different AM technologies, spanning the material categories of ceramic, metallic, and polymer materials (ISO/ASTM, 2015).

Direct ink writing (DIW) – or robocasting – is an AM technology that is based on the selective deposition of a viscous ink by extrusion through a nozzle (Lewis et al., 2006)functional, and biomedical applications. One facile approach is direct ink writing (DIW. The ink (also called dispersion or slurry) usually consists of solid particles dispersed in a liquid phase, and is typically optimised with regards to its rheological properties by the use of additives, especially by modifying the ink to have it exhibit shear thinning behaviour for facilitated deposition (Dai et al., 2019). Additional additives may be used to further optimise the properties of the ink such as controlling the flocculation behaviour of the particles. Typical factors to consider when choosing the liquid phase for the ink are availability, its rate of evaporation, as well as its toxicity. Depending on the final use, the 3D-printed item, once manufactured, might be further processed, for example by sintering.

Combining additive manufacturing with ISRU is an attractive option, as a single technological system might be used to manufacture objects with differing geometries for a wide range of applications. Table 1 summarises published articles on the use of regolith as a material for additive manufacturing, as well as a minor selection of articles in which casting is used as a production method. It should be noted that test conditions (e.g. geometries, number of replicates, and the standards used) for the performed compressive strength measurements vary between sources, which in effect makes a direct comparison of the results of limited use. Still, the compressive strength has been included in the table to give a sense of the current state of each technology. It should also be noted that the availability of actual lunar regolith is highly limited. Therefore, research relating to this topic almost exclusively makes use of regolith simulants of terrestrial origin, the choice of which may affect the results.

| METHOD | SUBPROCESS | MATERIAL | COMPRESSIVE STRENGTH | REFERENCE |
|---|---|---|---|---|
| AM | Binder jetting | Regolith, Sorel cement, binder liquid | 20 MPa | (Cesaretti et al., 2014) |
| AM | Extrusion | Regolith (72 wt.%), urea, alkaline solution, Casted | 13 MPa | (Pilehvar et al., 2020) |
| AM | Extrusion | Regolith (56 wt.%), phosphoric acid, water, Machined | 20 MPa | (Buchner et al., 2018) |
| AM | Extrusion | Regolith (74 vol.%), PLGA, DCM, plasticizer | 19 MPa | (Taylor et al., 2018) |
| AM | Extrusion | Regolith (70 vol.%), PLGA, DCM, plasticizer | Not tested | (Jakus et al., 2017) |
| AM | Laser melting | Regolith | 31 MPa | (Caprio et al., 2020) |
| AM | Laser melting | Regolith | Not tested | (Goulas et al., 2016) |
| AM | Laser sintering | Regolith | Not tested | (Xu et al., 2019) |
| AM | Laser sintering | Regolith | Not tested | (Goulas & Friel, 2016) |
| AM | Laser sintering | Regolith | Not tested | (Fateri & Gebhardt, 2015) |
| AM | Laser sintering | Regolith | Not tested | (Balla et al., 2012) |
| AM | Microwave sintering | Regolith | Not tested | (Allan et al., 2013) |
| AM | Solar sintering | Regolith | 2 MPa | (Meurisse et al., 2018) |
| Casting | Geopolymer | Regolith (76 wt.%), liquid silicate, alkaline solution | 16 MPa | (Montes et al., 2015) |
| Casting | Sulphur concrete | Regolith (65 wt.%), sulphur | 31 MPa | (Toutanji et al., 2012) |
| Casting | Thermite reaction | Regolith (67 wt.%), aluminium powder | 18 MPa | (Faierson et al., 2010) |

TABLE 1 Overview of reported use of regolith together with mainly additive manufacturing processes.

## Innovation

This work focuses on the use of an extrusion-based additive manufacturing technology – direct ink writing – using a formulation that is both non-toxic and easy to produce in situ. Indeed, the current extrusion-based processes described in the literature often use additives that are hazardous (e.g. DCM, phosphoric acid) and/or difficult to produce in situ (e.g. plasticizers). The selection criteria for the proposed formulation were in this instance, in descending order, low toxicity, potential in-situ availability, and low technological complexity in order to increase the robustness of the system.

Water was chosen as the liquid phase owing to its non-toxicity and potential availability on the Moon (Colaprete et al., 2010). Sodium alginate (SA) and methyl cellulose (MC), two bioorganic compounds, were both identified as suitable binding agents for the dispersion. A scenario is envisioned here in which either sodium alginate or methyl cellulose is produced in situ on the Moon by the use of microorganisms and bioreactors, utilising CO2 exhaled by astronauts (Menezes et al., 2015; Way et al., 2011)all of which can be

generated by means of biosynthesis. Synthetic biology has the potential to generate organisms designed for supplying human nutritional needs in space. Photosynthetic microbes may be ideal for this purpose, as they are more efficient per volume cultivated than green plants at conversion of light to chemical energy, biomass and nutritional molecules. In addition, microbes are easier and faster to genetically engineer, facilitating not only design and terrestrial manufacture of organisms optimized for growth and nutrient production in the artificial conditions of space, but superior ability in space to develop organisms suited to newly discovered environments. The rapid ability to adapt and create new microbes to suit new circumstances when in space offers significant potential for risk reduction. Development of sun-driven microbial production of nutritional chemicals would also have terrestrial benefits in commerce and sustainability. A synthetic biology approach to chemical production would not be based on fossil fuels as such fuels do not exist on other planets. This approach would highlight a synergistic relationship between outer space and 'spaceship earth', illustrating NASA's role in stimulating technology development with terrestrial application. Two specific approaches deserve consideration: production by traditional photosynthetic microbes, or by the newly appreciated capacity of some bacteria to absorb electric current (e.g. solar panels. In such a scenario, all the ingredients for the dispersion – regolith, water, and binding agent – could be sourced locally once the initial infrastructure has been installed.

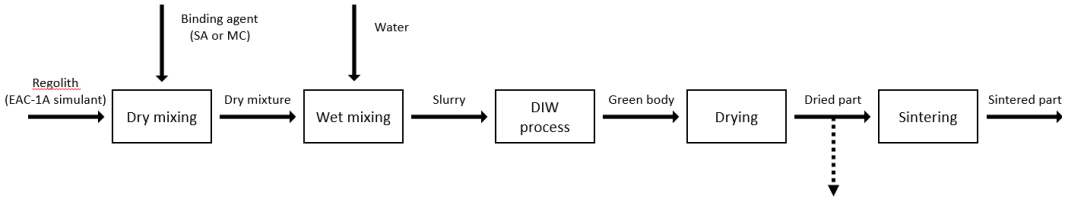


FIGURE 1 Proposed process for 3D parts production using regolith slurry.

A schematic of the proposed process is presented in Figure 1. The regolith (i.e. EAC-1A simulant) is first mixed with the powdered binding agent (SA or MC) to form a dry mixture. A slurry is then produced by addition of deionized water and thorough mixing. This slurry is a viscous fluid loaded in regolith, which can be used for DIW. A 3D-printing rig is used to extrude the slurry on a build-plate and produce a 3D geometry. The printed green body is air-dried to obtain a dried part, which can be used as is or sintered in a furnace to obtain the final sintered part.

In this paper, the feasibility of the proposed process is demonstrated through experimental results. A working set of process parameters is establish, and the properties of the produced parts are assessed.

## Experimental methods

### Materials

EAC-1A, a lunar regolith simulant developed by ESA, was used for this work. It is readily available and has been shown to be comparable to other frequently used regolith simulants (Engelschiøn et al., 2020). The material composition in wt.% as reported in the literature is summarised in Table 2. The grain size for

the material ranges between 0.02–1.0 mm. In terms of granulometry, EAC-1A mostly falls within the range of values observed in Apollo samples, with a slight underrepresentation of particles between 200 µm and 70 µm. The elemental composition of EAC-1A is closest to the one observed in the Apollo 17 samples.

EAC-1A, as any other regolith simulant, does differ from actual lunar regolith in a few aspects relevant to this work. First of all, lunar regolith grains have very irregular shapes, and are often elongated with sharp edges and corners. As a terrestrial simulant, EAC-1A displays more rounded grain shapes. This may affect the mechanical properties of the slurry, such as its flowability or its cohesion strength. Actual lunar regolith also has a large glass fraction (up to 60%wt), which is difficult to reproduce in terrestrial simulants. The absence of this glass phase in EAC-1A could affect the sintering behaviour of the produced green bodies.

| OXIDE | WT.% |
|---|---|
| $SiO_2$ | 43.70 |
| $Al_2O_3$ | 12.60 |
| $Fe_2O_3$ | 12.00 |
| MgO | 11.90 |
| CaO | 10.80 |
| $Na_2O$ | 2.90 |
| $TiO_2$ | 2.40 |
| K2O | 1.30 |
| $P_2O_5$ | 0.60 |
| MnO | 0.20 |
| Total | 98.40 |

TABLE 2 Chemical composition of the lunar regolith simulant EAC-1A in wt.%.

Two dispersions were prepared by mixing ingredients according to the ratios given in Table 3, with 'LA' referring to 'Low Additive' content and 'HA' referring to 'High Additive' content respectively. HA samples had an increased concentration of additive by a factor of 3.6. Dispersions were prepared using either methyl cellulose (MM = 160000 g/mol) or sodium alginate (both Carl Roth GmbH + Co. KG, Germany) as additives. EAC-1A regolith simulant was mixed with the powdered additive, to which de-ionised water was then added. The mixture was hand stirred for at least 5 minutes using a mortar and pestle. The resulting dispersion was transferred to a 60 ml syringe for immediate use. After finishing a print, the resulting items were left to dry under ambient atmospheric conditions for 72 h before sintering.

| | EAC-1A | WATER | ADDITIVE |
|---|---|---|---|
| LA | 1 | 0.40 | $5.6 \cdot 10^{-3}$ |
| HA | 1 | 0.45 | $2.0 \cdot 10^{-2}$ |

TABLE 3 Dispersion content as component mass/EAC-1A mass ratio. (LA: Low Additive, HA: High Additive).

## 3D printing

An overview of the key components of the 3D printer used in this work is given in Figure 2. It is a 3-axis system, allowing a custom slurry extruder to be moved along the X,Y, and Z directions over a fixed printbed. The custom unit is controlled through a controller board which has a graphical user interface and that runs a

modified version of the Marlin firmware. The X- and Y-axes (lateral axes) are belt driven by stepper motors connected to microstep drivers for current regulation and step size control. The Z-axis (vertical axis) is a rack and pinion system driven by a stepper motor, on which the extruder subunit can be mounted. The extruder has a stepper motor which actuates a leadscrew with a custom plunger attached to its end that fits into a 60 ml syringe with a 28 mm chamber diameter. The 3D printer takes G-code files as input. The movement speed for the X- and Y-axes was set to 7 mm/s and the extrusion speed was set to 4 µm per mm X and Y travel, which corresponds to 28 µm/s or a volumetric flow of 17 $mm^3/s$. The system parameters of importance are listed in Table 4.

To perform the printing operation, the slurry is loaded into the extruder syringe and deposited onto an unheated ceramics buildplate. Since the slurry formulations used were subject to air-drying, the printing operation was undertaken within 30 minutes after slurry production. After printing, the parts were left on the printbed to dry at room temperature for at least 72 hours. This allowed the sample to build enough strength to be separated from the printbed for further processing without damaging the geometry.

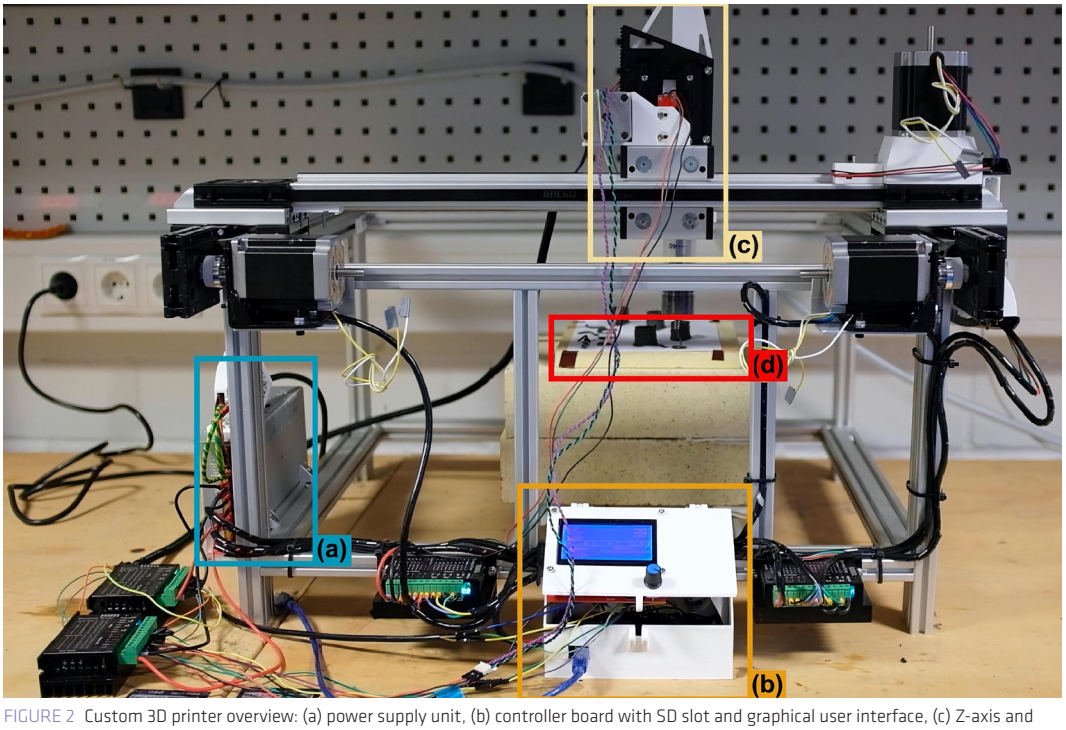


FIGURE 2 Custom 3D printer overview: (a) power supply unit, (b) controller board with SD slot and graphical user interface, (c) Z-axis and extruder, (d) ceramic build plate.

| SYRINGE VOLUME | NOZZLE DIAMETER | X, Y MOVEMENT SPEED | EXTRUSION SPEED | VOLUMETRIC FLOW | LAYER HEIGHT |
|---|---|---|---|---|---|
| 60 ml | 2 mm | 7 mm/s | 28 µm/s | 17 $mm^3/s$ | 1.2 mm |

TABLE 4 System parameters for the custom 3D printer.

## Sintering

The sintering was carried out using a Paragon SC-Series 1680 W Kiln with a specified max. temperature of 1093 °C, with an actual max. temperature varying around 1080 °C during sintering. The sintering was carried out over three steps, listed in Table 5, and the kiln was then left to cool to room temperature over a period of approximately 2 h. The total process took approximately 8.5 h from start to finish.

| STEP | TARGET TEMPERATURE | HEATING RATE | HOLDING TIME |
|---|---|---|---|
| Drying | 120 °C | 5 K/min | 45 min |
| Debinding | 500 °C | 5 K/min | 45 min |
| Sintering | 1080 °C | 10 K/min | 120 min |

TABLE 5 Sintering steps.

### Characterisation

A Hitachi TM-1000 scanning electron microscope with an accelerating voltage of 15.0 kV was used for this work. A Shimadzu AGX universal testing machine with a force accuracy of ±0.5% was used at a speed setting of 1 mm/min for the compressive testing.

## Results and discussion

### Slurry preparation

When only regolith and water are mixed, the mixture separates into its solid and liquid components as regolith lacks the cohesiveness of clay materials, meaning that water itself is not sufficient to create a self-supporting and extrudable slurry. By using methyl cellulose or sodium alginate as a binding agent, the viscosity of the dispersion is markedly increased as the additive comes in contact with water. The dispersion may be modified from being water-like with high flowability, to being a thick, nonflowing paste, by altering the concentration of additive. Both SA and MC behaved in similar way in this study. In a shear thinning liquid, such as one that is ideally used for 3D-printing applications, an increase in the strain rate will lead to a decrease in viscosity. Both SA and MC slurries reportedly exhibit this behaviour (Liu et al., 2018; Schlordt et al., 2013).

There was an observed increase in rigidity of an extruded strand of dispersion during this work as the concentration of additive was increased. An extruded segment of the higher additive 'HA' concentration dispersion resisted attempts at indentation with a sharp object, while the lower additive 'LA' concentration did not do so. It is possible that this increase in observed rigidity counteracts the interaction and bonding between subsequent layers. This might increase anisotropy in the material due to the reduced bonding strength between layers, similar to what is commonly observed in thermoplastic 3D printing (Hart et al., 2018). As a result, it is suggested that a higher concentration of additive will result in weaker structures if a certain threshold value of additive is surpassed due to reduced layer bonding.

Mixing is an important step to ensure a well dispersed slurry, and the use of a ball mill instead of mortar and pestle might improve the distribution and dispersion of particles in the slurry. At higher concentrations of additive, it was difficult to manually homogenise the slurry, as the material had the viscosity of a thick paste. It has been suggested elsewhere that the ratio of nozzle size to maximum particle diameter should be 10, which equals particles with a maximum size of 200 µm for a 2 mm nozzle, like the one used here (Perrot et al., 2018). As already mentioned, the particles used in this work ranged between 0.02 and 1 mm in diameter (before mixing), which might lead to non-optimal flow behaviour.

## 3D printing

The prepared dispersions proved to be extrudable using the 3D printer system available for this work. A selection of parts printed using this setup are presented in Figure 3.

Experiments using higher concentrations of additive than those reported here were also conducted, but extrusion was no longer possible due to the limitations of the setup. Similarly, tests were performed using finer nozzle sizes (0.8 mm and 1.2 mm) in combination with the sieved fraction EAC-1A, with the result that the system again was not able to extrude the dispersion. This indicates that an upgraded setup with higher extruding pressure may help improve the process. Indeed, the feature size of printed items depends on the nozzle size, meaning that a finer nozzle enables higher resolution.

It is also important that the printed items exhibit a high green strength to support the subsequent layers as they are deposited. Figure 3 (a) displays a printed hollow cylinder that is approximately 20 mm tall, consisting of 15 layers, in which SA was used at a low concentration ('LA'). This object demonstrates that the prepared dispersion has enough shape retention to carry its own weight at this scale. The cylinder is not perfectly straight, but it is not certain if this is due to self-buckling of the structure, small inaccuracies in the movement of the printhead, or to slight deviations in how the dispersion expands and contracts after extrusion, which, as the print progresses, may lead to dimensional inconsistencies.

It has been reported that a difference of only 2 vol.% in solid loading for a ceramic dispersion can have a significant impact on the buckling behaviour of the ink (Rueschhoff et al., 2016; Tang et al., 2019), which may be an important consideration when seeking to avoid any self-buckling tendencies of the ink.

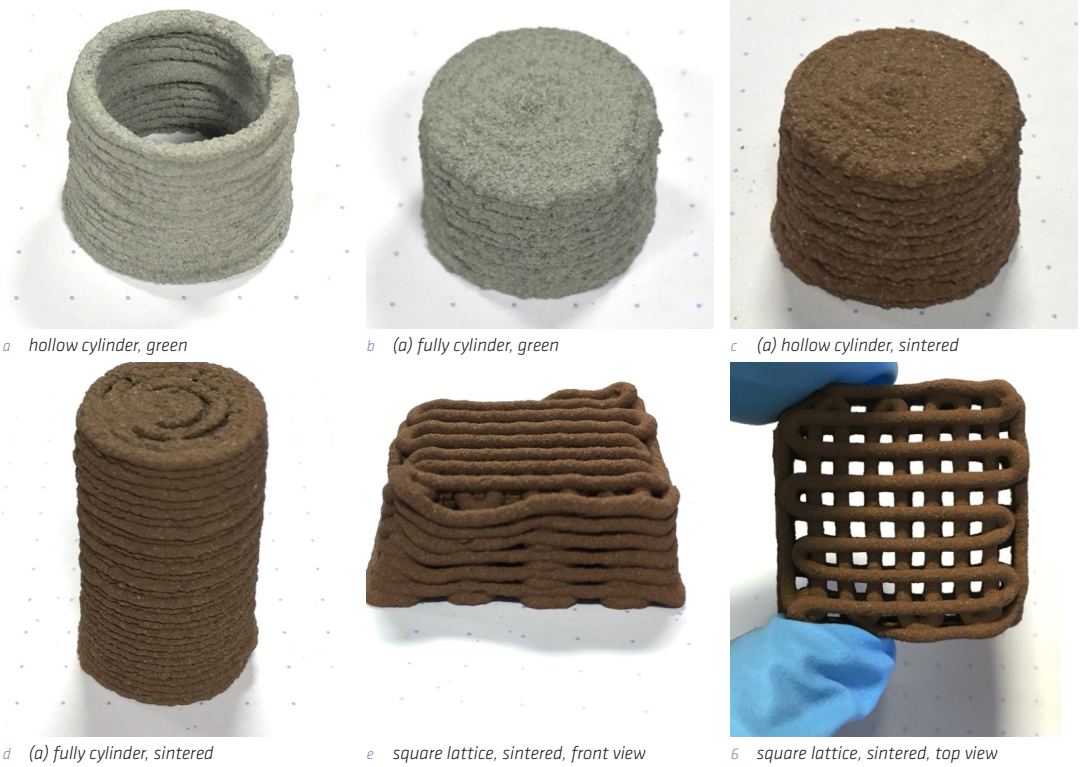

*a* hollow cylinder, green

*b* (a) fully cylinder, green

*c* (a) hollow cylinder, sintered

*d* (a) fully cylinder, sintered

*e* square lattice, sintered, front view

*6* square lattice, sintered, top view

FIGURE 3 Parts produced by direct ink writing of regolith simulant slurry (distance between the dots is 10 mm)

Figure 3 (e) & (f) shows a 3D printed lattice structure after sintering, the dispersion used being low additive ('LA') with SA as a binder. It can be seen that the structure has collapsed at the unsupported sections, creating a defect along the side that progressively worsens. However, this collapse had little influence on the actual inner grid structure, which retained its shape relatively well, as seen in the figure. It should be noted that for the commonly used thermoplastic fused filament fabrication (FFF) process, overhangs exceeding 45° are generally not printed without the use of a support structure, and it should therefore not be surprising to observe that the dispersion used here is unable to support 90° overhangs. If a finer grid had been printed, it is possible that the structure would be able to support itself, as can already be observed in certain places.

Figure 3 (d) depicts a 3D-printed cylinder that is 33.8 mm tall created with the 'LA' dispersion using SA. As demonstrated by this structure, solid objects exhibit structural integrity both during and after printing. The gaps seen at the top are believed to be due to dispersion shrinkage after deposition as water evaporates. A way to compensate for this would be to use a line width during printing that is slightly less than the nozzle diameter, e.g. 1.8–1.9 mm instead of the 2 mm used here.
An observation when using the 'HA' concentration of sodium alginate to print a set of rectangular objects was that a crack evolved in all the objects along the same direction on the underside that was in contact with the ceramic build plate. These cracks were noticed after the drying period of 72 h, and it is therefore not known when they developed as the underside of the samples were not visible until the objects were turned, but this is likely due to the drying process.

A possible explanation for this behaviour is that the outer surface of the objects dries at a higher rate than the inside of the objects. As water evaporates, the volume of the item will decrease, and this shrinkage will be more pronounced at the outer edges of the samples. If the object is relatively stiff, as noticed when using the 'HA' concentration, the parts of the sample with a less pronounced shrinkage (i.e., the inner regions) will 'resist' this shrinkage, and the tension arising in the sample will give rise to the observed crack. No cracks were observed in samples prepared using the 'LA' concentration, and it is believed that the reduced stiffness or rigidity of the 'LA' concentration creates less build-up of tension in the samples during the drying process compared to the 'HA' concentration, or that the tension is more easily dissipated in the 'LA' concentration samples. Another explanation could be the difference in liquid-to-powder ratio between 'LA' and 'HA' concentrations, as this will affect the capillary action – i.e., the transport of the liquid phase – and porosity in the material. In any case, this observation suggests that there is an upper limit to the amount of additive that should be used, which is below the value at which the dispersion still shows good printability during the AM process, as was the case for the high additive concentration slurry used here.

It is likely that the direct ink writing process – due to the use of a liquid phase – inevitably will produce relatively loosely packed samples, at least when compared to other green body preparation processes such as compaction through an external force. There is a risk that this porosity will have a detrimental effect on the sintering step. This might be mitigated by reducing the non-solid mass of the slurry as much as possible, i.e., by optimising the dispersion with regards to a low water content. Still, the achievement of dense ceramic bodies has been reported for the DIW process (Rueschhoff et al., 2016).

## Sintering

Figure 3 (a) & (b) show the same 3D-printed solid cylinder before and after sintering, using the 'LA' dispersion and SA as an additive. There is little observable difference between the two, with the noticeable exception of hematite formation, which takes place during sintering in an oxygen rich

environment and gives rise to the observed reddish-brown colour (Zocca et al., 2020). If regolith is sintered under oxygen-deprived conditions – e.g. vacuum – the objects retain their greyish colour (Taylor et al., 2018)"ISSN":"00945765","abstract":"The development of in situ fabrication methods for the infrastructure required to support human life on the Moon is necessary due to the prohibitive cost of transporting large quantities of materials from the Earth. Cellular structures, consisting of a regular network (truss.

No significant densification of the samples was observed in this work as the items retained most of their initial volume after sintering. Small dimensional deviations in the sample made it difficult to determine its volume with a sufficient degree of accuracy when using a hand measuring tool. Otherwise, if the volume was known, it would be possible to determine the degree of densification during sintering.

A comparison that was performed of the mechanical strength between a sintered and an unsintered sample under compression with a hand tool suggests that the strength of the sintered sample is only slightly higher than that of the unsintered sample. An explanation for this could be a less-than-optimal sintering process. It might be tempting to view the colour change of the samples as a sign of successful sintering, but hematite formation is already significant at temperatures around 850 °C, well below the reported sintering start at 1091 °C for particles with a diameter of 100 µm or smaller (Zocca et al., 2020). As the sintering temperature reached for this work – 1080 °C – is less than the reported sintering start, and also considering that the grain size distribution for the samples prepared in this work range between 20–1000 µm, i.e. containing particles larger than 100 µm, it is reasonable to believe that the sintering was limited in its effect, if it even took place at all.

The heat rate of the sintering protocol (not only the temperature) is also expected to influence the mechanical properties of the sintered objects. Here, a heat rate of 5 K/min was chosen for the initial drying and debinding steps. The choice of this heat rate was motivated by reported heat rates for sintering of regolith material found in the literature (Taylor et al., 2018; Zocca et al., 2020)"ISSN":"00945765","abstract":"The development of in situ fabrication methods for the infrastructure required to support human life on the Moon is necessary due to the prohibitive cost of transporting large quantities of materials from the Earth. Cellular structures, consisting of a regular network (truss. Decreasing the heat rate during sintering will allow for a more uniform heating and cooling of the object, which in turn reduces the risk of crack formation during sintering due to temperature gradients in the material. It might be beneficial to the mechanical strength of the objects to reduce the heat rate even further than was done in this work, although there is likely to be a trade-off between mechanical strength and considerations associated with an increased processing time such as cost and practicability.

It should also be expected that the complex mineralogy found within regolith will give rise to complex melting behaviour (Meurisse et al., 2017). Certain minerals – or additives – in the material, having different melting temperatures than that of the rest of the matrix, could give rise to liquid phase sintering of the material. This in turn might facilitate the densification of a porous sample, as the liquid phase is able to penetrate voids in the sample.

## SEM

The SEM analysis was performed on the cross section of a sintered rectangular sample manufactured using the 'LA' concentration of sodium alginate. The images obtained at magnifications of x100, x500, and x1000 can be seen in Figure 4. Figure 4 (a) displays a low magnification image of the sample, illustrating the heterogeneous nature of the material, with particles visible in a variety of shapes and sizes, the largest of

them appearing to be about 200 µm. As mentioned previously, the EAC-1A feedstock material used has a grain size range of 0.02-1.0 mm. The apparent absence of >200 µm grains can be explained by the grinding that occurs during slurry preparation, done with a pestle and mortar. It is proposed that this leads to the 0.2-1.0 mm grains being broken down into smaller grains <200 µm.

We also observe high porosity in the sample, which can further be seen in Figure 4 (b), taken at a higher magnification. Again, a large spread in particle sizes and shapes is observed, and the sample may be classified as being highly porous due to the significant amount of void space between particles, as seen in the figure. It is possible that a finer particle size of the material than that used here would allow a higher degree of close packing of particles, which in turn would facilitate sintering as discussed previously. Furthermore, an increase in solid phase during slurry preparation – i.e. a reduced water content – might lead to a denser sample, as the void volume that is observed here is likely to previously have been occupied by the gel-phase that is evaporated during the drying and sintering stages.

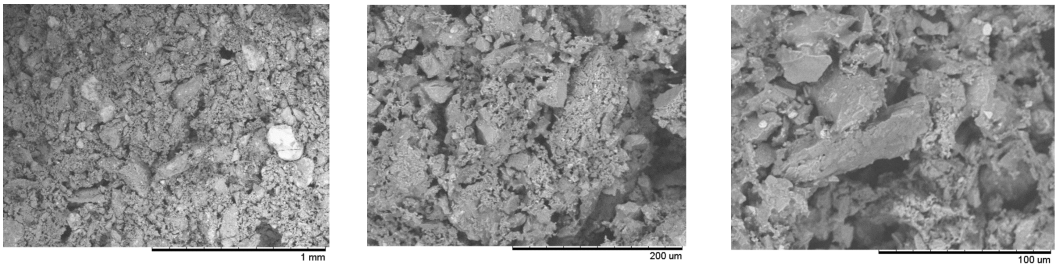


*a Sample section at x100 magnification* *b Sample section at x500 magnification* *c Sample section at x1000 magnification*

FIGURE 4 SEM analysis of sintered 'LA' sample produced by DIW.

In Figure 4 (c), jagged particle shapes can be observed throughout the sample; it is not clear whether this is a result of the slurry preparation step, or a property of the stock material, even though it is reasonable to believe that the pestling during the slurry preparation would influence particle morphology. The average sphericity F for the material has been reported as being in the range 0.59–0.60 F, where a sphere equals unity, indicating a moderate sphericity for the stock material (Engelschiøn et al., 2020).

## Compression testing

Sintered solid cylinder samples such as the one shown in Figure 3 (a) & (b) above were used for compression testing. Four samples with an average diameter of 18.5 mm and an average height of 14.6 mm were tested. During the initial phase of the test, the load was concentrated on surface irregularities on the top of the samples; as these gave way, the load was spread evenly over the top surface of the cylinder. Before reaching the recorded maximum load of each test, cracks were observed that propagated throughout the samples. An example of a force/displacement curve obtained is shown in Figure 5.

The average value for the compressive strength of the samples was recorded to be 2.4 Mpa, with a standard deviation of 0.2 MPa. Compared with the values in Table 1, the compressive strength in this work is about one order of magnitude less than what is commonly reported. As discussed previously, it is believed that less-than-optimal sintering was achieved during our experiments, which would explain the low value for compressive strength.

An average value for the Young's modulus of the samples was calculated to be 36.8 MPa, with a standard deviation of 10.9 MPa. This value was calculated from the measured peak force and associated displacement at the end of the linear region of the plot. However, this value is not believed to be an accurate representation of the material's Young modulus. Indeed, it is proposed that the linear region of the plot does not correspond to an elastic compression of the sample (associated with Young's modulus), but is due to the progressive compaction of the sample through local rupture of the weak inter-grain links. This mechanism explains the low value obtained, as well as the discontinuities that can be observed in the linear region, resulting from non-homogenous compaction of the sample.

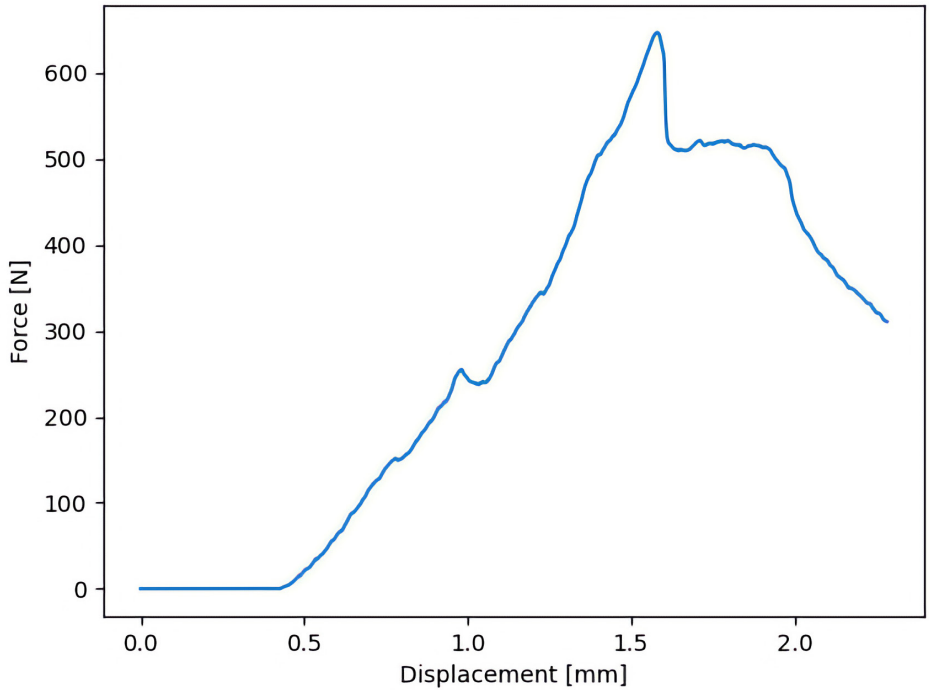


FIGURE 5 Force vs displacement curve measured during compressive testing of sample 2.

## Conclusions

A new approach to additive manufacturing using regolith simulant as feedstock in the form of the direct ink writing process was proposed, in which an extrudable dispersion is prepared with regolith simulant, water, and a binding additive. Two such binding additives were identified – sodium alginate and methyl cellulose – and the feasibility of the DIW process was demonstrated through the manufacture of objects with varying geometries.

The compressive strength for sintered samples produced with this method was measured to be 2.4 MPa with a standard deviation of 0.2 MPa (n = 4), which is about one order of magnitude less than what is typically reported in the literature. It is believed that a non-ideal sintering process was carried out in this work. This is supported by the results from the SEM analysis, showing a highly porous inner structure of the sintered samples.

The main advantage of the proposed process is that it only uses resources which can be produced in situ on the lunar surface. Regolith and water can be sourced locally, while the additives can be produced in bio-reactors. Furthermore, the proposed process only requires a small amount of additives (about 1 wt.%) and only uses non-toxic additives.

The comparatively low compressive strength observed for the parts produced with this process limits its usefulness for manufacturing structures or functional parts. However, there are applications that could benefit from the ability of the produced parts to maintain their shape while being relatively fragile. A good example of this would be mould production for metal casting in a lunar environment. Using the presented approach, complex and diverse mould geometries could be printed on-demand using only local resources. Those moulds could then be used to produce casted metal parts, for example from recycled aluminium.

The next steps to develop this process further will focus on increasing both the compressive strength and geometrical accuracy of the parts produced. Optimizing the sintering procedure in terms of temperatures and durations should allow for more complete sintering and therefore higher mechanical strength.
In addition, improving the extrusion parameters, such as the extrusion pressure and positioning accuracy, should allow the green bodies to have more precise and finer geometrical features. This could also increase the density of the green bodies, leading again to improved sintering behaviour.

## References


Allan, S., Braunstein, J., Baranova, I., Vandervoort, N., Fall, M., & Shulman, H. (2013). Computational modeling and experimental microwave processing of JSC-1A lunar simulant. *Journal of Aerospace Engineering*. https://doi.org/10.1061/(ASCE)AS.1943-5525.0000245

Anand, M., Crawford, I. A., Balat-Pichelin, M., Abanades, S., Van Westrenen, W., Péraudeau, G., Jaumann, R., & Seboldt, W. (2012). A brief review of chemical and mineralogical resources on the Moon and likely initial in situ resource utilization (ISRU) applications. *Planetary and Space Science*, *74*(1), 42–48. https://doi.org/10.1016/j.pss.2012.08.012

Balla, V. K., Roberson, L. B., O'Connor, G. W., Trigwell, S., Bose, S., & Bandyopadhyay, A. (2012). First demonstration on direct laser fabrication of lunar regolith parts. *Rapid Prototyping Journal*, *18*(6), 451–457. https://doi.org/10.1108/13552541211271992

Buchner, C., Pawelke, R. H., Schlauf, T., Reissner, A., & Makaya, A. (2018). A new planetary structure fabrication process using phosphoric acid. *Acta Astronautica*, *143*(June 2017), 272–284. https://doi.org/10.1016/j.actaastro.2017.11.045

Caprio, L., Demir, A. G., Previtali, B., & Colosimo, B. M. (2020). Determining the feasible conditions for processing lunar regolith simulant via laser powder bed fusion. *Additive Manufacturing*, *32*(July 2019), 101029. https://doi.org/10.1016/j.addma.2019.101029

Cesaretti, G., Dini, E., De Kestelier, X., Colla, V., & Pambaguian, L. (2014). Building components for an outpost on the Lunar soil by means of a novel 3D printing technology. *Acta Astronautica*, *93*, 430–450. https://doi.org/10.1016/j.actaastro.2013.07.034

Colaprete, A., Schultz, P., Heldmann, J., Wooden, D., Shirley, M., Ennico, K., Hermalyn, B., Marshall, W., Ricco, A., Elphic, R. C., Goldstein, D., Summy, D., Bart, G. D., Asphaug, E., Korycansky, D., Landis, D., & Sollitt, L. (2010). Detection of water in the LCROSS ejecta plume. *Science*, *330*(6003), 463–468. https://doi.org/10.1126/science.1186986

Dai, L., Cheng, T., Duan, C., Zhao, W., Zhang, W., Zou, X., Aspler, J., & Ni, Y. (2019). 3D printing using plant-derived cellulose and its derivatives: A review. *Carbohydrate Polymers*, *203*(March 2018), 71–86. https://doi.org/10.1016/j.carbpol.2018.09.027

Engelschiøn, V. S., Eriksson, S. R., Cowley, A., Fateri, M., Meurisse, A., Kueppers, U., & Sperl, M. (2020). EAC-1A: A novel large-volume lunar regolith simulant. *Scientific Reports*, *10*(1), 1–9. https://doi.org/10.1038/s41598-020-62312-4

Faierson, E. J., Logan, K. V., Stewart, B. K., & Hunt, M. P. (2010). Demonstration of concept for fabrication of lunar physical assets utilizing lunar regolith simulant and a geothermite reaction. *Acta Astronautica*, *67*(1–2), 38–45. https://doi.org/10.1016/j.actaastro.2009.12.006

Fateri, M., & Gebhardt, A. (2015). Process parameters development of selective Laser Melting of lunar regolith for on-site manufacturing applications. *International Journal of Applied Ceramic Technology*, *12*(1), 46–52. https://doi.org/10.1111/ijac.12326

Goulas, A., & Friel, R. J. (2016). 3D printing with moondust. *Rapid Prototyping Journal*, *22*(6), 864–870. https://doi.org/10.1108/RPJ-02-2015-0022

Goulas, A., Harris, R. A., & Friel, R. J. (2016). Additive manufacturing of physical assets by using ceramic multicomponent extra-terrestrial materials. *Additive Manufacturing*, *10*, 36–42. https://doi.org/10.1016/j.addma.2016.02.002

Hart, K. R., Frketic, J. B., & Brown, J. R. (2018). Recycling meal-ready-to-eat (MRE) pouches into polymer filament for material extrusion additive manufacturing. *Additive Manufacturing*, *21*(February), 536–543. https://doi.org/10.1016/j.addma.2018.04.011

Hinterman, E. (2020). Simulating oxygen production on Mars for the Mars Oxygen In-Situ Resource Utilization Experiment. *Acta Astronautica*, *170*(October 2019), 678–685. https://doi.org/10.1016/j.actaastro.2020.02.043

ISO/ASTM. (2015). INTERNATIONAL STANDARD ISO / ASTM 52900 Additive manufacturing – General principles – Terminology. *International Organization for Standardization*. https://doi.org/10.1520/ISOASTM52900-15

Jakus, A. E., Koube, K. D., Geisendorfer, N. R., & Shah, R. N. (2017). Robust and Elastic Lunar and Martian Structures from 3D-Printed Regolith Inks. *Scientific Reports*, *7*, 1–8. https://doi.org/10.1038/srep44931

Jakus, A. E., Taylor, S. L., Geisendorfer, N. R., Dunand, D. C., & Shah, R. N. (2015). Metallic Architectures from 3D-Printed Powder-Based Liquid Inks. *Advanced Functional Materials*, *25*(45), 6985–6995. https://doi.org/10.1002/adfm.201503921

Lewis, J. A., Smay, J. E., Stuecker, J., & Cesarano, J. (2006). Direct ink writing of three-dimensional ceramic structures. *Journal of the American Ceramic Society*, *89*(12), 3599–3609. https://doi.org/10.1111/j.1551-2916.2006.01382.x

Liu, Q., Li, Q., Xu, S., Zheng, Q., & Cao, X. (2018). Preparation and properties of 3D printed alginate-chitosan polyion complex hydrogels for tissue engineering. *Polymers*, *10*(6). https://doi.org/10.3390/polym10060664

Menezes, A. A., Cumbers, J., Hogan, J. A., & Arkin, A. P. (2015). Towards synthetic biological approaches to resource utilization on space missions. *Journal of the Royal Society Interface*, *12*(102). https://doi.org/10.1098/rsif.2014.0715

Meurisse, A., Makaya, A., Willsch, C., & Sperl, M. (2018). Solar 3D printing of lunar regolith. *Acta Astronautica*, *152*(September), 800–810. https://doi.org/10.1016/j.actaastro.2018.06.063

Meurisse, A., Beltzung, J.C., Kolbe, M., Cowley, A., & Sperl, M. (2017). Influence of Mineral Composition on Sintering Lunar Regolith. *Journal of Aerospace Engineering*. 30. 04017014. https://doi.org/10.1061/(ASCE)AS.1943-5525.0000721

Montes, C., Broussard, K., Gongre, M., Simicevic, N., Mejia, J., Tham, J., Allouche, E., & Davis, G. (2015). Evaluation of lunar regolith geopolymer binder as a radioactive shielding material for space exploration applications. *Advances in Space Research*, *56*(6), 1212–1221. https://doi.org/10.1016/j.asr.2015.05.044

Nieke, P., Kita, J., Häming, M., & Moos, R. (2019). Manufacturing dense thick films of lunar regolith simulant EAC-1 at room temperature. *Materials*, *12*(3). https://doi.org/10.3390/ma12030487

Perrot, A., Rangeard, D., & Courteille, E. (2018). 3D printing of earth-based materials: Processing aspects. *Construction and Building Materials*, *172*, 670–676. https://doi.org/10.1016/j.conbuildmat.2018.04.017

Pilehvar, S., Arnhof, M., Pamies, R., Valentini, L., & Kjøniksen, A. L. (2020). Utilization of urea as an accessible superplasticizer on the moon for lunar geopolymer mixtures. *Journal of Cleaner Production*, *247*. https://doi.org/10.1016/j.jclepro.2019.119177

Rueschhoff, L., Costakis, W., Michie, M., Youngblood, J., & Trice, R. (2016). Additive Manufacturing of Dense Ceramic Parts via Direct Ink Writing of Aqueous Alumina Suspensions. *International Journal of Applied Ceramic Technology*, *13*(5), 821–830. https://doi.org/10.1111/ijac.12557

Schleppi, J., Gibbons, J., Groetsch, A., Buckman, J., Cowley, A., & Bennett, N. (2019). Manufacture of glass and mirrors from lunar regolith simulant. *Journal of Materials Science*, *54*(5), 3726–3747. https://doi.org/10.1007/s10853-018-3101-y

Schlordt, T., Schwanke, S., Keppner, F., Fey, T., Travitzky, N., & Greil, P. (2013). Robocasting of alumina hollow filament lattice structures. *Journal of the European Ceramic Society*, *33*(15–16), 3243–3248. https://doi.org/10.1016/j.jeurceramsoc.2013.06.001

Sherwood, B. (2019). Principles for a practical Moon base. *Acta Astronautica*, *160*(March), 116–124. https://doi.org/10.1016/j.actaastro.2019.04.018

Song, L., Xu, J., Fan, S., Tang, H., Li, X., Liu, J., & Duan, X. (2019). Vacuum sintered lunar regolith simulant: Pore-forming and thermal conductivity. *Ceramics International*, *45*(3), 3627–3633. https://doi.org/10.1016/j.ceramint.2018.11.023

Tang, S., Yang, L., Li, G., Liu, X., & Fan, Z. (2019). 3D printing of highly-loaded slurries via layered extrusion forming: Parameters optimization and control. *Additive Manufacturing*, *28*(February), 546–553. https://doi.org/10.1016/j.addma.2019.05.034

Taylor, S. L., Jakus, A. E., Koube, K. D., Ibeh, A. J., Geisendorfer, N. R., Shah, R. N., & Dunand, D. C. (2018). Sintering of micro-trusses created by extrusion-3D-printing of lunar regolith inks. *Acta Astronautica*, *143*(September 2017), 1–8. https://doi.org/10.1016/j.actaastro.2017.11.005

Taylor, S. L., Jakus, A. E., Shah, R. N., & Dunand, D. C. (2017). Iron and Nickel Cellular Structures by Sintering of 3D-Printed Oxide or Metallic Particle Inks. *Advanced Engineering Materials*, *19*(11). https://doi.org/10.1002/adem.201600365

Toutanji, H. A., Evans, S., & Grugel, R. N. (2012). Performance of lunar sulfur concrete in lunar environments. *Construction and Building Materials*, *29*, 444–448. https://doi.org/10.1016/j.conbuildmat.2011.10.041

Way, J. C., Silver, P. A., & Howard, R. J. (2011). Sun-driven microbial synthesis of chemicals in space. *International Journal of Astrobiology*, *10*(4), 359–364. https://doi.org/10.1017/S1473550411000218

Xu, J., Cao, H., Sun, X., Tang, H., Ma, H., Song, L., Li, X., Duan, X., & Liu, J. (2019). *3D printing of hypothetical brick by selective laser sintering using lunar regolith simulant and ilmenite powders*. *1084208*(February 2019), 9. https://doi.org/10.1117/12.2505911

Zocca, A., Fateri, M., Al-Sabbagh, D., & Günster, J. (2020). Investigation of the sintering and melting of JSC-2A lunar regolith simulant. *Ceramics International*, *February*, 0–1. https://doi.org/10.1016/j.ceramint.2020.02.212

# Combined Airborne Wind and Photovoltaic Energy System for Martian Habitats

**Lora Ouroumova, Daan Witte, Bart Klootwijk, Esmée Terwindt, Francesca van Marion, Dmitrij Mordasov, Fernando Corte Vargas, Siri Heidweiller, Márton Géczi, Marcel Kempers, Roland Schmehl** [1]

[1] *Delft University of Technology*
*Faculty of Aerospace Engineering*
*Delft, the Netherlands*

## Abstract

Generating renewable energy on Mars is technologically challenging. Firstly, because, compared to Earth, key energy resources such as solar and wind are weak as a result of very low atmospheric pressure and low solar irradiation. Secondly, because of the harsh environmental conditions, the required high degree of automation, and the exceptional effort and cost involved in transporting material to the planet. Like on Earth, it is crucial to combine complementary resources for an effective renewable energy solution. In this work, we present the results of a design synthesis exercise, a 10 kW microgrid solution, based on a pumping kite power system and photovoltaic solar modules to power the construction and subsequent use of a Mars habitat. To buffer unavoidable energy fluctuations and balance seasonal and diurnal resource variations, the two energy systems are combined with a compressed gas storage system and lithium-sulphur batteries. The airborne wind energy solution was selected because of its low weight-to-wing-surface-area ratio, compact packing volume, and high capacity factor which enables it to endure strong dust storms in an airborne parking mode. The surface area of the membrane wing is 50 $m^2$ and the mass of the entire system, including the kite control unit and ground station, is 290 kg. The performance of the microgrid was assessed by computational simulation using available resource data for a chosen deployment location on Mars. The projected costs of the system are €8.95 million, excluding transportation to Mars.

## Keywords

Mars, Renewable Energy, Airborne Wind Energy, Kite Power, Microgrid, Solar Energy, Photovoltaics, Space Systems Engineering

## DOI

https://doi.org/10.7480/spool.2021.2.6058

## Introduction

Several governmental space agencies and private corporations have proposed human missions to Mars with the goal of establishing a habitat. Because such missions are extremely costly and transportation capacity is limited, in-situ material and energy utilization will be crucial (Horneck et al, 2003). The environmental conditions on Mars, and thus the renewable energy sources, differ substantially from those on Earth. For example, surface temperatures range from -140 to 30 degrees Celsius, surface pressure is more than 100 times less compared to Earth, and the solar irradiance is only 43 percent of that on Earth (Williams, 2020). Solar irradiance is reduced further by strong seasonal dust storms (Fraser, 2009). Wind speeds, on the other hand, can be higher than on Earth. At the Viking landing sites, the wind speeds varied between 2 to 7 m/s during summer, 5 to 10 m/s during fall and 17 to 30 m/s during dust storms, resulting in an average of 10 m/s (Boumis, 2017). The main impeding effect of the dust storms is the irradiation on solar panels, rather than the corrosive effect (Mersmann, 2015). As on Earth, natural energy sources vary across shorter (minute, hour, and day) and longer (year) time scales. For that reason, any renewable energy system on Mars would ideally use complementary types of energy and combine these with energy storage solutions. Yet, it is not only these resource characteristics that make energy harvesting on Mars challenging, but also the required high degree of automation and the aggressive environment created by the dust storms, the intense cosmic ionising and solar radiation, and extreme temperatures and associated fluctuations.

The use of wind energy on Mars was analysed by Haslach (1989), who concluded that despite the low density of the Martian atmosphere, wind speeds are high enough to make wind energy competitive with nuclear power in terms of power produced per unit mass. He proposed the design of a mobile and lightweight vertical axis wind turbine, but also identified the variability of the wind as a critical point that would deserve further attention. An extensive study on utilizing local material and energy sources for a Martian outpost was presented by James et al (1998), covering geothermal, solar, and wind resources and confirming that the exploitation of wind power would be feasible. Bluck (2001) investigated the combined use of solar and wind energy systems to power a sustainable Mars base, suggesting using modified cold-weather wind turbines to cover for the lacking solar power during month-long Martian global dust storms. Delgado-Bonal et al (2016) on the other hand, came to the conclusion that the use of wind power on Mars is ineffective, due to insufficient wind speeds. A lightweight, horizontal-axis wind turbine was proposed by Holstein-Rathlou et al (2018) and tested in a wind tunnel in a simulated Martian atmospheric environment. A very similar, rapidly deployable turbine concept has been developed commercially by the Danish start-up KiteX, promising a power-to-mass ratio of 75 W/kg at a wind speed of 7.5 m/s (KiteX, 2020).

A further reduction of the structural mass required to harvest wind energy can be achieved by airborne wind energy systems. The innovative technology is based on tethered flying devices, either combining onboard wind turbines with a conducting tether, or converting the pulling power of the flying devices with ground-based generators (Schmehl, 2019). Another advantage, besides the reduced mass, is that the flight operation of the systems can be adjusted continuously to the available wind resource, by which the capacity factor can be maximized for a given wind profile (Bechtle et al, 2019). Major advances in automatic flight control over the past two decades have contributed to the commercial development of airborne wind energy for terrestrial applications (Vermillion et al, 2020) and a number of different implementations have reached the prototype stage (Nelson, 2020). Within this context, researchers from NASA have proposed using kites for wind energy harvesting on Mars (Silberg, 2012). A factor supporting the operation of airborne wind energy systems on Mars, where aerodynamic forces are generally much lower than on Earth, is the lower gravity.

In this paper, we present a hybrid wind-solar energy system to power the construction and subsequent use of a subsurface Mars habitat. The central component of this microgrid is an airborne wind energy system

based on a remote-controlled flexible membrane wing operated in pumping cycles. The 20 kW demonstrator system that has been developed at TU Delft for terrestrial applications is illustrated in Figure 1.

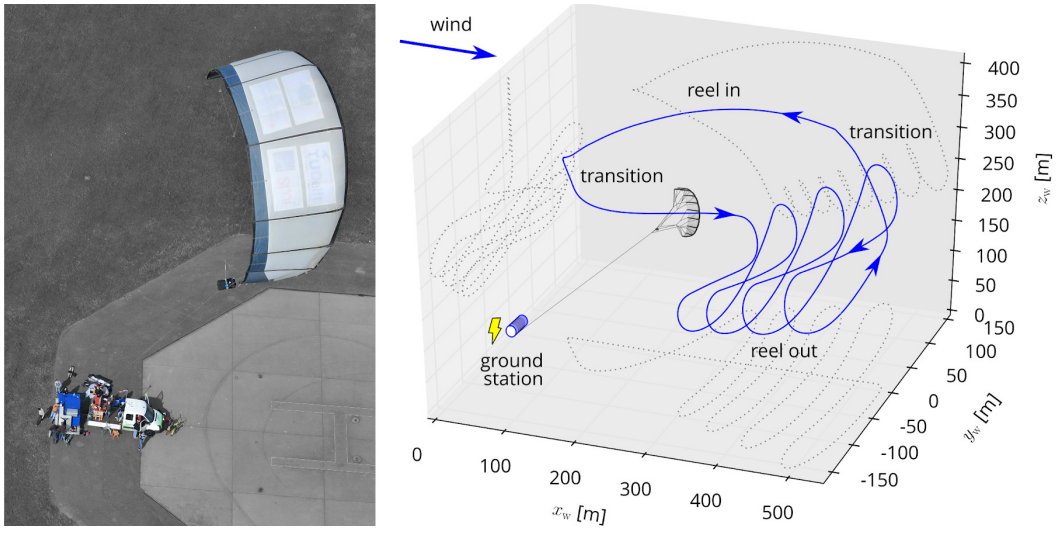


FIGURE 1 Kite power system of TU Delft in operation and simulated pumping cycle (Fechner, 2016).

During transport, the inflatable lightweight wing can be packed into a compact volume. The generator has a nominal power of 18 kW and produces an average electrical output of about 7 kW in good wind conditions (Van der Vlugt, 2013). This power is sufficient for about 14 Dutch households. To adapt the system to the lower atmospheric density on Mars, the wing surface area has been increased. The sizing and design of the kite power system is based on a validated performance model (Van der Vlugt, 2019). The complete microgrid solution also includes photovoltaic (PV) modules and electrical storage to buffer in periods of low wind.

The paper summarizes the results of a design synthesis exercise conducted at the Faculty of Aerospace Engineering of TU Delft (Corte Vargas et al, 2020), which succeeded the submission of a proposal to an ESA ideas competition (Bier, 2019). The key contribution of this work is a performance analysis of the combined airborne wind energy and photovoltaic renewable energy solution, accounting for the demand and resource profiles and the coupling of all subsystems. Because little quantitative information about the energy consumption needed for the robotic construction of the habitat was available at the time of the study, the design of the microgrid mainly covers the usage period of the habitat. It is planned to also integrate the construction phase in a future study. The paper is structured as follows. First, the site for the habitat is selected and the entire mission outlined. Then, the energy system architecture and energy demand of the habitat are defined. Following that, the performance of the energy system is analysed and the design of the microgrid concretized. Subsequent sections detail the sizing of the airborne wind energy subsystem, the solar energy subsystem, and the storage solution. Finally, the power management and distribution system are described, followed by conclusions.

## Site and Mission

The siting of the habitat needs to account for several requirements. For one, the basic requirements for a manned mission have to be fulfilled, such as the availability of water and a maximum allowed elevation for landing of -1000 m MOLA (Mars Orbiter Laser Altimeter) (Chen, 2014). This elevation limit ensures

sufficiently high aerodynamic drag for the braking of the entry module. In addition, the underground has to be suitable for the excavation of the subsurface structures of the planned habitat. Finally, the site must also provide for reasonably good renewable energy sources. Areas on Mars where useful resources for an Earth-independent human settlement are present had already been explored systematically in previous research, for example, by James et al (1998). For this project, the site selection started with seven sites chosen from the first round of the NASA landing site selection workshops (NASA, 2020) and from the known SpaceX landing site candidates for its upcoming Mars Starship mission (Foust, 2017). Key selection criteria were the availability of water ice, low elevation, and the possibility of in situ resource utilization (ISRU), with the presence of usable water being the most crucial one. Based on this preselection, a detailed trade-off was conducted, and the Dichotomy Boundary Deuteronilus Mensae (DBDM) exploration zone (EZ) identified as the most suitable landing site. This circular area with a radius of 100 km and centred at 39.11°N 23.199°E is located at the southern border of the Deuteronilus Mensae region (Head et al, 2015). It is at an elevation of -4000 m MOLA, surrounded by cliffs and ridges at higher elevations, and possibly the remains of a northern low-lands ocean. The terrain features expose all three major geological eras including various rock samples as well as climate and possible glacial ice history. Continuous water ice is located in high concentrations 10-15 m below the surface (Plaut, 2009) and there is an abundant supply of materials that can be used for ISRU and in-space manufacturing (ISM) to construct the habitat (Rummel et al, 2014). Even though solar and wind resources are scarcer in the northern polar region than around the equator, it was concluded that the presence of water and a low elevation were key criteria for the habitat.

The mission starts by launching and deploying the cargo needed for the construction of the habitat. In addition, the servicing orbiter and the Mars Ascent Vehicle (MAV) are sent to Mars. The main goal of the orbiter is to produce, assemble, and perform maintenance on larger-than-payload structures, as well as serving as a gateway between Earth and Mars. The MAV is designed for traveling repeatedly from the Martian surface to orbit and back. Following this preparation phase, the first crew lands to initialize the deployment and installation of the energy system. Once this system is generating sufficient energy, the construction and subsequent operation of the habitat is begun. The energy system will then provide renewable energy to the habitat for a lifespan of 5 Martian years throughout the different seasons, varying between using wind and solar energy as the main source of energy. Finally, after the end-of-life of the energy system has been reached, the system can be retired and its different components disposed of either on Mars or by sending them back to Earth.

## Energy System Architecture and Performance

The hybrid architecture of the energy system is illustrated in Figure 2, highlighting the connections and interfaces between the subsystems and the external links to the environment, habitat, and maintenance system. The five main components are the power management system, the energy storage system, the central control system, and the two energy generation subsystems. The primary generation subsystem is based on wind energy, using a flying kite to convert the kinetic energy of the wind into a resultant aerodynamic force and corresponding tether force, which are further converted by the ground-based reeling mechanism and connected generator into shaft power and electrical power, respectively (see Figure 1). The subsystem is equipped with its own control unit and super-capacitor to balance the energy production and consumption phases of the pumping cycles. Solar PV technology is considered as a secondary generation subsystem, having been used successfully for earlier Mars missions (Delgado-Bonal et al, 2016). The subsystem is equipped with dust protection and tilting mechanisms to minimize losses and ensure the best incidence angle of the radiation. The energy storage system includes short-term storage, using lithium-sulphur batteries to cover the nights, and long-term storage, using CO2 compressed into

underground cavities to cover months with lower resource availability. Carbon dioxide makes up roughly 95% of the Martian atmosphere and the analysis showed that its use for compressed air energy storage (CAES) met the long-term energy storage requirements of the mission. The power management system handles the energy flows from the generation subsystems to the storage system and the habitat. The various configurations of the power distribution subsystem are evaluated and a thorough trade-off resulted in a direct current (DC) microgrid as the most suitable option. The electrical infrastructure is elaborated in section 3.5. The central control system manages the communication of all system components, ensuring the proper functioning of all components.

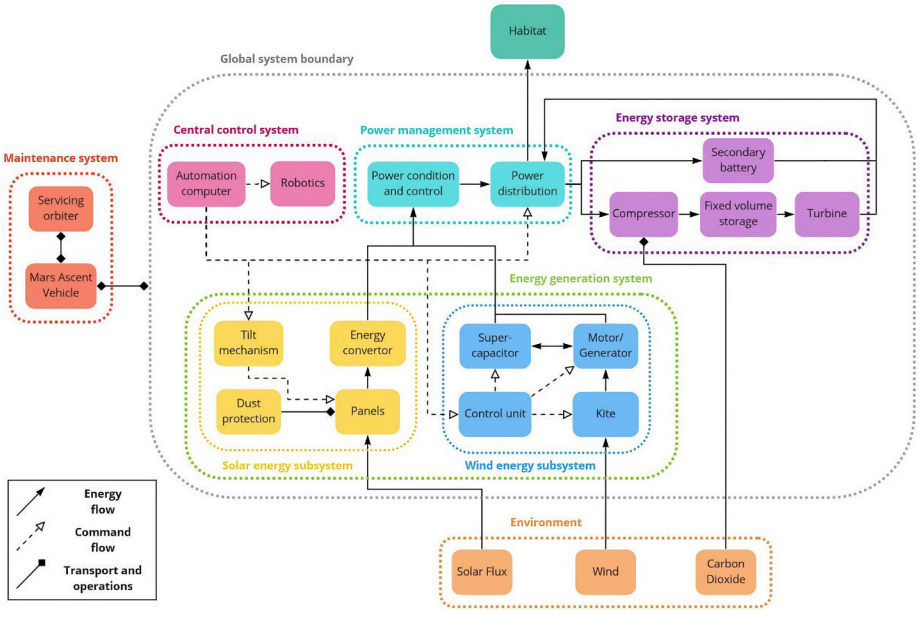


FIGURE 2 Architecture and interfacing of the entire renewable energy system. Schematic from Corte Vargas et al (2020).

The design of the energy system depends on the energy demand profile of the habitat, the performance of the microgrid (including the conversion performances of the PV modules and the kite power system), and the availability of the respective energy resources. To determine the energy demand of the habitat, we note that the electrical energy consumption of humans is generally irregular as a result of varying daily activities. Previous research indicates that the mental and physical health of the crew is best maintained throughout the entire mission by adhering to a regular schedule, which helps the human circadian rhythm to remain synchronized with the day-night cycle on Earth (Horneck et al, 2003; Basner, 2013) To aid human adaptation and to ease time keeping, a time-keeping scheme with days of 24 hours of equal length is considered. Every hour consists of 60 equally long minutes and each minute is also composed of 60 seconds. However, a second on Mars is approximately 1.0275 times longer than on Earth. Work and rest periods with different power consumption are distinguished. While work periods require an average of 10 kW for scientific and domestic activities on top of the basic energy requirements of the habitat, rest periods require less power for maintaining basic habitat activities and covering the base loads of the life-support systems. Examining and interpreting data from experiments in the Hawaii Space Exploration Analog and Simulation (HI-SEAS) habitat (Barnard et al, 2019; Engler, 2017; Engler et al, 2019), we propose a schedule alternating between 14 Martian work hours, lasting from 9am until 11pm, and 10 rest hours with energy requirements of 10 kW and 5 kW, respectively. This leads to a constant daily energy demand of 190 kWh[1].

1 Energy units kWh and MWh refer to Martian hours

## Performance Model

With the energy demand of the habitat established, the design of the energy system can be determined in multiple iterations between the actual design specification of the five subsystems and the expected performance levels to meet this demand. The process also yields how much of the generated energy is directly used to cover the demand and how much of it is used for short- and long-term storage to cover later periods of demand. This performance analysis is based on a computational model of the energy system, which is programmed in Python and which accounts for the performance characteristics and efficiencies of all system components included in Figure 2. The iterative procedure is required to account for the various interdependencies between system components. For example, the microgrid efficiencies depend on the nominal power fed into the grid, while the total energy and power generation depend on the microgrid efficiencies. Also, the outputs of the system model are inputs for the sizing of the subsystems, which is described in the following sections, and vice versa, as the results of the sizing are inputs for the performance analysis.

The computational model is implemented in six successive steps (Corte Vargas et al, 2020):

- Define daily operational conditions
- Calculate direct supply conditions
- Evaluate resource conditions
- Evaluate wind, solar, battery and CAES performance
- Evaluate power generation for seasonal storage
- Evaluate power mix values, total energy, and nominal powers

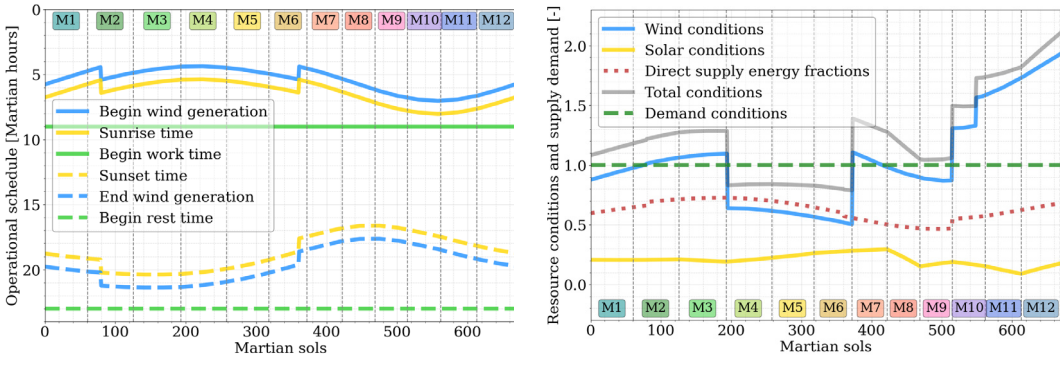


a b

FIGURE 3 Yearly operational schedule (a) and energy conditions (b). A sol is a solar day on Mars, spanning 24 Martian hours, while one year on Mars lasts 669 sols. In the graphs, the twelve Martian months (corresponding to a solar longitude change of 30 degrees each) are distinguished by the vertical dashed lines and their number given in the labels as adapted from the Mars Climate Database (2006). Every three months, the season changes, starting with the northern hemisphere spring equinox at a solar longitude of 0 degrees and Sol 1. Diagrams adapted from Corte Vargas et al (2020).

The results of steps 1 and 2 are illustrated in Figure 3 (left) which shows the astronauts' schedule and the resource availability over a complete Martian year. Solar energy is available between sunrise and sunset (Delgado-Bonal et al, 2016), while the availability of the wind resource is determined by the diurnal cycle, with average wind speeds generally dropping at night (Read et al, 2015; Viúdez-Moreiras et al, 2020). Because atmospheric circulation is caused by the differential heating between the equator and the poles and the rotation of the planet, we assume, as a first approximation, that wind energy can be harvested from one hour before sunrise until one hour after sunset in spring, summer, and autumn, while during winter it can be harvested from two hours before sunrise until two hours after sunset. The severely limited direct

energy supply at night requires that a considerable fraction of the energy needed at night has to be supplied by short-term storage. Thus, during wind and solar harvesting periods, sufficient energy both for the daytime demand and for battery charging needs to be generated.

In step 3, we evaluate the normalized wind and solar energy available, which we denote as wind and solar conditions, or, more generally, as resource conditions. The wind conditions are determined by dividing the daily energy production of the kite by the daily energy demand of the habitat. The demand ranges from 231.5 to 246.4 kWh, accounting for the base demand (190 kWh) and losses due to seasonal fluctuations as well as iterated supply path and subsystem losses. A value of 1 means that the wind energy fully meets the daily demand. The evolution of the wind conditions is obtained from the resource conditions and supply path specifications, while its magnitude is determined by the size of the kite.

Similarly, for the evolution of the solar conditions, the daily irradiance is normalized by the maximum irradiance over the year and divided by a factor representing the averaged supply path losses of that sol. As solar is the secondary/complementary source, the magnitude of the conditions is iterated in the course of the design process by manually changing the maximum solar condition (resulting in a final value of 0.29). The computed resource conditions are illustrated in Figure 3 (right). Based on the energy conditions, the distribution process of the power management system is simulated considering the dominant and auxiliary source and how they compare to the direct energy supply fraction. For the resulting system design, wind energy is considered to be the dominant source throughout the entire year, as for our design wind conditions are always superior to solar conditions. The dominant source is used for direct supply, as this minimizes losses. If the dominant source is greater than one, the excess energy is used to charge the battery (months 2, 3, 7, and 10 to 12). If it is greater than the direct energy fraction but lesser than one, the auxiliary source (solar energy) is also used to charge the battery for night-time energy consumption (months 1, 8, and 9). Any excess energy generated in those months is redirected to the CAES facility for storage purposes. Furthermore, in summer when the sum of the conditions is less than one (months 4 to 6), the CAES facility is used to compensate for the lack of generation.

Lastly, the design is iterated by changing the magnitude of the wind condition, which depends on the kite size, and complementary solar conditions, which depend on the prescribed maximum condition at the end of month 7 as an input. During the iterations, steps 3-6 are repeated with the new input. The nominal power flow in the microgrid is monitored and path losses altered, if necessary. The charging cycles of the CAES facility are examined to guarantee yearly net positive charge, to evaluate the required capacity, and estimate the feasibility of the design. On the same note, the energy required based on the system analysis is compared to the energy generated by the wind and solar subsystems as illustrated in Figure 4, which shows the differences between actually generated and demanded values as modelling errors. A breakdown of the yearly energy flow is illustrated by the Sankey diagram in Figure 5 .

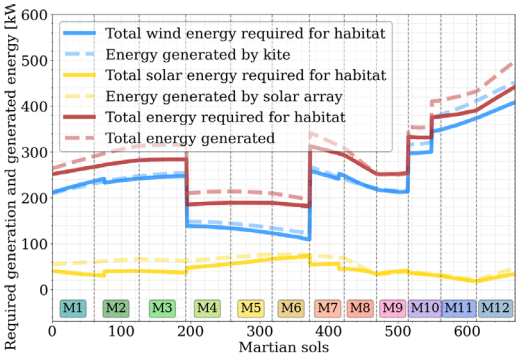


FIGURE 4 Wind energy required by the system performance analysis and actual output of the designed kite, solar energy required by the system performance analysis and actual energy output of the designed PV array, and total energy required and generated. Diagram adapted from Corte Vargas et al (2020).

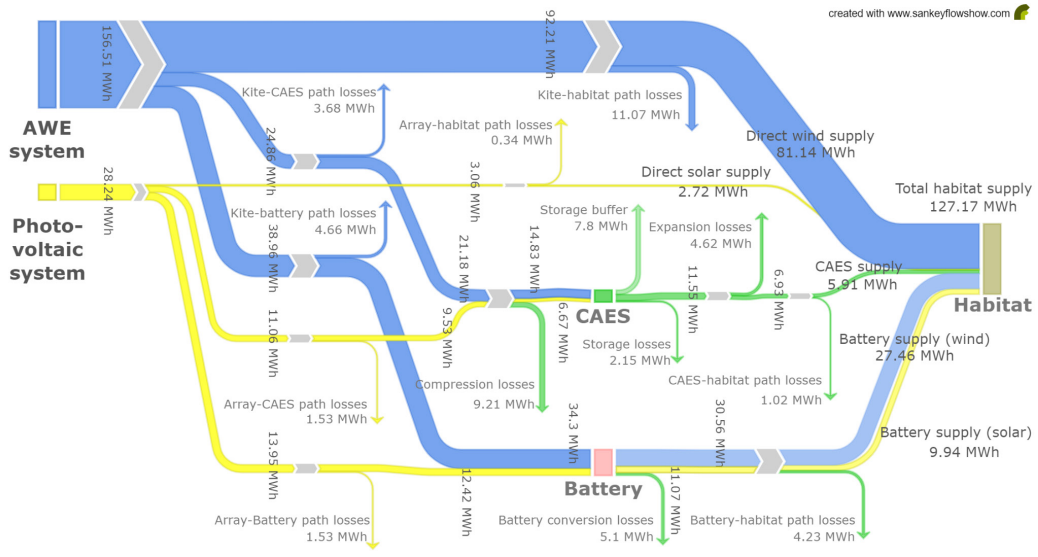


FIGURE 5 Sankey diagram of total yearly energy generation, losses and supply in Martian MWh.

The resulting annual energy mix shares based on the annual supply demand (669 sols x 190 kWh = 127.17 MWh) are summarized in Table 1. In conclusion, the required rechargeable battery capacity is 116 kWh, and the microgrid should be able to facilitate a power input of 26 kW, all with a contingency of 5%. The required supply via the CAES is 6.5 MWh with a contingency of 10%. Furthermore, from the net charge of the CAES it could be derived that the mission should be started in autumn/winter to save up enough energy for the summer supply.

| DIRECT WIND | DIRECT SOLAR | THROUGH BATTERY | THROUGH CAES | TROUGH WIND | THROUGH SOLAR | THROUGH CAES |
|---|---|---|---|---|---|---|
| 81.14 MWh | 2.72 MWh | 37.4 MWh | 5.91 MWh | 108.6 MWh | 12.66 MWh | 5.91 MWh |
| 63.84 % | 2.14 % | 29.37 % | 4.65% | 85.44 % | 9.91 % | 4.65 % |

TABLE 1 Total annual energy and energy mix for direct and through-storage supply (left) and for daily and seasonal supply (right).

## Airborne Wind Energy Subsystem

The choice of a pumping kite power system with a flexible membrane wing was the result of an initial trade-off analysis in which the suitability of different wind energy technologies was assessed for the planned space mission. Horizontal-axis and vertical-axis wind turbine variants were ruled out due to their prohibitive mass and volume. The low specific mass and transportation volume of tethered flying systems make them a generally interesting option for wind energy harvesting on other planets with an atmosphere. In particular, inflatable wings with rigid reinforcements can be scaled up efficiently to compensate for the substantially lower atmospheric density on Mars (Breuer & Luchsinger, 2010). An example for the effect of the lower atmospheric density and gravity on Mars is the aerodynamic design of NASA's Ingenuity drone (NASA, 2020; Chi, 2020).

As illustrated in Figure 1, the pumping kite power system is operated in alternating energy-generating tether reel-out and energy-consuming reel-in phases. When reeling out, the kite performs cross-wind manoeuvres to maximize the flight speed and pulling force. When reeling in, the crosswind manoeuvres are discontinued and the kite is depowered to minimize the pulling force and retraction time. The inflatable wing is actuated by a kite control unit (KCU). This suspended cable robot is responsible for steering the wing and changing

its angle of attack to modulate the pulling force (Van der Vlugt, 2013). A flight path planner adjusts the planned path to the instantaneous wind conditions and a flight controller uses sensor data from kite and ground station to ensure that the kite follows the planned path (Jehle & Schmehl, 2012; Fechner & Schmehl, 2018; Rapp & Schmehl, 2019). The ground station is responsible for controlling the tether force and thereby optimising the generation of power (Fechner & Schmehl, 2013). The functional architecture of the pumping kite power system adapted to operation on Mars is shown in Figure 6.

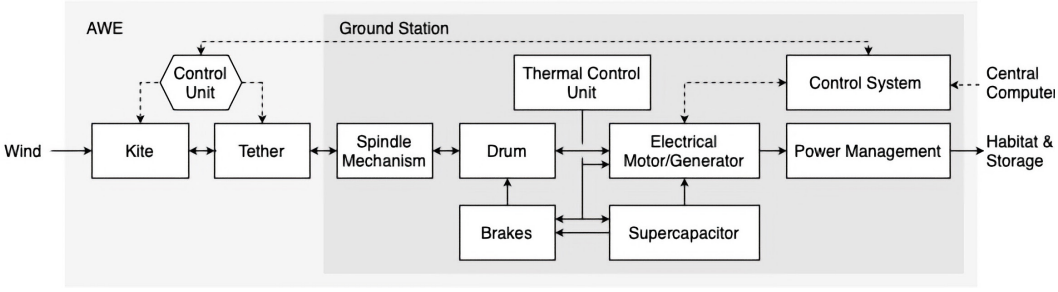


FIGURE 6 AWE system architecture for operation on Mars. Solid lines denote energy flows, dotted lines communication flows. Schematic from Corte Vargas et al (2020).

To size the AWE system as the primary energy supplier of the microgrid, a computational model was developed in Python accounting for the main aspects of the system: kite operation (Luchsinger, 2013), axial flux generator (Fechner & Schmehl, 2013), and tether (Bosman et al, 2013). Outputs of the model include the weight of the AWE system along with its energy output throughout the year. The model is embedded in the iterative design procedure, such that the sizing of all subsystems of the microgrid can be done concurrently, while ensuring that all requirements are met. The computational model was verified and validated by comparing the results to a validated performance model of the pumping kite power system (Van der Vlugt et al, 2019; Schelbergen & Schmehl, 2020).

As a result of this analysis, we found that a 50 $m^2$ kite with an average annual power output of 25 kW is needed to sustain the habitat. The AWE system has a total mass of 290 kg, can be compacted to a volume of 0.7 $m^3$, and costs approximately €70,000. Suitable materials were determined by trade-off analyses for all system components, considering the mass, structural properties, and sustainability of the materials. It was found that to retire the AWE system on Mars, many of the components and materials can be reused to minimize the environmental impact.

## Solar Energy Subsystem

Because of its high technology readiness level (TRL), reliability, and mass performance, solar PV was identified as the most suitable secondary energy technology for the planned mission. To compensate for the low solar irradiance and dust storms on Mars, we selected a dual-axis support system with a sun simulation for sun tracking to reduce the incidence angle on the panels. As for the dust settling on the panels, we propose an experimental coating (Zhou, et al, 2019) that was tested under simulated Mars conditions and is expected to be able to remove more than 90% of all dust from the panels by inclining them, while having a negligible effect on the transparency of the panel cover.

Space-grade solar panels are usually designed for optimal performance at an Air Mass 0 (AM0) spectrum, considering direct light from the sun that has not interacted with an atmosphere (Funde, 2020). Compared

to AM0 and the spectrum on the surface of Earth, the spectrum at the surface of Mars differs substantially as the shorter wavelengths are filtered out to a large extent by the red dust (Landis & Hyatt, 2006). When using multijunction solar cells – which would be required because of their higher conversion efficiency, leading to lower required volume and mass – the change in spectrum could render the solar cells no longer current matched. To counteract this, Landis & Hyatt (2006) found that triple-junction GaInP/GaAs/Ge cells could be adapted to the Mars surface spectrum, as its specific band gaps are well suited for the long wavelength-rich spectrum, having an energy conversion efficiency of approximately 32%.

During their operative lifetime, the PV panels will produce no emissions and thus will leave little to no impact on Mars. However, the production of the panels results in waste due to the refinement of rare metals needed for the triple-junction cells. At end of life, most of the subsystems and the panels can be recycled, although specialized facilities are needed to disassemble the panels and purify the metals for reuse. This cannot be done on Mars, as it is assumed that the required facilities will not be built in the timespan of the mission. Thus, to reduce the impact on the Mars environment, it is advised to return the panels to Earth for recycling at mission end.

A system for the cooling of the PV panels is still to be developed. As the atmosphere is thinner on Mars, the panels do not cool as effectively as they would in an Earth environment and thus the efficiency of the panels is reduced according to an initial estimation by Delgado-Bonal et al (2016). Assuming that an efficient cooling solution can be developed, the area of the solar array required for supplementing the wind energy system would be approximately 70 $m^2$. The complete cost of the solar energy system would amount to an estimated €6,800,000, with a mass of around 790 kg.

## Energy storage Subsystems

Apart from production and distribution of energy, buffering and storage are key aspects of any autarkic renewable energy system. In our case, the energy produced is distributed via three different paths: a part of the energy is directly supplied to the habitat, while the excess is captured by rechargeable batteries for short-term storage covering the nights and by compressed air energy storage (CAES) for covering seasonal generation shortages. An initial study led to a required cavern volume and pressure ratio of 107,500 $m^3$ and 175, respectively. The mass of $CO_2$ to be stored annually is 301,812 kg, roughly 86% of the total storage system weight, disregarding the regolith that is mined and used as inner structural lining material. Because of mechanical, thermal and electrical losses of the cycle components (expander, compressor, convertors), the overall efficiency of the CAES system is around 45%. The cavern volume is limited by the maximum stresses that the rock-mass formation of Martian terrain can handle. Further investigations into the local rock quality are recommended to provide more insight to the maximum storage capacity and required distance from the habitat, to reduce the operational risk. The costs of the CAES system are estimated to be €2,000,000 for development, transport, and subsystem-specific mission operations.

Although lithium-ion batteries have become a standard in the space industry, lithium-sulphur batteries were chosen for the systems' day-to-day storage, because these batteries are well recyclable (Deng, 2017) and their energy density (350 Wh/l) is higher than that of lithium-ion batteries (200 Wh/l). The batteries are charged during the day and discharged during the night. A volume of 0.1 $m^3$ and a mass of 120.4 kg were determined by the system performance analysis based on the required capacity needed to get through the longest nights on Mars (Wertz, 1999). The batteries will have to be stored in a protective container shielded from Mars' environment and they will be modular to allow for easy replacement or repairs. Finally, the cost of the batteries will end up at an estimated €6450.

## Power Management and Distribution System

A well-engineered power management and distribution system is critical to ensure a reliable delivery of the electrical power to the habitat, where it is consumed. This is achieved by a direct current microgrid, which connects the habitat and the various energy generation and storage systems. A DC microgrid is preferred to the more widely applied alternating current (AC) alternative, because this grid type requires less power conversion devices, which is favourable in terms of overall mass, volume, efficiency, and reliability. The critical system elements of the microgrid are schematically illustrated in Figure 7.

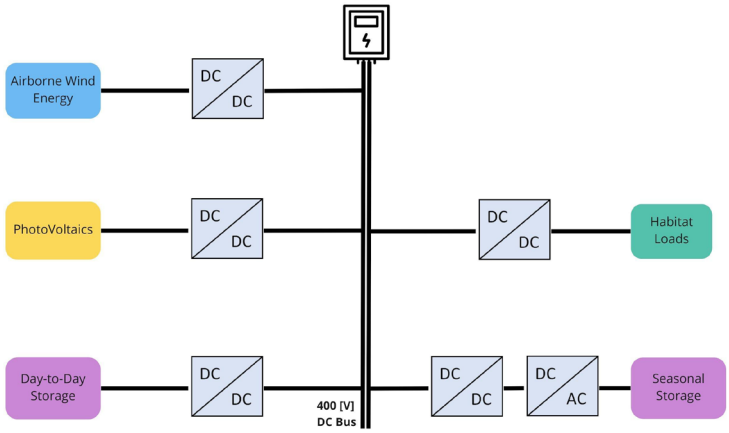


FIGURE 7 Schematic of the microgrid system architecture, adapted from Corte Vargas et al (2020).

Electronic converters are used to convert the electrical power that is injected into (or withdrawn from) the microgrid to the correct current and voltage levels. State-of-the-art silicon-carbide (SiC) converters for aerospace applications were selected to facilitate high power densities and minimize power losses. A power distribution unit (PDU) is used for monitoring and controlling the power flow in the microgrid. Lastly, the DC bus is the common connection to which all power sources and sinks are connected in parallel. The power cables are laid under the Martian surface for better protection against the harsh environment. The grid voltage is maintained at 400 VDC, which has been determined to be the optimum voltage according to a study on voltage levels for DC microgrids (Anand & Fernandes, 2010).

Altogether, the power management and distribution system is designed to support a nominal power of 26 kW. The electrical path efficiencies, which indicate the power losses from supply to demand, are computed to be in the range of 73% to 89%. The total mass of the system is estimated at 200 kg, for a volume of 0.24 $m^3$ and an approximate cost of €70,000.

## Conclusion

The harsh environmental conditions on Mars due to dust storm seasons, low solar irradiation, and low atmospheric pressure require specific technical solutions. As for any space mission, a high degree of automation is required and the effort and costs to transport material have to be minimized. These requirements converge in the goal of designing an energy system for a Mars habitat that is sustainable, lightweight, and as low in costs as possible while reliably fulfilling the energy requirements.

To overcome the seasonal, monthly, and daily fluctuations in sustainable energy generation on Mars, the energy system is based on two different renewable energy technologies, a storage system, and a power management system. The primary energy system consists of a pumping kite power system with a semi-rigid inflatable kite. Due to the lightweight materials and large wing surface area, the kite system is able to perform at the low Martian atmospheric density. The lightweight materials and high foldability make it suitable for transportation to Mars. The secondary energy system uses solar PV panels with a dual axis-system support system. The panels follow the tracking of the sun to reduce the incidence angle and maximize the yield. To remove dust pollution from the PV panels, a coating is applied which removes over 90% of the dust by inclination of the panels without reducing transparency. In addition, the selected cells are able to perform at the long wavelength-rich Martian spectrum.

As both wind and solar energy are fluctuating resources, an energy storage system has been designed to which excess energy is charged during harvesting times. It consists of a day-to-day lithium-sulphur battery, which provides energy to the habitat overnight, and a seasonal compressed air storage system, to overcome seasons during which less energy can be produced. The latter makes use of a local cavity, reducing the transportation volume. Finally, the power management system connects the energy harvesting systems and the storage solutions, ensuring reliable electric delivery to the habitat. It makes use of a DC microgrid with underground power cables to protect against the harsh Martian conditions.

The combination of all these subsystems results in a design that can reliably produce and distribute enough energy for the Mars habitat, at a total base cost of €8.95 million, excluding transportation. This proves that renewable energy is a feasible option for a Mars mission and that further investigation needs to be done to finalize the design. For future work, we recommend determining the environmental conditions on Mars more accurately, in particular the wind resource, and to refine the system model and further details of the individual components of the microgrid. Moreover, from the price difference of the space-grade photovoltaic subsystem and the estimated cost of a space-grade AWE subsystem, it is evident that further research must be conducted to obtain a more practical expenditure prognosis for the kite and remaining subsystems.

## Acknowledgements

The authors would like to acknowledge the support of the coaches Dominic von Terzi, Botchu Jyoti, and Camila Brito, as well as the experts Angelo Cervone, Henriette Bier, Mark Schelbergen, Mihir Metha, Klaas Akkerman, Joep Breuer, and Henk Polinder during the design synthesis exercise.

## References


Anand, S., & Fernandes, B. G. (2010). Optimal voltage level for DC microgrids. IECON 2010 - 36th Annual Conference on IEEE Industrial Electronics Society, 3034–3039. https://doi.org/10.1109/IECON.2010.5674947

Barnard, A., Engler, S. T., & Binsted, K. (2019). Mars habitat power consumption constraints, prioritization, and optimization. Journal of Space Safety Engineering, 6(4), 256–264. https://doi.org/10.1016/j.jsse.2019.10.006

Basner, M., Dinges, D. F., Mollicone, D., Ecker, A., Jones, C. W., Hyder, E. C., Di Antonio, A., Savelev, I., Kan, K., Goel, N., Morukov, B. V., & Sutton, J. P. (2013). Mars 520-d mission simulation reveals protracted crew hypokinesis and alterations of sleep duration and timing. Proceedings of the National Academy of Sciences, 110(7), 2635–2640. https://doi.org/10.1073/pnas.1212646110

Bechtle, P., Schelbergen, M., Schmehl, R., Zillmann, U., & Watson, S. (2019). Airborne wind energy resource analysis. Renewable Energy, 141, 1103–1116. https://doi.org/10.1016/j.renene.2019.03.118

Bier, H. et al (2019) Rhizome: Development of an Autarkic Design-to-Robotic-Production and -Operation System for Building Off-Earth Rhizomatic Habitats. 2nd stage proposal for an ESA ideas competition. Retrieved May 14, 2020 from http://cs.roboticbuilding.eu/index.php/Shared:2019Final

Bluck, J. (2001) Antarctic/Alaska-Like Wind Turbines Could be Used on Mars. NASA Ames News Item. Retrieved May 14, 2020 from https://www.nasa.gov/centers/ames/news/releases/2001/01_72AR.html

Bosman, R., Reid, V., Vlasblom, M., & Smeets, P. (2013). Airborne Wind Energy Tethers with High-Modulus Polyethylene Fibers. In U. Ahrens, M. Diehl, & R. Schmehl (Eds.), Airborne Wind Energy (pp. 563–585). Springer. https://doi.org/10.1007/978-3-642-39965-7_33

Boumis, R. (2017) The Average Wind Speed on Mars. Sciencing. Retrieved May 14, 2020 from http://sciencing.com/average-wind-speed-mars-3805.html

Breuer, J. C. M., & Luchsinger, R. H. (2010). Inflatable kites using the concept of Tensairity. Aerospace Science and Technology, 14(8), 557–563. https://doi.org/10.1016/j.ast.2010.04.009

Chen, A. (2014, May 14) EDL Engineering Constraints [Workshop presentation]. Mars 2020 1st Landing Site Workshop., Pasadena, CA, United States. https://marsnext.jpl.nasa.gov/workshops/2014_05/05_LSW1_EDL_Eng_Constraints_v6.pdf (

Chi, C., Lumba, R., Jung, Y. S., & Datta, A. (2020, November 16). Preliminary Structural Design and Aerodynamic Analysis of Mars Science Helicopter Rotors. ASCEND 2020. ASCEND 2020, Virtual Event. https://doi.org/10.2514/6.2020-4025

Chuang, F.C., Crown, D.A. (2009) Geologic map of MTM 35337, 40337, and 45337 quadrangles, Deuteronilus Mensae region of Mars: U.S. Geological Survey Scientific Investigations Map 3079. https://pubs.usgs.gov/sim/3079/

Corte Vargas, F., Géczi, M., Heidweiller, S., Kempers, M.X., Klootwijk, B.J., van Marion, F., Mordasov, D., Ouroumova, L.H., Terwindt, E.N., Witte, D. (2020) Arcadian Renewable Energy System: Renewable Energy for Mars Habitat [Technical report]. Faculty of Aerospace Engineering, Delft University of Technology. http://resolver.tudelft.nl/uuid:93c343e5-ee79-4320-98a3-949d3e9c407d

Delgado-Bonal, A., Martín-Torres, F. J., Vázquez-Martín, S., & Zorzano, M.-P. (2016). Solar and wind exergy potentials for Mars. Energy, 102, 550–558. https://doi.org/10.1016/j.energy.2016.02.110

Deng, Y., Li, J., Li, T., Gao, X., & Yuan, C. (2017). Life cycle assessment of lithium sulfur battery for electric vehicles. Journal of Power Sources, 343, 284–295. https://doi.org/10.1016/j.jpowsour.2017.01.036

Engler, S. (2017). Forecasting of Energy Requirements for Planetary Exploration Habitats Using a Modulated Neural Activation Method. https://doi.org/10.11575/PRISM/26208

Engler, S. T., Binsted, K., & Leung, H. (2019). HI-SEAS habitat energy requirements and forecasting. Acta Astronautica, 162, 50–55. https://doi.org/10.1016/j.actaastro.2019.05.049

Fechner, U. (2016). A Methodology for the Design of Kite-Power Control Systems [Delft University of Technology]. https://doi.org/10.4233/UUID:85EFAF4C-9DCE-4111-BC91-7171B9DA4B77

Fechner, U., & Schmehl, R. (2013). Model-Based Efficiency Analysis of Wind Power Conversion by a Pumping Kite Power System. In U. Ahrens, M. Diehl, & R. Schmehl (Eds.), Airborne Wind Energy (pp. 249–269). Springer. https://doi.org/10.1007/978-3-642-39965-7_14

Fechner, U., & Schmehl, R. (2018). Flight Path Planning in a Turbulent Wind Environment. In R. Schmehl (Ed.), Airborne Wind Energy (pp. 361–390). Springer. https://doi.org/10.1007/978-981-10-1947-0_15

Foust, J. (2017) SpaceX studying landing sites for Mars missions. Retrieved December 1, 2020 from https://spacenews.com/spacex-studying-landing-sites-for-mars-missions/

Fraser S.D. (2009). Power System Options for Mars Surface Exploration: Past, Present and Future. In: Badescu V. (ed) Mars: Prospective Energy and Material Resources. Springer. https://doi.org/10.1007/978-3-642-03629-3_1

Funde, A., & Shah, A. (2020). Solar Spectra. In A. Shah (Ed.), Solar Cells and Modules (Vol. 301, pp. 17–32). Springer International Publishing. https://doi.org/10.1007/978-3-030-46487-5_2

Haslach, H.W. Jr (1989) Wind Energy: a Resource for a Human Mission to Mars. Journal of the British Interplanetary Society, Vol. 42, pp. 171–178. http://www.researchgate.net/publication/252363322_Wind_Energy_a_Resource_for_a_Human_Mission_to_Mars

Head, J., Dickson, J., Mustard, J., Milliken, R., Scott, D., Johnson, B., Marchant, D., Levy, J., Kinch, K., Hvidberg, C., Forget, F., Boucher, D., Mikucki, J., Fastook, J., & Klaus, K. (2015, October 27-30) Mars Human Science Exploration and Resource Utilization: The Dichotomy Boundary Deuteronilus Mensae Exploration Zone [Workshop presentation]. First Landing Site/Exploration Zone Workshop for Human Missions to the Surface of Mars. Houston, Texas, United States. https://www.hou.usra.edu/meetings/explorationzone2015/pdf/1033.pdf

Holstein-Rathlou, C. (2018) Wind Turbine Power Production Under Current Martian Atmospheric Conditions. Mars Workshop on Amazonian Climate 2018 (LPIContrib.No.2086) https://www.hou.usra.edu/meetings/amazonian2018/pdf/4004.pdf

Horneck, G., Facius, R., Reichert, M., Rettberg, P., Seboldt, W., Manzey, D., Comet, B., Maillet, A., Preiss, H., Schauer, L., Dussap, C. G., Poughon, L., Belyavin, A., Reitz, G., Baumstark-Khan, C., & Gerzer, R. (2003). Humex, a study on the survivability and adaptation of humans to long-duration exploratory missions, part I: Lunar missions. Advances in Space Research, 31(11), 2389–2401. https://doi.org/10.1016/S0273-1177(03)00568-4

James, G., Chamitoff, G., Barker, D. (1998) Resource Utilization and Site Selection for a Self-Sufficient Martian Outpost". NASA/TM-98-206538. https://ntrs.nasa.gov/citations/19980147990

Jehle, C., & Schmehl, R. (2014). Applied Tracking Control for Kite Power Systems. Journal of Guidance, Control, and Dynamics, 37(4), 1211–1222. https://doi.org/10.2514/1.62380

KiteX (2020) Windcatcher. Retrieved December 20, 2020 from http://kitex.tech/

Landis, G., & Hyatt, D. (2006). The Solar Spectrum on the Martian Surface and its Effect on Photovoltaic Performance. 2006 IEEE 4th World Conference on Photovoltaic Energy Conference, 1979–1982. https://doi.org/10.1109/WCPEC.2006.279888

Luchsinger, R. H. (2013). Pumping Cycle Kite Power. In U. Ahrens, M. Diehl, & R. Schmehl (Eds.), Airborne Wind Energy (pp. 47–64). Springer. https://doi.org/10.1007/978-3-642-39965-7_3

Mars Climate Database (2006) Martian Seasons and Solar Longitude. Retrieved March 22, 2021 from http://www-mars.lmd.jussieu.fr/mars/time/solar_longitude.html

Mersmann, K. (2015) The Fact and Fiction of Martian Dust Storms. NASA Goddard Feature. https://www.nasa.gov/feature/goddard/the-fact-and-fiction-of-martian-dust-storms

NASA (2020) Mars 2020 mission - For Scientists: Landing Site Selection. Retrieved May 11, 2020 from https://mars.nasa.gov/mars2020/mission/science/for-scientists/landing-site-selection/

NASA (2020) Mars helicopter. Retrieved December 20, 2020 from https://mars.nasa.gov/technology/helicopter/

Nelson, V. (2019). Innovative Wind Turbines: An Illustrated Guidebook (1st ed.). CRC Press. https://doi.org/10.1201/9781003010883

Plaut, J. J., Safaeinili, A., Holt, J. W., Phillips, R. J., Head, J. W., Seu, R., Putzig, N. E., & Frigeri, A. (2009). Radar evidence for ice in lobate debris aprons in the mid-northern latitudes of Mars: RADAR EVIDENCE FOR MID-LATITUDE MARS ICE. Geophysical Research Letters, 36(2). https://doi.org/10.1029/2008GL036379

Rapp, S., Schmehl, R., Oland, E., & Haas, T. (2019). Cascaded Pumping Cycle Control for Rigid Wing Airborne Wind Energy Systems. Journal of Guidance, Control, and Dynamics, 42(11), 2456–2473. https://doi.org/10.2514/1.G004246

Read, P. L., Lewis, S. R., & Mulholland, D. P. (2015). The physics of Martian weather and climate: A review. Reports on Progress in Physics, 78(12), 125901. https://doi.org/10.1088/0034-4885/78/12/125901

Rummel, J. D., Beaty, D. W., Jones, M. A., Bakermans, C., Barlow, N. G., Boston, P. J., Chevrier, V. F., Clark, B. C., de Vera, J.-P. P., Gough, R. V., Hallsworth, J. E., Head, J. W., Hipkin, V. J., Kieft, T. L., McEwen, A. S., Mellon, M. T., Mikucki, J. A., Nicholson, W. L., Omelon, C. R., … Wray, J. J. (2014). A New Analysis of Mars "Special Regions": Findings of the Second MEPAG Special Regions Science Analysis Group (SR-SAG2). Astrobiology, 14(11), 887–968. https://doi.org/10.1089/ast.2014.1227

Schelbergen, M., & Schmehl, R. (2020). Validation of the quasi-steady performance model for pumping airborne wind energy systems. Journal of Physics: Conference Series, 1618, 032003. https://doi.org/10.1088/1742-6596/1618/3/032003

Schmehl, R. (2019) Airborne Wind Energy - An introduction to an emerging technology. Retrieved May 14, 2020 from http://www.awesco.eu/awe-explained/

Silberg, B. (2012) Electricity in the air. NASA Jet Propulsion Laboratory News Item. Retrieved May 14, 2020 from https://climate.nasa.gov/news/727/electricity-in-the-air

van der Vlugt, R., Bley, A., Noom, M., & Schmehl, R. (2019). Quasi-steady model of a pumping kite power system. Renewable Energy, 131, 83–99. https://doi.org/10.1016/j.renene.2018.07.023

van der Vlugt, R., Peschel, J., & Schmehl, R. (2013). Design and Experimental Characterization of a Pumping Kite Power System. In U. Ahrens, M. Diehl, & R. Schmehl (Eds.), Airborne Wind Energy (pp. 403–425). Springer. https://doi.org/10.1007/978-3-642-39965-7_23

Vermillion, C., Cobb, M., Fagiano, L., Leuthold, R., Diehl, M., Smith, R. S., Wood, T. A., Rapp, S., Schmehl, R., Olinger, D., & Demetriou, M. (2021). Electricity in the air: Insights from two decades of advanced control research and experimental flight testing of airborne wind energy systems. Annual Reviews in Control, S1367578821000109. https://doi.org/10.1016/j.arcontrol.2021.03.002

Viúdez‐Moreiras, D., Newman, C. E., Forget, F., Lemmon, M., Banfield, D., Spiga, A., Lepinette, A., Rodriguez‐Manfredi, J. A., Gómez‐Elvira, J., Pla‐García, J., Muller, N., Grott, M., & the TWINS/InSight team. (2020). Effects of a Large Dust Storm in the Near‐Surface Atmosphere as Measured by InSight in Elysium Planitia, Mars. Comparison With Contemporaneous Measurements by Mars Science Laboratory. Journal of Geophysical Research: Planets, 125(9). https://doi.org/10.1029/2020JE006493

Wertz, J.R., Larson, W.J. (1999) Space Mission Analysis and Design. Space Technology Library, (Vol. 8., 4th ed.). Springer. ISBN 978-0-7923-5901-2

Williams, D.R. (2020) Mars fact sheet. Retrieved November 24, 2020 from https://nssdc.gsfc.nasa.gov/planetary/factsheet/marsfact.html

Zhou, S., Yang, H., Chen, C., Zhang, J., & Wang, W. (2019) Transparent dust removal coatings for solar cell on mars and its Anti-dust mechanism. Progress in Organic Coatings, 134, 312–322. https://doi.org/10.1016/j.porgcoat.2019.05.028

# The Interesting Challenges of Designing for Humans in Space

**Sandra Häuplik-Meusburger** [1], **Brand Griffin** [2]

[1] *TU Wien / space-craft Architektur*
*Vienna, Austria*

[2] *Genesis Engineering Solutions*

## Abstract

Extra-terrestrial living and working environments are characterized by significant challenges in logistics, environmental demands, engineering, social and psychological issues, to name a few. Everything is limited: physical volume, air, water, power, and medicine ... everything, even people, and therefore all is treated as valuable resource. This situation is complicated by the end product being the result of balancing many competing interests. The relationship between humans, space, and technology is forced, as well as a dynamic process. Although mathematical models for complex systems exist, long-term effects are hard to predict, and even more so to calculate. Even if we had technological solutions for all hazards and threats, there would still be the question of how these subsystems work together, how they are perceived, and if they are accepted by the inhabitants. Habitability design is vital to the success of future space exploration. Research into the dynamic system of 'living together in an isolated and extreme environment for a long time' does not lead to a single common solution. Instead, designers are left trying to translate differing first-person astronaut accounts into a solution bound by the constraints of physics, schedule, and cost. The early days of human spaceflight were all about discovery. Trying to replace conjecture with experience and fact. For example, the Moon was thought to have meters of soft dust that would swallow landing spacecraft. We have built on the successes and failures, but some achievements have also been forgotten. Today, we use these lessons to create effective designs for 'living together in the isolated and extreme environment (ICE)' of space. Following are descriptions of historical and newer examples of possible solutions that show what can be achieved when the demanding constraints of space inspire creative solutions for combining human needs with technological possibilities.

## Keywords

Space architecture, space history, habitability design, critical design challenges, design consequences, in-situ-resources,design innovation, creativity

## DOI

https://doi.org/10.7480/spool.2021.2.5267

## Introduction

From a technical and engineering point of view, one of the critical characteristics for human space operations and mission success is the dependency on the habitat, its technological capabilities as well as its provision of relevant resources for life-support. To sustain life, humans need oxygen at a minimum of 12.2 Kilopascal pressure. The Earth's atmosphere at sea level is 21 percent oxygen at 101.3 KPa. Space is a vacuum, the Moon is in a vacuum, and the Martian atmosphere unbreathable carbon dioxide at less than 1 percent of Earth atmospheric pressure. Therefore, all space habitats need to be constructed as pressure vessels. There is simply no human mission without (a lot of) technical subsystems.

With respect to upcoming and future human space missions, it will be important to build functional, supportive, persistent long-term infrastructure that extend the characteristics of survival shelters to become places that support all kinds of human activities. Integration of habitability in relation to human activity needs is key when mission length increases. As stated by Frances Mount (Mount 2002, p. 87): "*The impact of a poorly designed switch or lack of stowage area is different for a mission of six months compared to a mission of one week*."

At first sight, today's space habitats seem old-fashioned and not suitable for future space exploration. However, we should not forget the efforts that have been put into the design process. Designing a space station takes a long time and lot of people are involved. From the first idea to the actual realization, more ideas are discarded than advanced. It is a process of high creativity and also a process of selection. According to Kitmacher "*More than hundred different space stations were conceptualized [...] before the ISS became operational"* (Kitmacher, 2002 p.2) Fig. 1 and 2 show early concepts of Space Station Freedom, which was announced in 1984, slimmed down, and eventually realised as today's International Space Station (ISS).

FIGURE 1 Early space station concept by Boeing in 1984. At that stage, it was required to have two ways to exit each module. The modules would be linked in a loop configuration. (Illustration by Paul Hudson)

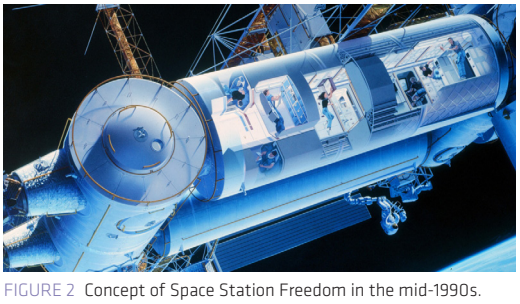

FIGURE 2 Concept of Space Station Freedom in the mid-1990s. That concept still included a habitation module that did not fly. (Illustration by Paul Hudson Design Boeing)

Over the years of designing and evaluating for today's International Space Station, a lot of features that would improve habitability were not included. The diameter of the modules was constrained to the Shuttle cargo bay. Yet, the ISS is the largest and most-advanced off-Earth architecture that has been built and it has been permanently inhabited for the last 20 years.

Human space exploration is as much a story of scientific discovery as one of optimizing humans and their newly created environments. Using selected historical examples, the authors will show what can be achieved when the demanding constraints of space inspire creative solutions for combining human needs with technological possibilities.

## How to fit it in – Mass, Volume, Form

"*Early spacecraft had been designed to be operated, not lived in*" (Compton and Benson 1983, p. 130). There is this famous saying that Mercury astronauts[1] did not climb into the spacecraft, *they put it on* (Img 3). The Mercury spacecraft was a 3.3m (10.8 ft.) tall, 1.85m (6 ft.) wide cone-shaped craft made for one astronaut. Spacecraft design remains primarily functional, and weight and size are among the major criteria for spacecraft design. Those restrictions also influenced criteria for astronaut selection, in that the astronauts also had a 'height limit' 1.82m (5ft. 11 in.) as a function of the spacecraft design (Burgess, 2011). It was at that time that the term 'tin can' as a synonym for the spacecraft and 'man in a (tin) can' as a synonym for an astronaut or cosmonaut were born.

FIGURE 3 Mercury 7 astronauts examine their 'couches'. Each astronaut's couch was moulded to fit his body to help withstand the G-loads of the launch.1959 (NASA)

FIGURE 4 Saturn V rocket launch, 1969 (NASA)

FIGURE 5 The space shuttle Discovery with its payload bay doors open. A module is resting inside the payload bay. (NASA)

## Consequences of the Transportation System

A space station in orbit or a habitat on the Moon or Mars is to a large extent a product of the launch system. The habitat size, mass, and very often the geometry depend upon the launch vehicle used. In terms of engineering and economic issues, there is a severe limitation on mass and volume. The Apollo flight system was made for only one flight and to land on the lunar surface, with only the command module returning to the surface of the Earth. The biggest portion of the available space within the Apollo spacecraft (Fig. 4) was occupied by enabling subsystems (structure, life support systems, propulsion systems, power systems, etc.).

No space station module has thus far had a larger diameter than the Skylab Space Station Orbital Workshop at 6.6m (22 ft.) diameter. And this was only possible because Skylab used one of the large Saturn V launch vehicle propellant tanks for the habitat/workshop. Skylab was launched first, followed by three separately-launched Apollo spacecraft carrying three astronauts each.

To create larger space station complexes, the Soviet planners used a modular approach using successive launches to build up the Mir space station. The International Space Station is also based on this assembled-in-space, modular architecture approach. As a consequence of integrating the Space Shuttle to reduce transportation costs, the modules were reduced in size to fit the Shuttle's payload bay of 4.5m (15 ft.) (Fig. 5).

1 Project Mercury was the first human spaceflight program of the United States and ran from 1958 to 1963.

While the Mir space station used solar panels for each of the modules (Fig. 6), the ISS has a truss structure with photovoltaic infrastructure (Fig. 7). Only the first modules of the ISS, Zarya and Zvezda, were independent, using solar panels attached to the module. In contrast, the European and US modules on ISS are much like houses in a village attached to a common utility source for electrical power, heat rejection, and communications. Interestingly the word "Mir" in Russian can be translated to "village", as well as "world" and "peace".

FIGURE 6 Russia's Mir space station in 1989, taken from Space Shuttle STS-89 mission (NASA)

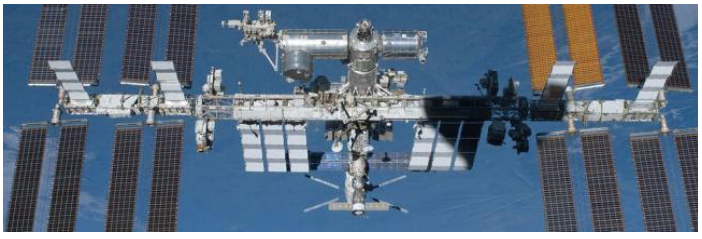

FIGURE 7 The International Space Station with its truss structure for the photovoltaic system, 2020 (NASA)

## The Rover Packaged in a Wedge

The Apollo programme was announced in 1960 as a follow up to the *Mercury Project*. At the time of the announcement, the flight configurations were not yet fixed yet. It is worth remembering that, while the first lunar landing took place in 1969, work on and designing of lunar missions began much earlier, even before the first human spaceflight. It is remarkable to note that in 1952 Werner von Braun was working on a lunar lander that would take 50 people to the Moon for six weeks. His ideas captured the interest of Walt Disney and were presented in a series of TV episodes (Fig. 9). He was also the one that promoted a lunar rover for expanding the exploration distance of future astronauts. Almost 20 years later, in 1969 von Braun would watch the first manned module land on the Moon.

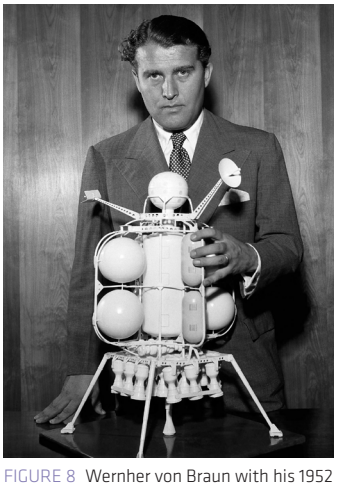

FIGURE 8 Wernher von Braun with his 1952 design of a lunar lander (Photo remastered by Dan Beaumont, original image US Information Agency)

FIGURE 9 Prototype of the Molab concept by General Motors in Hopi Buttes, AZ in 1967. It was scrapped in 1968. (U.S. Geological Survey USGS)

Along the way, there were many designs for lunar bases. Early base designs tended to be comprised of pre-integrated modules delivered from the Earth. In this way, the entire module could be fully tested before launch and immediately used on site. A disadvantage of this approach is that the weight and volume is limited to the launch vehicle payload capabilities. An innovative strategy to overcome the launch vehicle payload limitations was demonstrated by folding the lunar rover, then having it be deployed on the surface. Research into lunar surface rovers started in 1964. A variety of prototypes were designed, tested, and evaluated, as a lunar rover was intended to augment human exploration activities on the lunar surface. The MOLAB (Wright & Jaques, 2002) pressurized rover (Fig. 9) was successful in that it proved astronauts could stay in it for at least 18 days. However, it also proved that it would weigh so much that a Saturn V would have to deliver it ahead of the astronauts, which would have been too expensive. Eventually the MOLAB rover concept was dropped, and NASA gave up '*putting vehicles on the Moon*' (Riley et al., 2008). At General Motors, engineers started work on small unpressurized rovers and asked NASA HQ if there would be a possibility to include a rover. The answer was: "*If you could fit a vehicle in this triangular bay"* (in the descent stage, 1,5m (5ft) tall, wide, and deep), "*we might think about going again with a rover*" (Riley et al., 2008).

General Motors became a subcontractor of the Boeing Company and, working with NASA, delivered the Lunar Roving Vehicle that first flew folded into a small, wedge-shaped volume on Apollo 15. It was innovative because of its clever packaging and deployment as well as wheels made of wire (Fig. 10 and 11). Although astronauts had walked on the Moon, it was not clear how a rover would behave in the dust and lower gravity. The rover was powered by electric motors and designed to carry two astronauts. It was about 3m (10 ft. 2 in.) long, 1.1m (44 in.) high, with a 2.3m (7 ft. 6 in.) wheelbase. The finished lunar rover weighed only about 200kg (450 lb.), or just 34kg (75 lb.) in the Moon's gravity.

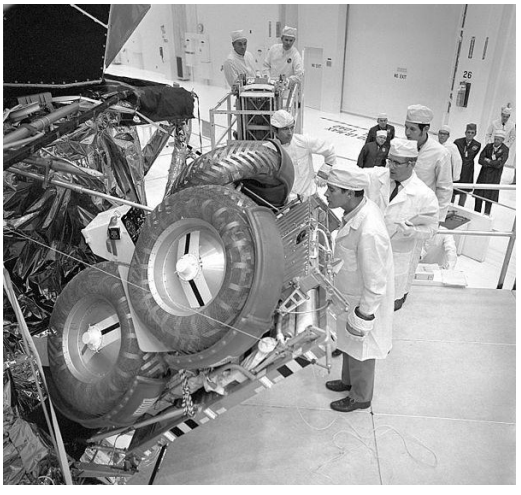

FIGURE 10 Apollo 16 Commander John Young and Lunar Module Pilot Charles M. Duke, inspect the Lunar Roving Vehicle during a deployment test in the Manned Spacecraft Operations Building at the Kennedy Space Center. November 1971. (NASA)

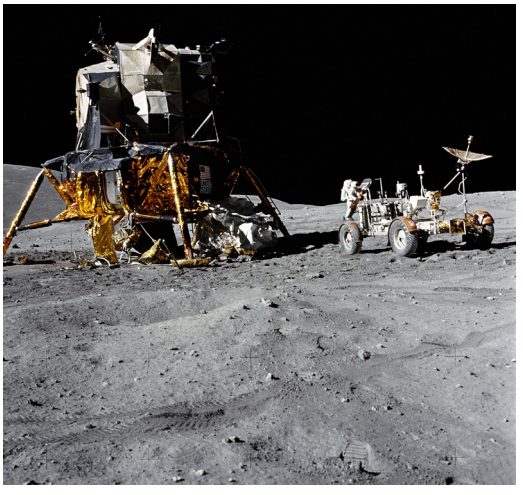

FIGURE 11 Image of the Lunar Module 'Orion', as photographed by astronaut Charles M. Duke during the first Apollo extravehicular activity. The lunar rover is visible in front of the triangular bay that hosted the folded rover. (NASA)

## Expandable Structures

Looking for on-orbit volumes larger than the launch vehicle diameter, engineers and designers explored expandable structures. One innovative concept proposed as early as the 1960s was an inflatable wheel-

shaped space station with a dimeter of 50m (162.5 ft.) (Fig. 12). In 1965, the Soviets equipped the manned spacecraft Voskhod 3KD with an inflatable airlock (Fig. 13) that enabled Alexei Leonov to conduct the worlds' first EVA (Haeuplik-Meusburger and Ozdemir, 2012). Between 1997 and 2000, NASA developed the 'TransHab', an inflatable long duration habitat with a central core. Initially it was conceived as crew quarters for the ISS and later as a transit habitat to be used for Mars missions. It would expand to 8.2 m (26.7 ft.) diameter. The architects involved were Constance Adams and Kriss Kennedy.

FIGURE 12 This 1961 prototype of an inflatable space station concept with a solar power system collector was 7.3 m (24 feet) in diameter with an internal fabric bulkhead that could be separately pressurized in an emergency. (NASA)

FIGURE 13 The Volga airlock and Berkut spacesuit. Memorial Museum of Cosmonautics, Moscow, 1999. (Photo: Kucharek, Wikimedia)

FIGURE 14 Design for a Space Station in Low Earth Orbit. Diploma project at the TU Vienna by Matas Ivan (models and image: Matas Ivan, HB2, TU Wien)

Although the TransHab concept (Fig. 18) was discarded, it was highly successful insofar as it led to the development of the inflatable architecture by Bigelow Aerospace for a future space hotel, with NASA licensing the technology. Since 2016, the Bigelow Expandable Module (BEAM), which is a prototype for a future deployable space habitat, has been attached to the ISS as a temporary experimental module. The main purpose was to test its durability, but due to its engineering and performance assessment, it was decided to keep it in place until 2028. Today, it serves as a storage module. Fig. 14 shows a design for an inflatable research station based upon the Bigelow technology. The use of inflatables is currently the only way of producing larger volumes in LEO.

## Grappling with the Environment

The extra-terrestrial environment is lethal to humans. Humans can only survive within a protective pressurized habitat. The outer space and planetary environments on the Moon and Mars are zero to low pressure environments; therefore, these habitats need to be constructed as pressure vessels. To protect humans and equipment from radiation and micro-meteorites, additional protection layers and technologies have to be applied. Habitats must be thermo-regulated (active and passive) in order to maintain an even and comfortable internal temperature, to name but a few of the requirements.

Nowadays the space environment is well-understood and most of the technology is available to build a habitable extra-terrestrial environment. Threats like micrometeoroids, debris, and solar particle radiation events are unpredictable, but there are already solutions available to mitigate these hazards, at least close to Earth. The challenge is creating efficient and reliable spacecraft for long-term human transportation and exploration.

## Hazardous effects of Micrometeoroids and Space Debris

We tend to think of space as empty and, for the most part, that is true. In fact, when we encounter something in space, it is usually not good. Micrometeoroids are not present on Earth[2] and represent a major threat to spacecraft and space suited astronauts. Without protection, these fast-traveling bits of rock can penetrate the pressurized skin of habitable modules and space suits.

Similar to Earth architecture, the most effective approach for protection from different forces and environmental influences is layering. The space suit, as the smallest possible protective skin, is a good example. A space suit is a highly compact technological system for sustaining human activities in space (Fig. 15), composed of multiple layers, depending upon its purpose (Fig. 16). The American Extravehicular Mobility Unit (EMU) has 14 layers and a mass of about 145 kg (319 lb.). It consists of an upper and a lower torso and is fabricated at ILC Dover with modular components. In contrast, the Russian Orlan and Chinese Feitian suits are semi-rigid one-piece suits with a rear hatch entry.

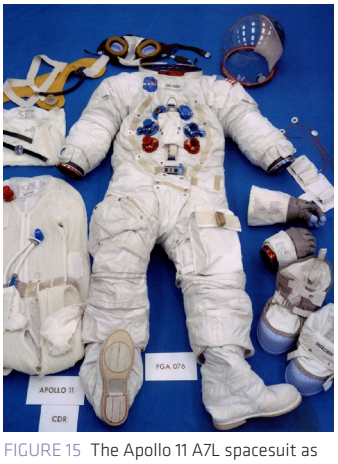


FIGURE 15 The Apollo 11 A7L spacesuit as worn by Neil Armstrong. (NASA)


FIGURE 16 Cutaway view of the first extravehicular spacesuit from the Gemini missions in 1965, showing the many layers. (NASA)

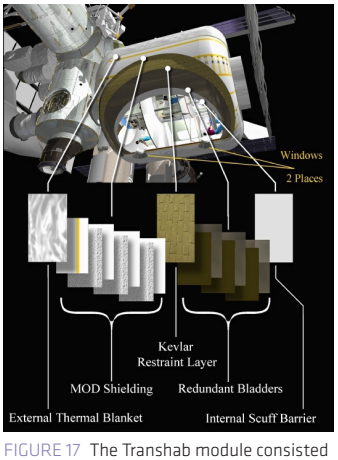


FIGURE 17 The Transhab module consisted of multiple layers: external thermal blanket, micrometeoroid and orbital debris (MOD) shielding, Kevlar restraint layer with three bladders of Combitherm, and an internal fireproof protective Nomex layer. (NASA)

The ISS modules also have layers of aluminium and Kevlar covering the pressurized module. In low Earth orbit there is the additional threat of debris from launch vehicles and other spacecraft. Image 17 shows a cut-away view of the Transhab module exemplarily representing the many layers of inflatable modules (Fig. 14). Transhab micrometeorite protection used twenty-four layers and was about one foot (0.3m) thick. The layers were used to break up particles of space debris and tiny meteorites that may hit the shell with a speed seven times as fast as a bullet. The outer layers protect multiple inner bladders, made of a material that holds in the module's air.

2 Meteoroids that enter the Earth's atmosphere are called meteorites and most burn up before hitting the surface.

## Making most out of the resources you have

Once you are off Earth, **all you have is what you bring** (which is highly restricted) **or what you can take advantage of** that is already there. One of the biggest issues for an extra-terrestrial habitat is its protection from solar radiation, in particular solar particle events. Galactic cosmic rays (GCRs) are ever present and virtually impossible to stop. On Earth, we are protected from hazardous radiation by the Earth's magnetic field and the atmosphere. Beyond low Earth orbit, radiation exposure can result in short term health risks and an increased probability of cancer or heart disease in the long term.

In August 1972, between the Apollo 16 and Apollo 17 missions to the Moon, the sun released powerful solar flares. It is believed that if this had occurred during one of these missions, the astronauts would have died. (NASA [SpaceWeather], 2020) Today, radiation protection remains a major concern for human missions to the Moon and, in particular for the long travel time required for Mars missions.

The challenge lies in finding the right protection with respect to mass and volume constraints. On Earth, nuclear power plants are screened by massive physical barriers. For space travel, a different approach has to be found. For solar protons, molecular hydrogen (H2) offers the most effective radiation protection. There is no easy design solution for using gaseous hydrogen, so the most manageable compromise is to use the hydrogen component in water or plastics to provide protection. For some Mars mission studies, the idea was to minimize the total mass by using the water content in strategically stored food to provide an added measure of protection. Of course, after the food was eaten, the water would need to be replaced.

FIGURE 18 Cutaway of the Transhab Module. The inner core is protected by a so-called radiation shield water tank. (NASA)

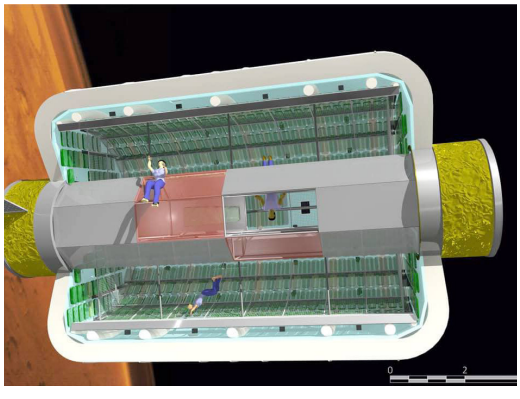

FIGURE 19 Longitudinal Section through a Bigelow 330 (TransHab type) space habitat, showing Water Walls Air Revitalization Bags installed around the inside perimeter and end walls of the inflatable pressure vessel. The water walls design concept includes algae and filters, which would replace solid waste and wastewater to be recycled for repeated human use. As published in Cohen et al. (2012) (NASA)

Recently, this approach was integrated into a radiation shielding concept in combination with the on-board life support and waste processing systems (Fig.19). The layout suggested for the use of the Water Walls Architecture uses radiation shielding wrapped around the whole module (Flynn et al. 2019). This is probably because it is not possible to predict solar flares on space transfer missions to Mars. Surrounding the entire habitat with water is a heavy solution. An alternative is the concept of a dedicated shelter. This shelter would be a protected location where the astronauts would retreat for the duration of the solar event. The logical place for the shelter is an area where the astronauts spend the most time. Typically, the astronauts will each spend 8 hours a day in their crew quarters, so shielding this area would provide a very effective, mass-sensitive solution (Fig. 18).

Other passive approaches to shielding available to astronauts on the surface of the Moon include in-situ resources. For example, using the lunar soil (regolith) has been proposed for shielding habitats. Several architectural approaches exist, including piling up regolith sand or bags filled with regolith, or recently, 3D printing or sintering structures with regolith (Fig. 20). Concepts of active shielding, based on the Earth's magnetic shielding, encompass electrostatic shielding, magnetic shielding, and plasma shielding. All require significant electrical power, so they are not appropriate for early missions.

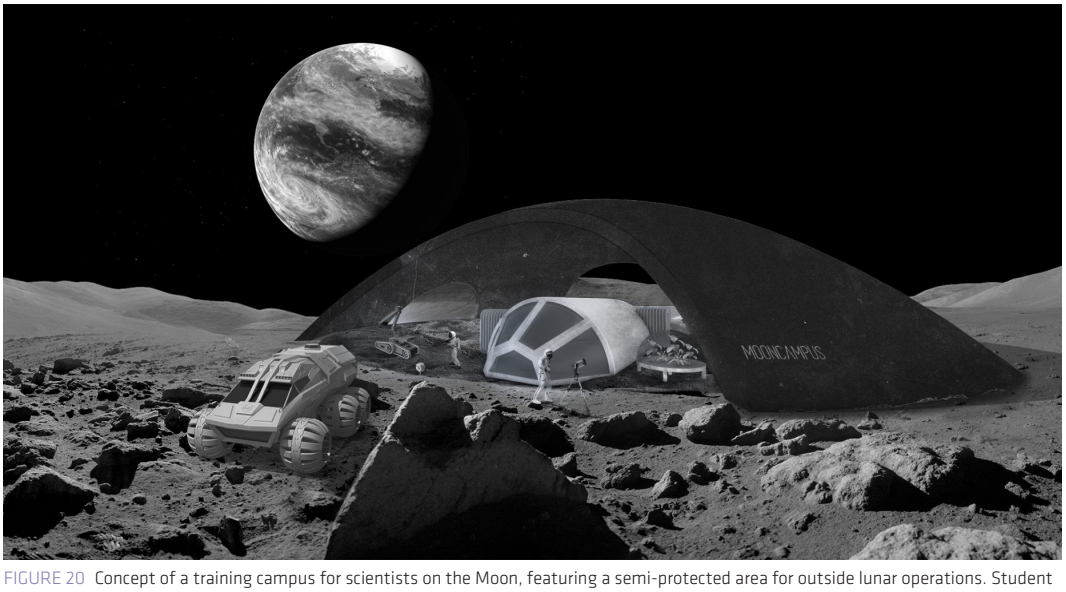


FIGURE 20 Concept of a training campus for scientists on the Moon, featuring a semi-protected area for outside lunar operations. Student project Moon Campus. (MoonVillage Design studio, HB2, TU Wien, by B. Dogan, J. Oblitcova)

## Getting in and out – dust free

During the Apollo missions, astronauts used a small hatchway to get in and out. Before getting out, astronauts had to put on their suits. Then they vented the air out of the lander cabin and started their Extra-Vehicular Activity (EVA). After their outside activities, astronauts were covered with dust, which can be seen on many images from the Apollo missions (Images 21 and 22).

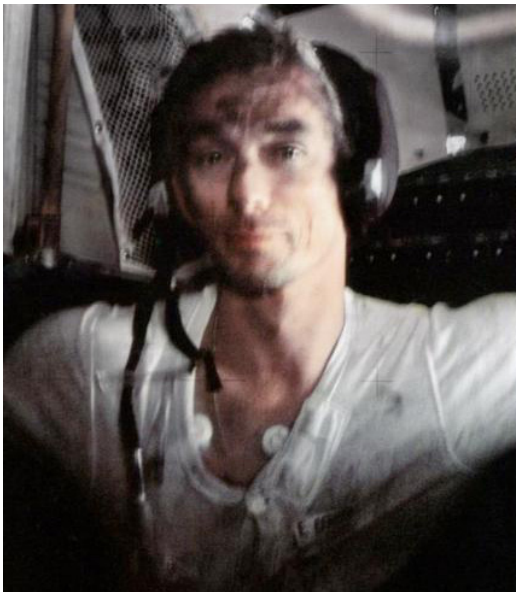

FIGURE 21 Gene Cernan covered in lunar dust (NASA)

FIGURE 22 Apollo 17 astronaut Harrison Schmitt, taking samples on the Moon. His suit is covered in lunar dust. (NASA, photo taken by Eugene Cernan)

**Lunar dust is not like Earth dust.** It is very abrasive because it was formed by meteoroid impacts resulting in shards of rock that have not been rounded-off by wind or water erosion. It can be toxic when breathed, clings to the suit, and gets into joints causing difficulty putting on gloves and helmet. Future explorers will also face the same problems that the Apollo astronauts had with dust. Lunar dust became a major problem not only inside the Lunar Module, but also inside the Command and Service Module, because the fine dust floated in microgravity and was too fine for the cleaning system (NASA [Debriefing A12], 1969; NASA [Dust Management], 2006). The filter system was possible upgraded for the Apollo 17 mission; Harrison Schmitt reported that most of the dust was filtered out of the cabin atmosphere (Schmitt, 2009).

During Apollo, the astronauts went straight from the cabin to outside. On the ISS, astronauts use an airlock to transition from inside to outside for EVAs. This is a small volume (module) that minimizes air loss between two different environments while not having to vent the cabin atmosphere (Griffin, 2010). Most concepts for future exploration include an airlock function. Different kinds of airlocks exist. Typically, they are cylindrical, just big enough for two suited astronauts. However, NASA is looking at a concept that uses a space suit with a hatch-like backpack that mates to a pressurized rover. The dusty suit remains outside while the astronauts enter and exit by opening the backpack into the rover. It is called the *suitport* (Fig. 23 and 24) and it allows faster egress and ingress while conserving atmosphere with the distinct advantage of minimizing lunar dust within the cabin. Future challenges include design for maintenance and repair by astronauts. Another open issue is related to the inhabitants. The space suits are still fitted to the astronaut's size and, so far, there is no spacesuit that fits all. With repeating missions, it has to be ensured that the attached spacesuits are just right for the crew working and living in the habitat.

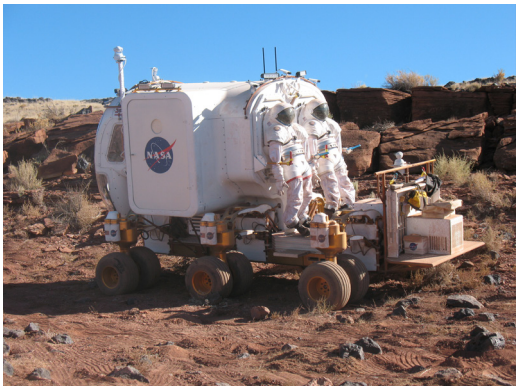

FIGURE 23 This is one prototype version for NASA's Lunar Electric Rover. This small pressurized rover is about the size of a pickup truck (with 12 wheels) and can house two astronauts for up to 14 days with sleeping and sanitary facilities. It is designed to require little or no maintenance, be able to travel thousands of miles climbing over rocks and up 40 degree slopes during its ten-year life exploring the harsh surface of the moon. Two spacesuits are attached to the rover suitlock. (NASA/Regan Geeseman)

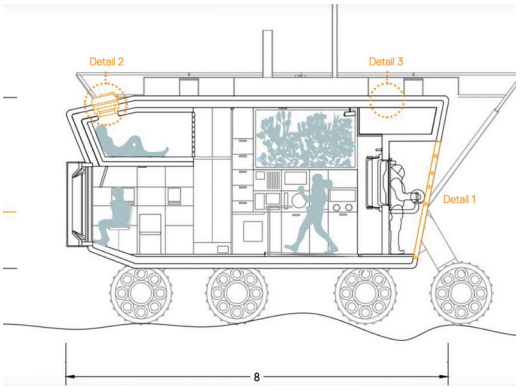


FIGURE 24 Section of a rover design with integrated suitport concept. (MoonVillage Design studio, HB2, TU Wien, by Günes Aydar, Emirhan Veyseloglu, Gözde Yilmaz)

## Humans in Micro Gravity

Humans outside the Earth environment are subject to lower gravity forces. Gravity is a strong force of nature. On Earth, this force is 1G (about 9.8 $m/s^2$) and represents the standard against which other gravity states are measured. In comparison to Earth, Moon gravity is about 1/6 and Mars about 1/3. All life that we know has developed in 1G and going into space means being subjected to a change of gravitational forces. This change affects a wide range of human activities, like body movement, posture, and locomotion. Furthermore, there are differences in human physiology. Most dramatic is weightlessness, or zero-g, in which physiological effects include calcium loss, fluid shifts, skeletal changes, muscle mass loss, and vestibular alterations (NASA [MSIS], 1995 p. 178). Changes in spatial orientation, movement, and sensory perception are among the most important aspects to consider when planning the habitat. Furthermore, without gravity there is no convection which means hot air does not rise, and there is no "natural" settling of heavier gases. Without careful attention to air flow, it is possible for the body's heat and exhaled carbon dioxide to surround the astronaut, which can lead to life-threatening consequences for the astronaut.

On Earth, we sit in chairs, lie down in beds, and get exercise just by walking. In zero-g, there is no need for chairs, astronauts sleep on the wall, and it takes special equipment to exercise. After going to the Moon, NASA created a space station using a large empty propellant tank that was outfitted as an orbital workshop. Before the Skylab mission, astronauts only knew the small, densely packed volume of a re-entry capsule. With Skylab it became evident that workstation designers have to take microgravity conditions into account. Following this experience, an analysis of positions in microgravity was conducted in 1975.

### Designing for the Unknown: The Zero-G-Posture

*"On Earth, gravity is holding the feet to the floor. In zero-g [an astronaut] must have restraints for that purpose."* (NASA [Bull. 7], 1974 p. 2)

Skylab's long duration missions and large open volume (Fig. 25 and 29) provided the opportunity to – for the first time – document the neutral body position in space. The neutral body posture is when all muscles are in their neutral state without requiring extra effort. There is a clear difference from the neutral body position in space compared to Earth (Fig. 27). At that time, when the measurements were taken during the Skylab missions, it was believed that "*there is a definable relaxed body posture in zero-g and that the eligible flight crew population can be fitted to that posture*" (NASA [Bull.17], 1975 p. 2). Today, we know that the range between those positions varies much more and also relates to the individual astronaut. However, there are some similarities that have large consequences for the design of the whole space station interior (Griffin 1978). **The head is tilted down, the arms and legs lift up, and there is no pooling of fluids in the lower extremities.** The neutral body position in 0 gravity is called the Zero-g posture (Fig. 26).

FIGURE 25 Mission Specialist Carl Meade at the Spacelab glovebox, rack # 12. (NASA)

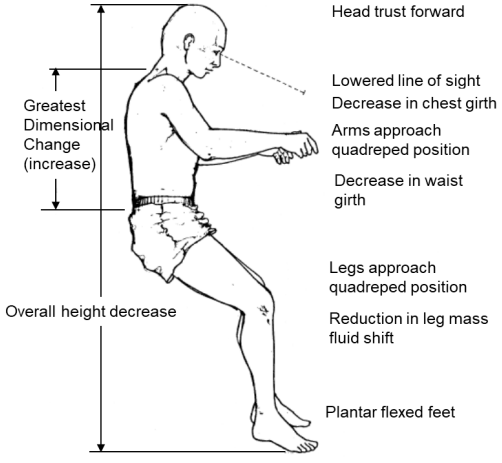


FIGURE 26 Description of the main characteristics of the zero-g posture, the neutral body position in space. (Brand Griffin)

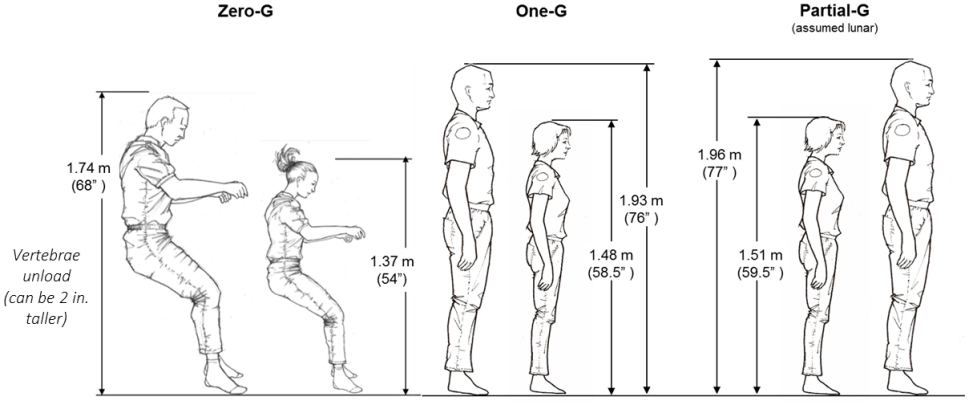


FIGURE 27 Comparison of the neutral body position depending on different gravity conditions. (Brand Griffin)

Some tasks require the use of both hands and a stable body position. In microgravity this is particularly essential, because without some type of restraint (which is the floor on Earth), an astronaut trying to tighten a screw will do the turning, not the screw. The solution for Skylab was to create a shoe with a triangular cleat on the sole which was secured to an open triangular grid (Fig. 28 and 29).

The grid proved useful for attaching equipment and tools. But as each crew became quickly familiar with motion and restraint on Skylab, the shoe was not used much. In order to operate the control panel for the Apollo Telescope Mount, one of the astronauts thought that a chair-like body restraint would be useful. Later, this, along with a fireman's pole were abandoned and considered unnecessary. (NASA [Bull.10], 1974; NASA [Bull.11], 1975)

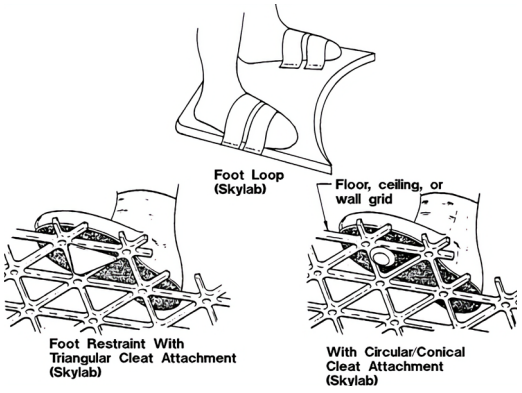


FIGURE 28 Selection of foot restraints used during the Skylab missions. (NASA)


FIGURE 29 Internal arrangement of the Skylab Orbital Workshop. From left to right is the dining area, waste management, and sleeping quarters. Portable restraints are on the wall beside the sleeping quarters. The walls are all made of a triangular grid as restraints. (NASA)

On the Salyut and Mir space stations the walls were also used as storage and utility areas (Fig. 30) Today, there are many restraints, such as handholds, waist restraints, and foot restraints. Velcro is used all over the International Space Station to hold things in place (Fig. 31)

FIGURE 30 Cosmonaut Dorin Prunariu onboard the Salyut 6 space station in 1981. Rubber bands are used to hold things in place. (Courtesy: Dorin Prunariu)

FIGURE 31 Japan Aerospace Exploration Agency (JAXA) astronaut Takao Doi, STS-123 mission specialist, looks over his choices of beverages and snacks in the galley on the middeck of the Space Shuttle Endeavour while docked with the International Space Station. Note the many Velcro patches to secure all different kinds of things to the wall. (NASA)

## Same, same, but different - Human Activities in Space

**Weightlessness changes (almost) everything.** While the feeling of weightlessness is the most unusual and most desired experience of the astronauts (see Fig. 25), as "*you can use it to make your life easier*" and "*you can use all surfaces*" (Clervoy 2009), the physical effects are a challenge for the human body. Most severe is the change in cardiovascular, bone, and hormonal physiology. The astronauts' heart rate and blood pressure decrease in space, as does the variability in heart rate and blood pressure. Astronauts' bones lose calcium and strength, their muscles lose mass. In strong contrast to Earth, where exercise is mostly seen as a leisure activity, in space it is essential for staying healthy and strong (Fig. 32).

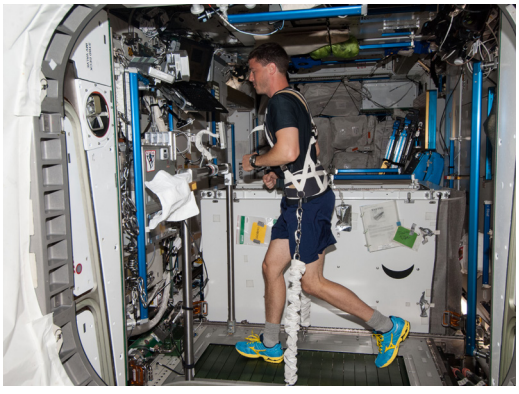

FIGURE 32 NASA astronaut Reid Wiseman, equipped with a bungee harness, exercises on the T2 treadmill. (NASA)

FIGURE 33 Canadian Space Agency astronaut Julie Payette preparing tortillas onboard the Space Shuttle Endeavour. Payette was a mission specialist on STS-127. (NASA)

Eating and drinking are also different. To prevent fluids and pieces of food from getting into electronics and equipment, the liquids are squeezed from tubes and other foods tend to have a paste-like consistency. Because there is no natural drainage in the head, the concentration of fluids affects the taste of food. It is not uncommon for astronauts to bring a spicy sauce and be inventive to liven up the dull taste (Fig. 33). With that, cleanliness and personal hygiene have been considered from early on. Most Apollo astronauts shaved during the mission. Although space stations are considered 'clean', in total three shower systems have been developed for use in microgravity, and were used during the Skylab, Salyut, and Mir missions. Opinions vary. In-space showering was considered a pleasant experience, but at the same time too time-consuming. As a compromise, in the case of Mir, the shower cabin was used as a sauna, before it was removed because it took up too much space. ISS does not have a shower; instead, the crew use wet wipes (Häuplik-Meusburger, 2011). For future long-term missions, the system of full-body cleansing will become important again.

## Not all things change: Local Vertical

The first impression is that without gravity there is no need for a floor or ceiling. That is true, but our human form and Earth conditioning yearn for a reference system. Without the natural orientation of gravity, the solution is to create a local vertical that provides a common up and down across the spacecraft. This establishes the orientation for controls, displays, and labelling and is useful in face-to-face communication. We do not like looking directly into the light source; therefore, overhead lighting not only provides the preferred illumination, it is also used to imply an 'up' direction. Furthermore, because there is no natural convection of gases, it is conceivable to generate a bubble of body heat and exhaled carbon dioxide around

the body. So, rather than blowing air up the nose, the accepted design creates a head-to-toe airflow reinforcing the up-down orientation. (Img 34). In the weightless environment, hands are more important than on Earth. In addition to normal tasks, astronauts use their hands for translation and stabilize themselves. Because this prevents two-handed operations, having floor-mounted foot restraints provides stability while freeing up both hands. Although zero-g seems to offer unconstrained freedom, there are good reasons to retain a floor and ceiling along with a local vertical orientation for some human activities.

## The ongoing debate on windows

Nobody would question having a window in a house on Earth. In space, it's different; the inclusion of windows has been a delicate topic.

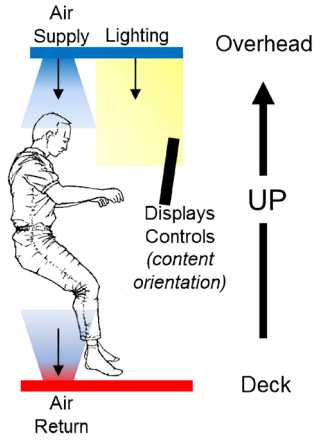


FIGURE 34 Even in zero-g there are good reasons to have a floor and ceiling with a local vertical orientation.

FIGURE 35 Astronaut Susan Helms views the Destiny module of the International Space Station from the Nadir window in the US Laboratory. This is a picture of that particular window from the time when no restraint was installed. (NASA)

FIGURE 36 Astronaut Chris Hadfield strums his guitar in the International Space Station's Cupola, in 2012. (NASA)

Early spacecraft had windows that were mission relevant. The discussion of including a window next to the eating area for the Skylab space station has become famous. It was argued that it was too expensive, that developing it would take too long, that it would weaken the structure, and at last it seemed not to be essential to mission success. After long discussions, the window in the wardroom was finally integrated and also appreciated by the astronauts. As a piece of side information, the astronauts could not see much out of this particular window because of the space station's orientation in relation to Earth. The Multiple Docking Adapter windows were much preferred because they were arranged in a 90-degree angle.

Nowadays, windows in space stations are flat windows integrated within a module. They usually have two interior and one outer redundant glass pane separated by a vented space. For micrometeoroid and debris protection, windows are equipped with external shutters. It has been established that looking out of the window is the favourite astronaut leisure activity. The neglect of that human activity led to a leak in the ISS in 2004. Due to a lack of appropriate handholds, the astronauts repeatedly held onto the air hose when looking out of the window (Fig. 35). This unplanned practice finally resulted in a leaky hose, through which internal air left the station (cf. Haeuplik-Meusburger, 2011).

Today, the ISS has a protruding window assembly, which is essentially a small enclosure with 6 windows and called a cupola (Fig. 36). The debate for the future even includes the discussion of what can substitute for a lack of outward-facing windows. Examples are virtual technology and the clever placement of greenhouses.

## Summary Observations

Support and evidence for the need of integrating habitability can be found in every decade. In view of future and long-term missions, habitability design integration is an important aspect as it becomes even more important when mission length and crew numbers increase.

The history of space travel shows that much has been learned from a technological point of view. Life support systems, food systems, and the development of new technologies and materials are only a few examples of how much has been achieved in the last 50 years. But, when it comes to designing for living in space, there is still a lot to do. Knowledge transfer from one environment to the other, as well as from one generation to the next one can become tricky. Political and economic decisions can slow down and even freeze a whole programme, regardless of its originally innovative concept.

Despite, the focus of early spacecraft design on mission success defined by pure survivability, the examples show creative solutions for combining human needs with technology that are possible within the severe constraints of space flight. The examples also show that a lot of creative potential has not yet been used and remains to be uncovered, and that learning from the past can be part of a promising future. We have to bear in mind the difference between planning and realising projects, and that we will need the best minds from many different professions to let the dream of sustainable space travel come true.

## References


Burgess, C. (2011). Selecting the Mercury seven: The search for America's first astronauts. Springer in association with Praxis Pub.

Clervoy, Jean-François. (2009). Transcript not published [Unpublished interview]. Sandra Häuplik-Meusburger. Paris, France, June 2009.

Cohen, M., Flynn, M., Levy, F., Mancinelli, R., Matossian, R., Miller, J., & Parodi, J. (2012). Water Walls Life Support Architecture: 2012 NIAC Phase 1 Final Report. https://www.nasa.gov/sites/default/files/atoms/files/niac_2012_phasei_flynn_waterwallsarchitecture_tagged.pdf

Compton, W. D., & Benson, C. D. (1983). Living and Working in Space, A History of Skylab. National Aeronautics and Space Administration.

Flynn, M. T., Cohen, M., Matossian, R. L., Gormly, S., Mancinelli, R., Miller, J., Parodi, J., & Grossi, E. (2019). Water Walls Architecture: Massively Redundant and Highly Reliable Life Support for Long Duration Exploration Missions. https://ntrs.nasa.gov/citations/20190001191

Griffin, B. N., Lewin, J. L., & Louviere, A. J. (1978). The influence of zero-G and acceleration on the human factors of spacecraft design. JSC-14581, NASA-JSC.

Griffin B. (2010). Lunar Surface Airlocks. In A.S. Howe, B. Sherwood (Eds.) Out of This World: The New Field of Space Architecture, Reston, Virginia, USA, AIAA

Griffin, B. N., Smitherman, D. V., & Howe, S. A. (2013). Internal layout for a cis-lunar habitat. In AIAA SPACE 2013 Conference and Exposition (p. 5433).

Häuplik-Meusburger, S. (2011). Architecture for Astronauts: An Activity-based Approach (Springer Praxis Books). Springer.

Haeuplik-Meusburger S. and Bishop S. (2021). Space Habitats and Habitability: Designing for Isolated and Confined Environments on Earth and in Space. Springer Nature .

Haeuplik-Meusburger, S., & Ozdemir, K. (2012). Deployable lunar habitation design. In Moon (pp. 469-502). Springer, Berlin, Heidelberg.

Kitmacher, G. H. (2002). Design of the Space Station Habitable Modules. 53rd International Astronautical Congress, Houston, Texas. IAC-02-IAA.8.2.04.pdf

Mount, F. E. (2002). Habitability: an Evaluation. In H. W. Lane, R. L. Sauer, D. L. Feeback (Eds.), Isolation: NASA Experiments in Closed-environment Living: Advanced Human Life Support Enclosed System Final Report. American Astronautical Society.

NASA [Bull.7]. (1974). Skylab Experience Bulletin No. 7: An Overview of IVA Personal Restraint Systems. Lyndon B. Johnson Space Center. JSC-09541.

NASA [Bull.10]. (1974). Skylab Experience Bulletin No. 10: Body Restraint Systems. Lyndon B. Johnson Space Center, JSC-09544.

NASA [Debriefing A12]. (1969). Apollo 12 – Technical Crew Debriefing. Manned Spacecraft Center, 1969.

NASA [Dust Management]. (2006). The Apollo Experience Lessons Learned for Constellation Lunar Dust Management. Houston, Texas, US : Sandra A. Wagner, Johnson Space Center, 2006. NASA/TP-2006-213726

NASA [MSIS]. (1995). Man-Systems Integration Standards (MSIS) (Revision B ed., Vol. 1). NASA. NASA-STD-3000.

NASA [SpaceWeather]. (2020). NASA Space Weather History. http://spaceweatherlivinghistory.org/timeline/31

Riley, C., Copp, D., & Davidson, N. (Directors). (2008-2009). Moon Machines [Documentary] Science Channel.

Schmitt, H. (2009). Transcript not published [Unpublished interview.] Sandra Haeuplik-Meusburger. Vienna, Austria, 2009.

Wright, M., Jaques B. (2002). A Brief History of the Lunar Roving Vehicle. https://www.hq.nasa.gov/alsj/MSFC-LRV.pdf

# Dialogues on Architecture

**Henriette Bier** [1, 2, 3], **Paul Chan** [1], **Advenit Makaya** [4], **Angelo Cervone** [1]

[1] *Delft University of Technology*
*Delft, the Netherlands*

[2] *Politecnico di Milano*
*Milan, Italy*

[3] *Anhalt University of Applied Sciences*
*Dessau-Rosslau, Germany*

[4] *European Space Agency*
*Noordwijk, Netherlands*

## Abstract

Dialogues on Architecture is a series of dialogues between researchers and practitioners, who are embracing the intellectual model of high technology and are involved in its advancement and application in architecture. Dialogue #4 focuses on the technology transfer between on- and off-Earth research and its impact on society, and in particular on industry and education. The dialogue takes place between Henriette Bier (HB), Paul Chan (PC), Advenit Makaya (AM), and Angelo Cervone (AC).

## Keywords

Architecture, Construction, Robotics, In-Situ Resource Utilisation, Human-Computer and Human-Robot Interaction, Industry 4.0

## DOI

https://doi.org/10.7480/spool.2021.2.6057

## Technology Transfer between on- and off-Earth Research and its Impact on Industry and Education

**HB:** Even though buildings have been gradually incorporating some level of robotic aspects since the '70s (inter alia Eastman, 1972; Negroponte, 1975), building processes have been slow in adopting new technologies, which has a major impact on productivity and safety. Compared with other industries, building construction productivity has lagged behind and remained one of the most dangerous activities in the EU, involving more fatalities than any other sector[1].

One way of accelerating new technologies' adoption in building construction could be through technology transfer from off-Earth applications, which return benefits back to Earth applications in areas such as materials, advanced robotics, engineering, etc. Various projects such as the Foster and Partners' Lunar habitat, built using an autonomous swarm of robots,[2] or AI Space Factory's MARSHA habitat that used a biopolymer basalt composite material for 3D printing,[3] etc. are examples in which the potential of technology transfer is highlighted.

**PC:** The architecture, engineering, and construction (AEC) sector is known for its conservative outlook on innovation. As a mature sector with a long-established structure of professional roles and disciplines, ways of producing, constrained by a tight regulatory regime, are well entrenched. Not all of these constraints are necessarily bad. Clear roles and responsibilities coupled with a strong regulatory framework can safeguard against problems of health and safety, and stop buildings from collapsing. Thus, the fact that there are institutionalised ways of working should not be disregarded simply as resistance to technological change. There is a need to examine why current business models persist in the AEC sector.

The ongoing Covid-19 crisis has shown the potential of digital transformation in what is traditionally a sector characterised (to a greater or lesser extent) by on-site production. Hours of virtual meetings have replaced handshakes in the boardrooms with some suggesting that virtual engagements can create more equity and egalitarianism. Advanced robotics and drone technologies coupled with increasing sensing capabilities can help create a more resilient AEC sector by reducing reliance on conventional craft skills. Big Data analytics can unlock the puzzle to produce more liveable built environments in future cities. It seems that technological imagination never fails to amaze.

The Fourth Industrial Revolution (or Industry 4.0) is poised to transform the AEC sector. Through a constellation of technologies – ranging from robotics to advanced sensing, machine learning for Big Data analytics, augmented and virtual reality, and digital twins – Industry 4.0 promises greater efficiency in designing, constructing, and managing the built environment. In a recent McKinsey report, The Next Normal in Construction, the technological wonder of Industry 4.0, is laid out in their manifesto to turn the AEC sector into a truly global sector, offering customisable and on-demand solutions in a mass-production world.

1 Eurostat document: https://ec.europa.eu/eurostat/statistics-explained/index.php/Accidents_at_work_-_statistics_by_economic_activity

2 Link to Lunar habitat: https://www.fosterandpartners.com/projects/lunar-habitation/

3 Link to Marsha: https://www.aispacefactory.com/marsha

**HB:** No doubt that robotics can help the construction sector to not only increase productivity, sustainability, and thus profitability, but also deliver superior products and services at affordable prices. According to McKinsey[4] (2017), almost half the activities in the global economy have the potential to be automated but less than 5 percent of all occupations can be automated entirely. People will, thus, continue working alongside machines.

In terms of the process, the tasks that can be automated need to be first identified, then physical automation of those tasks and processes has to be implemented similarly to the way the car industry has automated its tasks and processes. Then data-driven automation relying on CPS,[5] involving not only Human-Computer but also Human-Robot Interaction (C/HRI), predictive analytics, and Machine Learning (ML), will follow. The human remains in the loop as there are tasks such as human-level pattern recognition as well as tasks requiring subjective assessment or high-level strategic planning. Once processes and activities that have high automation potential are identified, whole process sequences could be redefined. The labour skill shift will be a societal challenge and architects, construction engineers, and workers will need to develop skills suited for the automation age. New activities and jobs will be created for which retraining and skill-raising programmes will be important to support workers shifting to new roles.

Considering the expected labour skill shift, the question is also how academic education responds to the challenges of robotization and the subsequent requirement that architects, construction engineers, and workers develop new skills. Contrary to the preconception that robotization is not architecture related in its essence, the challenge is to understand the same way the modernist architects understood that the industrial revolution 2.0 and new materials fundamentally change architecture, that industrial revolution 3.0 and 4.0 with their robotic, AI, and IoT applications have a major impact on architecture, transforming not only its design and production but also its operation towards becoming a cyber-physically enhanced (production and operation) system.

In this context, accelerating the adoption of new technologies in building construction through technology transfer from off-Earth applications, which return benefits back to Earth applications in areas such as materials, advanced robotics, engineering, etc., needs further definition.

**AM:** Obviously, off-Earth infrastructure construction needs to respond to the limited manpower available for the construction operations, as well to the difficulty of verifying the items built on site. This requires making full use of existing and upcoming capabilities in the design and modelling of constructed parts, process modelling, process automation, in-process monitoring, as well as automation and robotic manufacturing. The collection and use of a substantial amount of data is also particularly relevant, to build models of the constructed elements, for monitoring of their behaviour and predictive maintenance. Those are key aspects of the ongoing development of Industry 4.0 and the associated technological capabilities. Off-Earth construction can therefore be an end user and a catalyst of such technological developments. Off-Earth construction can also, to some extent, be considered as the application of construction techniques which are routinely applied on Earth, to a different, more challenging environment. The wealth of experience and know-how from terrestrial industry can therefore be highly beneficial, if appropriate bridges can be

4 Mckinsey's report: https://www.mckinsey.com/~/media/mckinsey/featured%20insights/digital%20disruption/harnessing%20automation%20for%20a%20future%20that%20works/a-future-that-works-executive-summary-mgi-january-2017.ashx

5 CPS embed computer networks that monitor and control physical processes, with feedback loops between physical and computational processes.

established between space engineering and relevant terrestrial sectors such as architecture, construction, mining, and sustainable energy.

**AC:** On-Earth research is indeed fundamental to correctly prepare and plan the establishment of off-Earth habitats. Most currently envisaged programmes for the human exploration (or, in the longer term, even colonization) of extra-terrestrial celestial bodies need to be widely prepared by means of targeted activities on Earth, with two main objectives: the training of astronauts, and the demonstration/validation of technologies.

The Mars environment especially has a number of similarities with the terrestrial one, including a comparable duration of the day and a very similar seasonal alternation. This allows for very good test facilities to be set, with sufficiently relevant experimental conditions, in some specific locations on Earth. However, the results of these validation activities need to be scaled very carefully to also take into account the differences between the terrestrial and Martian conditions. The most important differences include, just as examples, the significantly lower gravity on Mars, the completely different composition and density of the atmosphere, and the extremely toxic nature of Martian regolith.

Ultimately, the most important technologies that will need to be developed and carefully demonstrated on Earth, in order to allow for the establishment of habitats on other celestial bodies, are: technologies for the in-situ extraction, production and utilization of materials (e.g. planetary mining, 3D printing, autonomous manipulation, etc.); body protection equipment and suits; facilities for the production of food/water and the recycling of human waste; sufficiently reliable power generation plants, including facilities for the production of rocket propellants.

Of course, the opposite is also true, with aspects of off-Earth research becoming relevant to on-Earth applications. This is nothing new; from the engineering point of view, space research has always experienced a continuous synergy with research for terrestrial applications, in a wide range of fields from medicine to air/road transportation, from innovative materials to computer software and hardware, to everyday products. Unsuspected products and technologies that come directly from space engineering developments include, just as examples: the LASIK surgery technique for vision correction (NASA Technology Transfer Program, 2003)[6]; innovative technologies for durable gold-plating of objects (NASA Technology Transfer Program, 2018[7]); super-strong materials for car tyres; water purification systems; and even special supplements for baby food.

When it comes to off-Earth space research, one aspect that needs to be taken very carefully into account is sustainability. Can human colonization of other, non-Terrestrial, planetary environments be considered sustainable at all? This is a very widely debated question, see for example: Levchenko et al., 2019; Smith et al., 2019; Anker, 2005. It is more an ethical and political question than a technical one, but it still has a huge impact on engineering aspects too; which materials can be brought from Earth, and which ones need to be procured and used directly on-site? To what extent can humans alter the planetary environment with constructions and habitats? What debris and how much of it can be left on an extra-terrestrial planet? All these questions have a direct impact on the development of technologies for off-Earth habitats.

**PC:** Similarly, for on-Earth applications, there are ethical questions that need to be raised with respect to determining what a world driven by algorithmic ways of designing will look like. Will this necessarily

6 Link to NASA website: https://spinoff.nasa.gov/spinoff2003/hm_1.html

7 Link to NASA website: https://spinoff.nasa.gov/Spinoff2018/ip_4.html

lead to more equality and diversity? Or will algorithms further embed existing inequalities? How will Industry 4.0 lead to better employment and societal outcomes? And how can society safeguard against technological mega-corporations controlling the narrative of building future cities? Technology is thus the question, not the answer.

**HB:** These questions need to be addressed and the challenge is to also introduce them in education in order to prepare future engineers for the challenges of the 21st century.

**AM:** Because off-Earth infrastructure construction and manufacturing can be best implemented in a multidisciplinary context - involving expertise in space engineering, planetary science, civil engineering, architecture, and advanced manufacturing - such multidisciplinary approach should be promoted in the education of future professionals involved in space infrastructure development. This could be achieved through concurrent engineering projects and by ensuring exposure of non-space students to space engineering aspects and space environment constraints, while making space engineering students are acquainted with topics such as human-centred design, psychological aspects, and spatial planning.

**AC:** Education has a crucial role in particular when it comes to outside-the-box, futuristic research as, for instance, in the final BSc project (called Design Synthesis Exercise) offered at the Aerospace Engineering faculty, Delft University of Technology, where groups of 10 students work full-time for 10 weeks on a design project proposed by academic staff of the faculty. In the framework of this course, several projects related to off-Earth research and planetary exploration were recently proposed, such as: the design and planning of a comprehensive programme for the human colonization of Mars; the design of a planetary protection mission against potentially hazardous asteroids (Radu et al., 2019), etc. These projects have led to extremely interesting, outside-the-box design ideas, taking advantage of the fresh mindset and creativity of young BSc students.

Another education element that allows for the exploration of off-Earth concepts and injecting new, exciting ideas in them is, of course, the MSc theses of students. An example is a thesis that focuses on a preliminary study of technologies for in-situ production of rocket propellant on the Moon. It is easy to imagine the potential game changer this would represent for interplanetary travel; it would be possible to build "re-fuelling stations" orbiting the Moon, limiting the demand for propellant required to be broughtfrom Earth and thus allowing for faster, better-performing travels to Mars or other planets (Schluter & Cowley, 2020). It's not a technology to be developed in the next few years – it will take a bit longer –but when developed it will bring disruptive advantages to (human) space travel. And these students, with their projects, will definitely be precursors to these disruptive technologies.

## References


Anker, P. (2005). The ecological colonization of space. *Environmental History, 10(2), 239-268.*

Eastman, C. (1972). Adaptive Conditional Architecture. *Research Report Carnegie-Mellon University Institute of Physical Planning.*

Levchenko, I., Xu, S., Mazouffre, S., Keidar, M., & Bazaka, K., (2019). Mars colonization: beyond getting there. *Global Challenges, 3(1).*

Negroponte, N. (1975). The architecture machine. *Computer-Aided Design*, *7(3).*

Radu, S., Speretta, S., & Cervone, A. (2019). Pico-Satellite Platforms as Effective Sensors for In-Situ Asteroid Characterization. *Proceedings of the IAF 70th International Astronautical Congress*.

Schlüter, L. & Cowley, A. (2020). Review of techniques for In-Situ oxygen extraction on the moon. *Planetary and Space Science, 181.*

Smith, K. C., Abney, K., Anderson, G., Billings, L., Devito, C. L., Green, B. P., ... & Wells-Jensen, S. (2019). The great colonization debate. *Futures, 110, 4-14.*

# spool

www.spool.ac



ISBN 9789463664592